2001

The effect of oxygen on the growth and relaxation of Ag thin films and associated nanostructures deposited on Ag(100)

Anthony R. Layson
Iowa State University

INFORMATION TO USERS

This manuscript has been reproduced from the microfilm master. UMI films the text directly from the original or copy submitted. Thus, some thesis and dissertation copies are in typewriter face, while others may be from any type of computer printer.

The quality of this reproduction is dependent upon the quality of the copy submitted. Broken or indistinct print, colored or poor quality illustrations and photographs, print bleedthrough, substandard margins, and improper alignment can adversely affect reproduction..

In the unlikely event that the author did not send UMI a complete manuscript and there are missing pages, these will be noted. Also, if unauthorized copyright material had to be removed, a note will indicate the deletion.

Oversize materials (e.g., maps, drawings, charts) are reproduced by sectioning the original, beginning at the upper left-hand corner and continuing from left to right in equal sections with small overlaps.

Photographs included in the original manuscript have been reproduced xerographically in this copy. Higher quality 6" x 9" black and white photographic prints are available for any photographs or illustrations appearing in this copy for an additional charge. Contact UMI directly to order.

ProQuest Information and Learning
300 North Zeeb Road, Ann Arbor, MI 48106-1346 USA
800-521-0600

The effect of oxygen on the growth and relaxation of Ag thin films and associated nanostructures deposited on Ag(100)

by

Anthony R. Layson

A dissertation submitted to the graduate faculty

in partial fulfillment of the requirements for the degree of

DOCTOR OF PHILOSOPHY

Major: Analytical Chemistry (Chemical Instrumentation)

Major Professor: Patricia A. Thiel

Iowa State University

Ames, Iowa

2001

UMI Number: 3016719

UMI Microform 3016719

Bell & Howell Information and Learning Company
300 North Zeeb Road
P.O. Box 1346
Ann Arbor, MI 48106-1346

The effect of oxygen on the growth and relaxation of Ag thin films and associated nanostructures deposited on Ag(100)

Anthony R. Layson

Major Professor: Patricia A. Thiel
Iowa State University

We report the effects of oxygen on the nucleation, growth and relaxation of Ag nanostructures on Ag(100). Comparisons with previous observations on the clean, oxygen-free Ag(100) surface, provide an indirect method to determine how oxygen affects the atomic-scale diffusional processes on the surface. Experiments were performed in UHV using High-Resolution Low Energy Electron Diffraction and Variable Temperature Scanning Tunneling Microscopy. Oxygen exposures were performed prior-to, during, and after the deposition of Ag at temperatures usually ≤ 250 K.

Experimental data show that the mechanism for submonolayer-island coarsening changes from island diffusion/coalescence to Ostwald ripening after exposure to oxygen. The change in mechanism is manifest in an increase in the rate for island coarsening. Exposure to oxygen also enhances the rate for smoothing of mounded multilayer films. Decay analysis of multilayer island stacks reveals that oxygen adatoms (O_{ad}) are mobile on the Ag terraces, and are able to freely attach/detach from terrace steps. It is speculated that O_{ad} aids in the detachment of Ag_nO (n=1,2) from the surface steps, driving the coarsening process. After extended island evolution, Ag islands undergo a change in size and shape, with island and terrace steps adopting the less favorable (open) [100] orientation. The change in surface step geometry is a result of oxygen-induced formation and stabilization of kinks at the surface steps.

We also show that the presence of O_{ad} prior to the deposition of Ag results in the decrease in the initial island density of surface islands. This implies that mobile O_{ad} and/or Ag_nO interferes with Ag deposition. It is also possible that incorporation of oxygen destabilizes small Ag clusters, causing them to break apart, or makes the entire cluster itself mobile. Further analysis through multiple-step deposition experiments verifies the existence of mobile O-species. The change in island density demonstrates that the pre-exposure of the Ag surface to oxygen provides an interesting means to control the formation of Ag nanostructures during the deposition process.

Graduate College

Iowa State University

This is to certify that the Doctoral dissertation of

Anthony R. Layson

has met the dissertation requirements of Iowa State University

Signature was redacted for privacy.

Major Professor

Signature was redacted for privacy.

For the Major Program

Signature was redacted for privacy.

For the Graduate College

TABLE OF CONTENTS

I. GENERAL INTRODUCTION

1. Adsorbates in metal film growth

The deposition, growth, and equilibration of thin films and nanostructures hold considerable technological importance, and have recently been a subject of much interest [1]. For example, significant advancements in the field of thin films have driven the transistor size on integrated circuits down to the 100-nm regime. Fabrication of promising structures such as nanowires [2,3], quantum dots [4] and novel nanoelectromechanical devices [5] has also benefited from advancements in thin film growth techniques. However, consistency in the control and reproduction of nanostructures with very small lateral size ($\leq$ 10 nm) has proven to be difficult. To compound this problem, the interactions between these nanostructures with the surface, deposited atoms and other structures themselves are not fully understood.

As the size of the thin films and nanostructures continue to become smaller, manipulation and control over these structures depends on understanding the fundamental interactions between the substrate and deposited material. Ultimately this means understanding the growth process at the atomic level. To achieve this goal, experiments must be conducted in ultra-clean environments, free from interference from unwanted elements. Ultrahigh vacuum conditions are chosen to ensure the highest level of cleanliness so the interactions of interest proceed unimpeded. However, even in the cleanest environments, contamination from foreign species can never be entirely eliminated. Consequently contaminants, such as an adsorbate species, may adversely affect film growth and surface

interactions. Conversely, it is also possible for the presence of a foreign species to enhance the growth and properties of the film, such as adsorbate assisted layer-by-layer growth. Therefore, to understand the applicable characteristics of these films and structures, it is of the utmost importance to also understand the possible effects of adsorbed foreign species or contamination.

The specific use of adsorbed species, or surfactants, to aid in the growth of metal thin films and structures is well known. The addition of an Sb monolayer prior to deposition of Ag on Ag(111) is one of numerous examples in the use of metal surfactants to induce smooth layer-by-layer growth [6-10]. Gas adsorbates also find uses as surfactants in both homo and heteroepitaxial systems. For example, the use of fluorine on the Fe/Cu(100) [11] and oxygen on the Cu/Ru(0001) [12] heteroepitaxial systems, both promote smooth film growth. Oxygen has also been found to act as a surfactant in the homoepitaxial growth of Pt/Pt(111) [13] and Cu/Cu(100) [14].

While surfactants are purposely chosen for their properties in affecting film growth, it has long been known that spontaneously adsorbed species from the residual gas can also influence the film morphology during growth [15]. Several studies have shown that film growth on an adsorbate-precovered surface can be altered as compared to growth on the respective clean surface [16-18]. Adsorbate effects on nanostructure growth and equilibration have also been of considerable recent interest. For example, Au nanostructures on Au(111), which are stable in vacuum, decay rapidly when exposed to air [19,20]. The presence of minute amounts of CO affects the size, shape and density of the resultant islands during the deposition of Pt/Pt(111) [21]. A final example results in the rotation and elongation of the Ni islands deposited on an oxygen precovered Ni(100) surface [22].

Adsorbate induced evolution of step structures on low-index metal surfaces has also been studied extensively [23-26].

2. The Ag(100) Surface

The ultimate goal of our work is to try to understand the basic interactions of atoms on the surface and how the presence of an adsorbate alters those interactions. To accomplish this task, it is important that the system we choose be as simple as possible. The Ag(100) homoepitaxial system offers several advantages which make it an ideal surface for adsorbate studies. First, Ag(100) does not reconstruct upon annealing at high temperatures. Second, structures created on the surface are long lived and are easily monitored with our experimental methods. Most importantly, the Ag(100) surface is relatively unreactive and remains contaminant free during sample preparation and observation. This is particularly important in studying adsorbate/surface interactions, for contamination may hinder or contribute to, the true adsorbate interactions of interest.

Ag is an FCC metal with the (100) surface orientation exhibiting four-fold symmetry with rows of Ag atoms separated by rows of four-fold hollow sites (see Figure 1a). During the sample preparation, the crystal is cut with a slight misorientation from the (100) direction producing a surface consisting of terraces separated by single atom high steps. Two common step orientations exist: the close packed [110] step and the metastable [100] step (see Figure 1b). The [110] step is by far the more stable orientation and dominates the step structure on the clean Ag surface. 'Jogs' or irregularities in a [110] step produce sites that are known as kinks. The open nature of the [100] step can be described as a step comprised of a linear

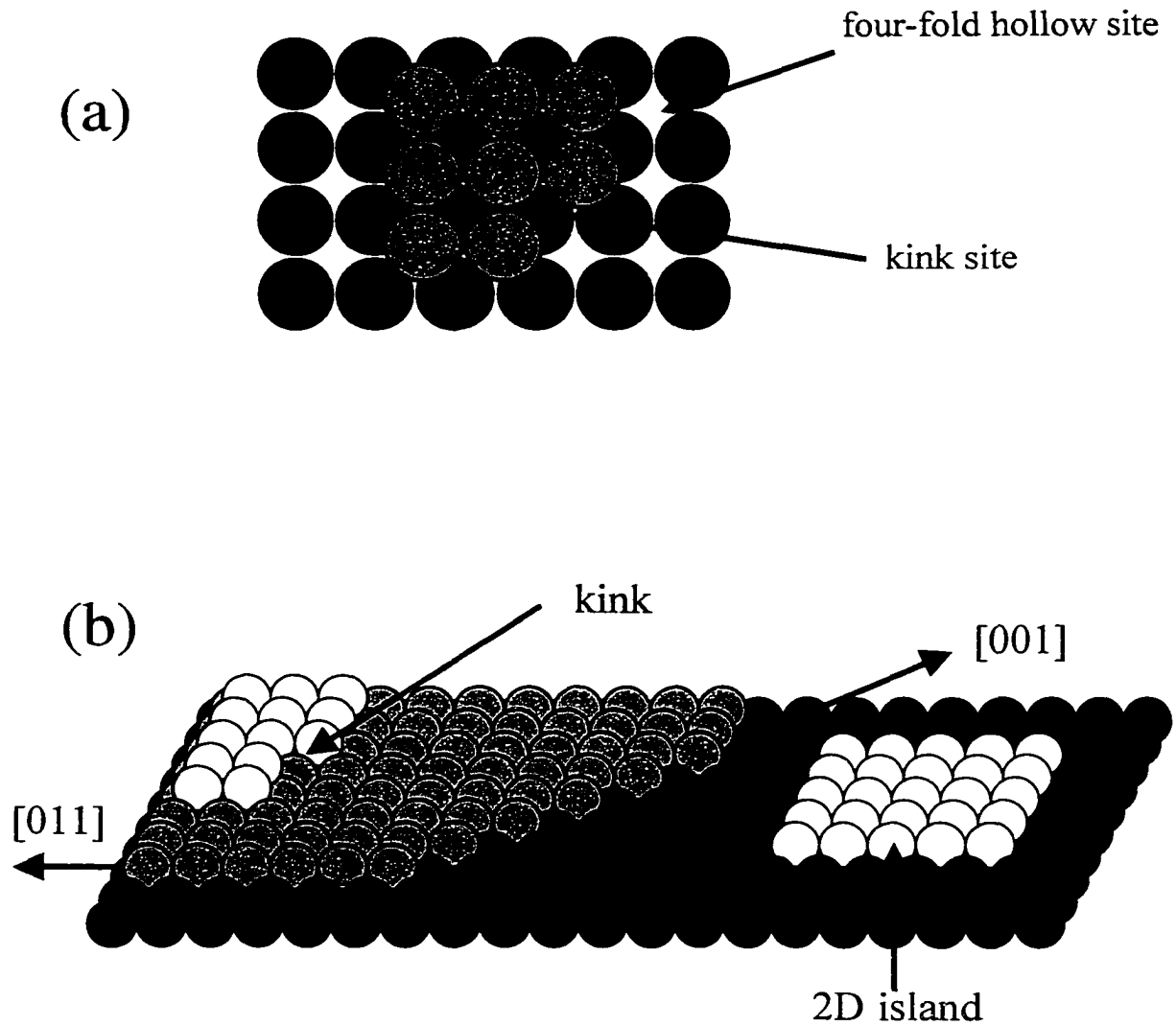

Figure 1. Views of the (100) surface. (a) Top view (b) '3-D' side view. Lighter atoms signify atoms occupying the next highest layer. The close-packed [110] and the open [100] step edge orientations are shown. The square geometry for surface structures is observed in the two-dimensional island. Kink site geometry is also illustrated, with the linear chain of kinks readily observed in the extended [001] step.

chain of kink sites. Deposition of Ag onto the (100) surface produces surface structures, such as submonolayer islands, with square equilibrium geometry and surface steps oriented in the [110] orientation.

3. O_2 on Ag(100)

The interaction of oxygen ($O_{2(g)}$)on Ag has a long history with industrial relevance in the ethylene epoxidation process, where Ag is the only known metal catalyst [27-30]. It has been recognized that the efficiency of this process is greatly determined by the mode of adsorption of $O_{2(g)}$ on the surface of the Ag catalyst [31,32]. Initial observations of the various low- index Ag surfaces showed that the (110) surface was quite reactive to $O_{2(g)}$ adsorption [33-37] while the (100) [34,38,39] and (111) [40,41] surfaces were considerably less reactive. As a result, a considerable amount of work concerning $O_{2(g)}$ on Ag(110) has been performed, while much less effort has been directed to similar studies on the (100) and (111) surfaces. At present, $O_{2(g)}$ interactions with Ag(100) are still relatively unstudied. However, some recent work has been done which has greatly enhanced our understanding of this system.

Adsorption of $O_{2(g)}$ on Ag(100) is characterized by a molecular chemisorption state at temperatures between 150-180 K [42]. This chemisorption state acts as precursor to a dissociative adsorption state at higher temperatures. The dissociative sticking probability of $O_{2(g)}$ on Ag(100) is 4.4×10^{-3} at 300K [43,44]. This is in stark contrast to the Ag(110) surface (where $O_{2(g)}$ adsorption is favorable) which has a sticking probability of 0.63 [44]. At temperatures above 180 K, the majority of oxygen molecules impinging on the surface

find the flat terraces, which are not favorable for adsorption, and the molecules promptly desorb [45,46].

As the temperature is increased, counter to intuitive thought, the oxygen-sticking coefficient actually increases. This implies that $O_{2(g)}$ dissociation is activated by thermally activated defects on the surface. Molecules finding the activated defect sites (identified as kink sites at the surface steps) are able to adsorb and subsequently dissociate [46-48]. It is not surprising that kink sites are favorable for $O_{2(g)}$ adsorption, for the kink geometry closely resembles (110)-sites, which as previously discussed, are favorable in oxygen adsorption.

Upon dissociation, the resultant oxygen adatoms (O_{ad}) on the (100) surface are quite stable and do not recombine and desorb. The stability is further witnessed in the inability to remove the O_{ad} by CO oxidation [49], which is readily accomplished for the other low index Ag surfaces [50,51]. Once in the atomic state, O_{ad} is able to diffuse from the kink site leaving the kink available for further oxygen dissociation events. At higher temperatures, fluctuations in the surface steps provide a constant source of fresh kink sites which further aids in oxygen dissociation. O_{ad} evolving from the kink sites is not restricted to diffusion along the surface steps. In chapter III we show that the oxygen atoms are able to diffuse across terraces as well as along steps. Additionally, about 0.8 eV/atom is released upon dissociation [40]. The additional energy may allow hyperthermal diffusion of O_{ad} to also occur [52,53]. High resolution electron energy loss spectroscopy (HREELS) studies also show that sub-surface incorporation of O_{ad} can also occur after dissociation [43]. An $O_{2(g)}$ molecule finding a kink site can adsorb in an 'end down' orientation with the primary axis directed toward the surface. This orientation offers an easy pathway for sub-surface

incorporation of the "hot" oxygen atoms. Temperature programmed desorption (TDS) shows no signal due to oxygen desorption upon annealing an oxygen exposed Ag(100) surface [43]. This further indicates that sub-surface incorporation of O_{ad}, and ultimately incorporation into the bulk, must occur.

To date, the majority of $O_{2(g)}$ on Ag(100) studies have focused primarily on observations concerning oxygen, such as oxygen dissociation, diffusion, binding sites and coverage. Far less studied are the effects of $O_{2(g)}$ on the Ag surface itself. The question then that needs to be asked is – what effect does $O_{2(g)}$ have on the morphology and structure of the Ag surface? Our research group has extensively studied the Ag(100) homoepitaxial system and has amassed extensive knowledge in the nucleation, growth and evolution of Ag nanostructures on this surface [54]. Past observations on the clean Ag(100) surface provide a convenient basis for comparison when the system is modified through the addition of oxygen.

The purpose of this dissertation is to observe the effects of $O_{2(g)}$ on the surface structure of Ag(100), as well its effects on thin films and nanostructructures created on the surface through Ag deposition. In chapters I and II we use two distinctly different instrumental techniques to observe the oxygen-induced evolution in coarsening and smoothing of submonolayer islands and multilayer mounds. Chapter III illustrates how controlled oxygen exposures, prior to Ag deposition, can be used as a means to control the growth of nanostructures on the surface. In addition, the growth experiments provide information on the atomic interactions of O_{ad} and Ag on the (100) surface. In chapter IV we take a closer look at surface structures to observe how the presence of O_{ad} affects the equilibrium shape of islands and steps through island-island and island-step restructuring

events. We also obtain insight into the restructuring dynamics at the island and surface steps by monitoring the restructuring events with time.

4. Instrumental methods

The principal experimental methods employed in the oxygen on Ag(100) studies are high-resolution low energy electron diffraction (HRLEED) and scanning tunneling microscopy (STM). While entirely different in their modes of operation and the data that they provide, the two techniques compliment each other extremely well, and when used in combination offer a powerful means for surface analysis.

HRLEED is a diffraction technique that provides information on atoms and structures at the crystal surface. The data obtained from this technique must be interpreted from reciprocal space diffraction patterns. Island separations and island densities are the most important pieces of information that HRLEED provides in the Ag(100) studies. Because HRLEED does not provide real-space information, it is not useful in monitoring individual events on the surface. However, the information contained in the diffraction profiles represents an average value that is derived over a large area on the surface. For this reason, HRLEED quickly provides very good statistical data for the system of interest. Additionally, HRLEED is easily operated over a large range of temperatures, and is stable enough that the surface can be monitored over extended periods of time. The primary disadvantage to the technique is that real-space information is not obtained. A more thorough explanation on how HRLEED is used in Ag(100) homoepitaxy is provided in Appendix D. Several interesting reviews by M. Henzler provide additional information on the technique [55-57].

Our primary experimental technique is STM, which offers several advantages. First, STM provides real-space images, therefore surface structures and surface features can be observed directly. Because the principal goal is to observe the surface structure, it is important that our imaging technique not interfere with the surface. STM is a logical choice for our studies in that there is no contact between the tip and surface. If correctly adjusted, imaging occurs free from surface/tip interference or perturbations. Second, the resolution in STM is extremely high allowing detailed images of surface structures down to the atomic level. This is very important in our experiments where surface islands may only be a few nanometers in size. Lastly, the STM provides sequential real-time imaging with a time scale of only minutes between images. Therefore, the evolution and dynamics of the surface structures can be observed. The microscope itself is easily adapted to ultrahigh vacuum conditions, which are necessary for our experiments. Additionally, our microscope is fitted with variable temperature capabilities, which allows us to explore the surface anywhere from 35 – 1000 K. A good summary of STM operation and applications can be found in C.J.Chen's book [58], "Introduction to Scanning Tunneling Microscopy."

A distinct disadvantage in using STM is that it only provides information on a small fraction of the surface. It is often difficult to draw concrete conclusions about the system of interest based on a single image or even a set of images. It is analogous to describing the landscape of the United States by reciting only what you see when you look out of your window. It is not a true representation of the country as a whole. The same can be true in STM. The only way to ensure consistency in measurements of extremely small areas is to probe many different areas on the surface or repeat the experiment many times. With lengthy or procedurally complicated experiments, this is often not possible. This is why the

combination of HRLEED and STM is so powerful. HRLEED results represent an average value for the surface features and events, over a large area of the surface. The data obtained hold significant statistical relevance, but lack detail on the minute scale. The strength of STM lies in the ability to directly observe the surface, with high resolution, over extended periods of time. While statistically the data may be poor, physical observation is the only way to truly discern what is occurring on the surface.

5. Dissertation Organization

This dissertation includes one published paper and three others that are either submitted or will be submitted for publication. Chapter II, "Testing 'realistic' environments for metal film growth and aging: chemical insights into the effects of oxygen on Ag/Ag(100)," appears in volume 472 of *Surface Science Letters* on pages L151-L156, 2001. Chapter III, "Additive-enhanced coarsening and smoothening of metal films: complex mass-flow dynamics underlying nanostructure evolution," has been submitted to *Physical Review Letters*. Chapter IV, " Use of Adsorbates to Manipulate Nanostructure Formation: O+Ag/Ag(100)," and chapter V, "The influence of oxygen on island shapes and restructuring dynamics on Ag(100)," will be submitted to *Surface Science*. General conclusions will be presented in chapter VI. Appendices A and B expand on material presented in the main chapters of this dissertation. The remaining appendices present additional material concerning Ag(100), Ag(110) and an database for STM and HRLEED experiments.

References

1. See, e.g. Science, 273 no. 5277 (1996)
2. See, e.g. MRS Bulletin, 23 no. 2 (1998)
3. See, e.g. MRS Bulletin, 23 no. 8 (1999)
4. Jiangtao Hu, Teri Wang Odom, and Charles M. Lieber, Acc. Chem. Res., 32 (1999) 435
5. See, e.g. Science, 290 no. 5496 (2000)
6. J. Vrijmoeth J. Vrijmoeth, H. A. van der Vegt, J. A. Meyer, E. Vlieg, and R. J. Behm, Phys. Rev. Lett. 72 (1994) 3843
7. V. Fiorentini, S. Oppo, M. Schleffler, Appl. Phys. A 60 (1995) 399
8. H.A. van der Vegt, H.M. van Pinxteren, M. Lohmeier, E. Vlieg, J.M.C. Thornton, Phys. Rev. Lett. 68 (1992) 3335
9. K. Fukutani, Surf. Sci. 281 (1993) 285
10. H. A. van der Vegt, J. Alverez, X. Torrellas, S. Ferrer, E. Vlieg, Phys. Rev. Lett. 68 (1992) 3335
11. W.F. Egelhoff Jr. Surf. Sci. 402-404 (1998) 32
12. H. Wolter, M. Scmidt, K. Wandelt, Surf. Sci. 298 (1993) 285
13. S. Esch, M. Hohage, T. Michely, G. Comsa Phys. Rev. Lett. 72 (1994) 518
14. M. Yata, H. Rouch, K. Nakamura, Phys. Rev. B 56 (1997) 10579
15. E. Bauer, Thin Solid Films 12, 167 (1972)
16. W. F. Englehoff and D.A. Steigerwald, J. Vac.Sci. Technol. A 7 (1989) 2167
17. J. Schröder, C. Günther, R.Q. Hwang, and R.J. Behm, Ultramicroscopy 42-44 (1992) 475

18. R.Q. Hwang, C. Günther, J. Schröder, S. Günther, E. Kopatzki, and R.J.Behm, J. Vac. Sci. Technol. A 10 (1992) 1970

19. B.H. Cooper, D.R. Peale, J.G. McLean, R. Phillips, E.Chason, Mat. Res. Soc. Symp. Proc. 280, 37 (1993)

20. D.R. Peale, B.H. Cooper, J. Vac. Sci. Technol. A 10 (1992) 2210

21. M. Kalff, G. Comsa, T. Michely, Phys. Rev. Lett. 81 (1998) 1255

22. E. Kopatgzki, S. Gunther, W. Nichti-Pecher, R.J.Behm, Surf. Sci. 284 (1993) 154

23. C.Y. Nakakura, E.I.Altman, Surf. Sci. 424 (1999) 244

24. Frank, J.Catal. 172 (1997) 406

25. C.Y. Nakakura, G.Zheng, E.I.Altman, Surf. Sci. 401 (1998) 173

26. T. Matsumoto, R.A. Bennett, P. Stone, T. Yamada, K. Domen, M. Bowker, Surf. Sci. 471 (2001) 225

27. C. Backx, C.P.M. de Groot, P. Biloen, Surf. Sci. 104 (1981) 300

28. R.A. van Santen, C.P.M. de Groot, Journal of Catal. 98 (1986) 530

29. R.A. van Santen, H.P.C.E. Kuipers, Adv. Catal. 35 (1987) 265

30. C.T. Campbell, Surf. Sci. 173 (1986) L641

31. H.H. Voge and C.R. Adams, Advan. Catalysis 17 (1967) 151

32. W.M.H. Sachtler, Catalysis Rev. 4 (1970) 27

33. A.M. Bradshaw, H.A. Engelhardt, D. Menzel, Ber. Bungsenges. Physik. Chem. 76 (1972)

34. H.A. Engelhardt, D. Menzel, Surf. Sci. 57 (1976) 591

35. H. Albers, W.J.J. vander Wal, O.L.J. Gijzerman and G.A. Bootsma, Surf. Sci. 77 (1978) 1

36. W.W. Pai, J.E. Reutt-Robey, Phys. Rev. B 53 (1996) 15997

37. WW. Pai, N.C. Bartelt, M.R. Peng, J.E. Reutt-Robey, Surf. Sci. 330 (1995) L679

38. C.S. Ares Fang, Surf. Sci. 235 (1990) L291

39. S.P. Mehandru and A.B. Anderson, Surf. Sci. 216 (1989) 105

40. C.T. Cambell, Surf. Sci. 157 (1985) 43

41. F. Bautier de Mongeot, M. Rocca, U. Valbusa, Surf. Sci. 339 (1995) 291

42. E.L. Garfunkel, X.Ding, G.Dong, S, Yang, X. Hou, X. Wang, Surf. Sci. 164 (1985) 511

43. F. Bautier de Mongeot, A. Cupolillo, U. Valbusa, Chem. Phys. Lett. 302 (1999) 302

44. F. Buatier de Mongeot, M.Rocca, U. Valbusa, Surf. Sci. 363 (1996) 68

45. F. Bauatier de Mongeot, M. Rocca,A. Cupolillo, U. Valbusa, H.J. Kreuzer, S.H. Payne, J. Chem. Phys. 106 (1997) 711

46. F. Bautier de Mongeot, A. Cupolillo, U. Valbusa, Chem. Phys. Lett. 270 (1997) 345

47. F. Bauatier de Mongeot, M. Rocca,A. Cupolillo, U. Valbusa, H.J. Kreuzer, S.H. Payne, J. Chem. Phys. 106 (1997) 711

48. G.Constantini, F. Bauatier de Mongeot,S.Rusponi, C. Boragno, U.Valbusa, L.Vattuone, U.Burghaus, L.Savio, M.Rocca, J. Chem. Phys. 112 (2000) 6840

49. U. Burghaus, L. Vattuone, P. Gambardella, M. Rocca, Surf. Sci. 374 (1997) 1

50. U. Burghaus, H. Conrad, Surf. Sci. 370 (1997) 17

51. U. Burghaus, H. Conrad, Surf. Sci. 331-333 (1995) 116

52. C. Engdahl, G. Wahnstrom, Surf. Sci. 312 (1994) 429

53. J. Wintterlin, R. Schuster, G. Ertl, Phys. Rev. Lett. 77 (1996) 123

54. P.A. Thiel, J.W. Evans J.Phys. Chem. 104 (2000) 1663 (and refe=rences within)

55. M. Henzler, Surf. Rev. Lett. 4 (1997) 489

56. M. Henzler, Surf. Sci. 357-358 (1996) 809

57. M. Henzler, Surf. Sci. 298 (1993) 369

58. C.J. Chen, *Introduction to Scanning Tunneling Microscopy*, 1 ed. (Oxford University Press, New York, 1993)

II. TESTING 'REALISTIC' ENVIRONMENTS FOR METAL FILM GROWTH AND AGING: CHEMICAL INSIGHTS INTO THE EFFECT OF OXYGEN ON Ag/Ag(100)

A paper published in Surface Science Letters

A.R. Layson and P.A. Thiel*

Abstract

We study the effect which exposure to molecular oxygen gas can have on the formation and aging of islands in a submonolayer Ag film on Ag(100). The technique used is high-resolution low-energy electron diffraction, and the surface temperature is 220-250 K. Oxygen has no discernible effect on the average separation of islands resulting from Ag deposition, implying that molecular oxygen does not interact with atomic Ag as it diffuses and nucleates islands on the terraces. However, oxygen serves to accelerate post-deposition coarsening, causing the average island separation to increase rapidly. We show that atomic, not molecular, oxygen is responsible for this effect. Dissociation of the molecule presumably takes place at kink sites, which are plentiful due to the abundance of island edges in the film, and can be triggered either by electron impact or by thermal activation.

There has been long-standing interest in the role of adsorbates, especially surfactants, on the final-state structures of films [e.g. 1-6]. These studies have been characterized, typically, by the deliberate pre-adsorption of a single strongly-bound species. There has been

much less work concerning the effect of species which may be weakly-bound or which may adsorb in a more realistic, but less-controlled environment, e.g. air. One intriguing investigation was carried out by Cooper and coworkers [7, 8]. They showed that relaxation of Au nanostructures occurred much more quickly in air than in ultrahigh vacuum [7, 8]. In other words, Cooper's work suggested that exposure to atmosphere can accelerate rearrangements of nonequilibrium nanostructures, such as those formed by film growth or by artificial manipulation. However, the component of air responsible for this effect—the underlying chemistry—remained a mystery. Obviously, it is important to identify and understand such effects, since they will have a direct bearing on the stability and lifetime of engineered metal nanostructures in realistic environments. The present paper deals with one such situation.

Previously, we have presented a detailed picture of nucleation, growth, and post-deposition relaxation of clean Ag/Ag(100) film structures in ultrahigh vacuum, i.e., in the absence of adsorbates or significant background gases[9]. While performing that work, we noticed on several occasions that accidental air leaks caused a great acceleration in the rate at which film structures coarsened. (Coarsening is an evolution toward fewer but larger, i.e. "coarser," features. For two-dimensional adlayers, coarsening is driven by the one-dimensional line tension associated with step edges.) For example, islands that would normally coarsen slowly over a period of hours, or even days, at pressures $\leq 1 \times 10^{-10}$ Torr, would vanish within minutes, in the presence of air at 10^{-7} Torr. This striking observation, which qualitatively paralleled that of Cooper et al., motivated us to investigate the effect of background gases more systematically. To that end, we studied and compared the effects of pure gases, introduced deliberately both *during* Ag deposition and *after* Ag deposition. We

found that Ar, a noble gas, had no effect, nor did CO, CO_2, or N_2, the latter two being major components of air. However, both water and oxygen—also major components of air--exerted strong (albeit dissimilar) effects. Details about water will be reported elsewhere. In the present paper, we discuss the *chemistry* underlying the effect of *oxygen*, insofar as we presently understand it. We pose four questions, then discuss the answers within the context of our data.

The **first question** is whether oxygen exposure affects nucleation and growth of the films. In the process of nucleation and growth, Ag atoms deposit randomly, then diffuse across the surface. Diffusion can lead to nucleation of new islands or aggregation with existing islands. The islands have a near-square shape, with close-packed <110>-type step edges. We choose to use the average separation of nucleated islands, L_s, as the main characteristic of the film. From basic nucleation theory, this quantity (during or immediately after deposition) should be determined by the ratio of the deposition flux, F, to the rate of atomic diffusion, D. For irreversible nucleation, the relationship should be

$$L_s \propto \left(\frac{D}{F}\right)^{1/6} \qquad (1)$$

From experiment, the island separation can be probed using high-resolution low-energy electron diffraction (HRLEED, also known as Spot Profile Analysis-, or SPA-LEED) to monitor a quantity known as the characteristic correlation length, L_c [10, 11]. This quantity, which is directly proportional to L_s, is derived from the reciprocal-space diameter, d*, of the halo surrounding integral-order diffraction spots (at fixed coverage):

$$L_s \propto L_c = \frac{4\pi}{d^*} \qquad (2)$$

It is reasonable to consider that oxygen might change the diffusion characteristics of atomic Ag on Ag(100). Other authors have noted that adsorbates can change the kinetics of metal atom diffusion across surfaces in other systems. For instance, hydrogen has been shown to exert both inhibiting and promoting effects; this is attributed in some cases to complexation between atomic hydrogen and the diffusing metal atom [12-15]. Equations 1 and 2 show that, if the rate of Ag diffusion increases in the presence of oxygen, one should measure a corresponding increase in L_c, as a function of oxygen exposure (for fixed F). However, Fig. 1 shows that the initial value of L_c has no dependence on oxygen exposure during deposition in this system. More quantitatively, the scatter in the values of L_c is no more than $\pm 3\%$, meaning that D can change by no more than $\pm 20\%$ in the presence of oxygen (cf. Eq. 1).

Another way of testing whether oxygen affects nucleation and growth is to compare the initial island separation obtained after *simultaneous* deposition of Ag and exposure to O_2 (as above), with that obtained after *sequential* deposition of Ag and exposure to O_2. If a complex forms between diffusing atomic Ag and oxygen, one might see a difference under the two conditions, because the abundance of Ag atoms should be different. This comparison is made by inspecting the circles and squares, respectively, in Fig. 1. There is no difference. Thus, during deposition, nucleation and growth of the islands is insensitive to oxygen.

The **second question** is whether oxygen affects relaxation and coarsening after the film stops growing. The answer, illustrated in Fig. 2, is positive. In the experiment, the stated exposure of oxygen took place *during* deposition of 0.3 monolayers (ML) of Ag at 250 K, although qualitatively similar results were obtained when exposure *followed* deposition at 250 K. The Figure shows L_c as a function of time, after the end of film growth and oxygen exposure. If the surface coarsens after deposition, L_c should increase; indeed, this is the behavior we have observed for the clean surface at room temperature [10, 16].

The horizontal line shows the behavior of the clean surface in the absence of oxygen at 250 K. At this low temperature, the clean islands do not coarsen—the film is entirely stable in UHV, over periods up to several hours. However, even a small exposure to oxygen (0.50 L) triggers an appreciable change in the kinetics, causing L_c to increase measurably and linearly with time. The slopes of the lines in Fig. 2 can then be equated to a coarsening rate. The data of Fig. 2 show that the coarsening rate increases with oxygen exposure up to about 4 L, with higher exposures having little additional effect. Details about the coarsening kinetics and mechanism will be reported elsewhere[17].

It may seem odd that oxygen affects post-deposition coarsening so dramatically, yet has no effect on island density during film growth. However, the time scales involved in the two processes are much different. Growth of the films only takes seconds to minutes, whereas coarsening takes place over periods of minutes to tens of minutes. Hence, oxygen does not accelerate coarsening appreciably on the time scale of the deposition experiments, but does accelerate it on the time scale of post-deposition observation. It should be noted that this clear demarcation probably results from the particular experimental

conditions—oxygen exposure and pressure, Ag deposition rate, temperature--employed (fortuitously) here.

A **third question** is whether the change in coarsening kinetics is due to atomically- or molecularly-adsorbed oxygen. The chemistry in our system is revealed by the effect of the HRLEED electron beam on the coarsening kinetics. Figure 3a shows an experiment in which 0.3 ML of Ag was deposited, followed by exposure to 4 L O_2 (gas) at 220 K. Three different time intervals separated the end of deposition and the beginning of the HRLEED measurement: 0, 20, and 32 minutes. The Figure shows that *coarsening occurs slowly until the electron beam is applied, at this temperature*. (For reference, the behavior of the system without oxygen is also shown—the horizontal line indicates, as in Fig. 2, no coarsening in UHV.) At a higher temperature—250 K, Fig. 3b—the electron beam is no longer necessary to initiate the coarsening.

To explain the data of Fig. 3, we hypothesize that molecular oxygen is adsorbed, at specific types of kink sites, [18, 19] up to about 220 K in UHV, beyond which it can dissociate thermally. This molecular oxygen does not affect the coarsening kinetics; the oxygen must dissociate in order for coarsening to accelerate. Dissociation can be initiated either by the electron beam, at 220K, or by the surface itself, at 250 K, on the time scale of our measurements. It is well known that electron beams can cause dissociation of adsorbates on metals, [20, 21] including oxygen on Ag(100) [22].

More insight into the mechanism of oxygen dissociation, particularly thermally-activated dissociation, is provided by a series of papers by Valbusa, Rocca, and co-workers, elucidating the dynamics and mechanisms of oxygen adsorption on Ag(100) [18, 19, 23, 24]. They demonstrated that dissociation of the molecule does not occur on the terraces, but can

occur at kink sites along <110>-type step edges [18]. By deliberately using sputtering to change the step density and step orientation and, necessarily, the kink site density, they showed that one can manipulate the ability of the surface to adsorb oxygen dissociatively [19]. In other words, the coverage of atomic oxygen depends sensitively upon kink site density. This is consistent with the fact that oxygen dissociates readily on Ag(110), which can be regarded as a surface comprised entirely of such kinks,[25] but less readily on 'perfect' Ag(100) surfaces [26]. In our experiments, we know that the nucleation and growth of many small Ag islands creates a significant density of <110>-type steps and also, necessarily, a significant density of kink sites. In a sense, film deposition is analogous to sputtering [19] in enhancing sites for dissociation. However, there is a barrier to dissociation even at the kink sites, a barrier that can be overcome either by electron bombardment, or by thermal activation.

In the work of Valbusa, Rocca, and coworkers [23] oxygen dissociation begins at about 180 K, whereas the threshold in our experiments is higher, at least 220 K. The difference may be due to inaccuracies in temperature measurement, primarily due to the fact that a thermocouple cannot be spotwelded directly to Ag. The difference may also reflect differences in time scales between the two types of experiments, since the extent of dissociation is not just a function of temperature, but also of time.

The requirement of kink sites for dissociation may account for the experimental data in Fig. 4, which compares coarsening rates as a function of oxygen exposure for the two different types of experiments, at constant temperature (250 K). In the top curve, the oxygen was admitted to the chamber *during* deposition of the film. In the lower curve, the oxygen was admitted to the chamber *after* deposition (post-deposition) of the film. For a given

oxygen exposure, the data show that post-deposition coarsening is always faster for simultaneous deposition-exposure, than for sequential deposition-exposure. We can envision two hypotheses to explain this effect. In the first, there is a higher concentration of kink sites during deposition (while the islands are in the process of forming) than after deposition (when they have, presumably, had a chance to restructure somewhat). The second hypothesis is that the density of kink sites is about the same under the two conditions. However, atomic oxygen becomes incorporated into the islands during deposition and somehow exerts a stronger influence on coarsening from that location, than if it dissociates on island edges after the islands are formed. In principle, the two hypotheses should be distinguishable by measuring oxygen coverage. The first hypothesis implies a difference in oxygen coverage between the two conditions of oxygen exposure, whereas the second hypothesis implies equal oxygen coverages. To that end, we attempted to use Auger electron spectroscopy to measure oxygen coverages. AES confirmed the presence of oxygen at the surface, but did not show any difference between the two conditions of exposure. However, the signal-to-noise was low, so we do not regard these data as conclusive.

A third hypothesis might be that atomic silver, diffusing across terraces, is active *in addition* to kink sites, in catalyzing oxygen dissociation. Diffusing silver atoms should be several orders of magnitude more abundant during deposition than after deposition. However, the difference in coarsening kinetics is only about a factor of two (Fig. 4). Hence, this hypothesis is unlikely.

A **fourth question** remains unanswered by the present work: Exactly how does atomic oxygen accelerate coarsening? Perhaps it forms a mobile Ag_2O species that diffuses faster than isolated Ag. Perhaps it serves to accelerate the attachment-detachment of Ag

atoms at island edges. Neither of these possibilities can be ruled out by the present work, nor by inspection of the literature.

Our results are reminiscent of those from Reutt-Robey's group, who found that oxygen can make another surface of Ag, the (110), very dynamic on an atomic scale, leading to reconstruction and/or facetting[27, 28]. Besenbacher and Norskov have noted that oxygen induces reconstructions of metal (M) surfaces in which -M-O-M-O- chains are a recurring structural motif [26]. This is certainly true for Ag(110), [28] and such chains have also been reported recently as a structural element of an oxygen-induced reconstruction on Ag(100) [24]. With this in mind, one could even imagine that polyatomic segments of chains detach from island edges and diffuse across the surface, although we have not seen evidence for this in STM.

In summary, the following picture emerges. Molecular oxygen adsorbs at kink sites in the low temperature range of our experiments. The kink sites are especially plentiful on the film surface because of the abundance of island edges. Molecular oxygen does not interfere with Ag atom diffusion and/or island growth. The oxygen at the kink sites can dissociate, either upon electron impact, or upon thermal activation at about 250 K (on the time scale of our measurements). The product atomic oxygen is responsible for accelerated coarsening of the Ag islands, although the mechanism by which it achieves this is not clear at present.

Acknowledgments. This work was supported by NSF Grant No. CHE-0078596. It was performed in the facilities of the Ames Laboratory, which is operated for the U.S. Department of Energy by Iowa State University under Contract W-7405-Eng-82.

References

1. M. Copel, M. C. Reuter, E. Kaxiras, R. M. Tromp, Phys. Rev. Lett. **63** (1989) 632.

2. R. Q. Hwang, J. Schröder, C. Günther, R. J. Behm, Ultramicroscopy **42-44** (1992) 475.

3. R. Q. Hwang, C. Günther, J. Schröder, S. Günther, E. Kopatzki, R. J. Behm, Journal of Vacuum Science and Technology **A 10** (1992) 1970.

4. J. Schroeder, C. Guenther, R. Q. Hwang, R. J. Behm, Ultramicroscopy (1992) submitted.

5. M. Scheffler, V. Fiorentini, S. Oppo, Surf. Sci. (1996) 219.

6. M. Kalff, G. Comsa, T. Michely, Phys. Rev. Lett. **81** (1998) 1255.

7. D. R. Peale, B. H. Cooper, J. Vac. Sci. Technol. A **10** (1992) 2210.

8. B. H. Cooper, D. R. Peale, J. G. McLean, R. Phillips, E. Chason, Mat. Res. Soc. Symp. Proc. **280** (1993) 37.

9. P. A. Thiel, J. W. Evans, J. Phys. Chem. **104** (2000) 1663.

10. L. Bardotti, M. C. Bartelt, C. J. Jenks, C. Stoldt, J.-M. Wen, C.-M. Zhang, P. A. Thiel, J. W. Evans, Langmuir **14** (1998) 1487.

11. L. Bardotti, C. R. Stoldt, C. J. Jenks, M. C. Bartelt, J. W. Evans, P. A. Thiel, Phys. Rev. B **57** (1998) 12544.

12. R. Stumpf, Phys. Rev. B **53** (1996) R4253.

13. G. L. Kellogg, Phys. Rev. Lett. **79** (1997) 4417.

14. G. L. Kellogg, Phys. Rev. B **55** (1997) 7206.

15. S. Horch, H. T. Lorensen, S. Elveg, E. Laegsgaard, I. Stensgaard, K. W. Jacobsen, J. K. Norskov, F. Besenbacher, Nature 398 (1999) 134.

16. J.-M. Wen, J. W. Evans, M. C. Bartelt, J. W. Burnett, P. A. Thiel, Phys. Rev. Lett. 76 (1996) 652.

17. A. R. Layson, P. A. Thiel, J. W. Evans, (2000) in preparation.

18. F. Buatier de Mongeot, A. Cupolillo, U. Valbusa, M. Rocca, Chem. Phys. Lett. 270 (1997) 345.

19. G. Costantini, F. Buatier de Mongeot, S. Rusponi, C. Boragno, U. Valbusa, L. Vattuone, A. Burghaus, L. Savio, M. Rocca, J. Chem. Phys. 112 (2000) 6840.

20. T. E. Madey, Science 234 (1985) 316.

21. T. E. Madey, Surf. Sci. 299/300 (1994) 824.

22. H. A. Engelhardt, D. Menzel, Surf. Sci. 57 (1976) 591.

23. F. Buatier de Mongeot, M. Rocca, A. Cupolillo, U. Valbusa, H. J. Kreuzer, S. H. Payne, J. Chem. Phys. 106 (1997) 711.

24. M. Rocca, L. Savio, L. Vattuone, U. Burghaus, V. Palomba, N. Novelli, F. Buatier de Mongeot, U. Valbusa, R. Gunnella, G. Comelli, A. Baraldi, S. Lizzit, G. Paolucci, Phys. Rev. B 61 (2000) 213.

25. L. Vattuone, P. Gambardella, A. Burghaus, F. Cemic, A. Cupolillo, U. Valbusa, M. Rocca, J. Chem. Phys. 109 (1998) 2490.

26. F. Besenbacher, J. K. Norskov, Progress in Surface Science 44 (1993) 5.

27. J. S. Ozcomert, W. W. Pai, N. C. Bartelt, J. E. Reutt-Robey, Phys. Rev. Lett. 72 (1994) 258.

28. W. W. Pai, J. E. Reutt-Robey, Phys. Rev. B 53 (1996) 15997.

Figure Captions

1. Initial correlation length, L_c, as a function of oxygen exposure, at two different temperatures as indicated. The circles show the result for simultaneous deposition and exposure, the squares for sequential deposition and exposure. At both temperatures, the two data points at zero exposure are indistinguishable because of overlap. The Ag coverage was 0.3 ML, and the oxygen pressure during exposures was in the range 1×10^{-8} to 1×10^{-7} Torr. L_c is given in unites of Å, and is converted from the diameter of the reciprocal-space halo in HRLEED. [10, 11] The solid lines are drawn only to guide the eye.

2. Evolution of the correlation length, L_c, as a function of time at 250 K for various oxygen exposures. In these experiments, Ag deposition and O_2 exposure took place simultaneously, and the data shown were acquired after these procedures ended. The curve labels are the values of oxygen exposure in Langmuirs.

3. Evolution of the correlation length, L_c, as a function of time at (a) 220 K, and (b) 250 K. In both panels, curve (i) shows the coarsening behavior without oxygen.
   In all other curves, 0.3 ML of Ag was deposited, followed by exposure of 4 L of O_2. In panel (a), the time elapsed between exposure and the start of the HRLEED measurement was (ii) 0, (iii) 20, and (iv) 32 minutes. In panel (b), the time elapsed was (ii) 0 and (iii) 10 minutes.

4. Rate of change of L_c as a function of O_2 exposure at 250 K. The circles represent the kinetics after simultaneous Ag deposition and O_2 exposure, the squares after sequential procedures. In all cases, 0.3 ML of Ag was deposited. The solid lines are drawn only to guide the eye.

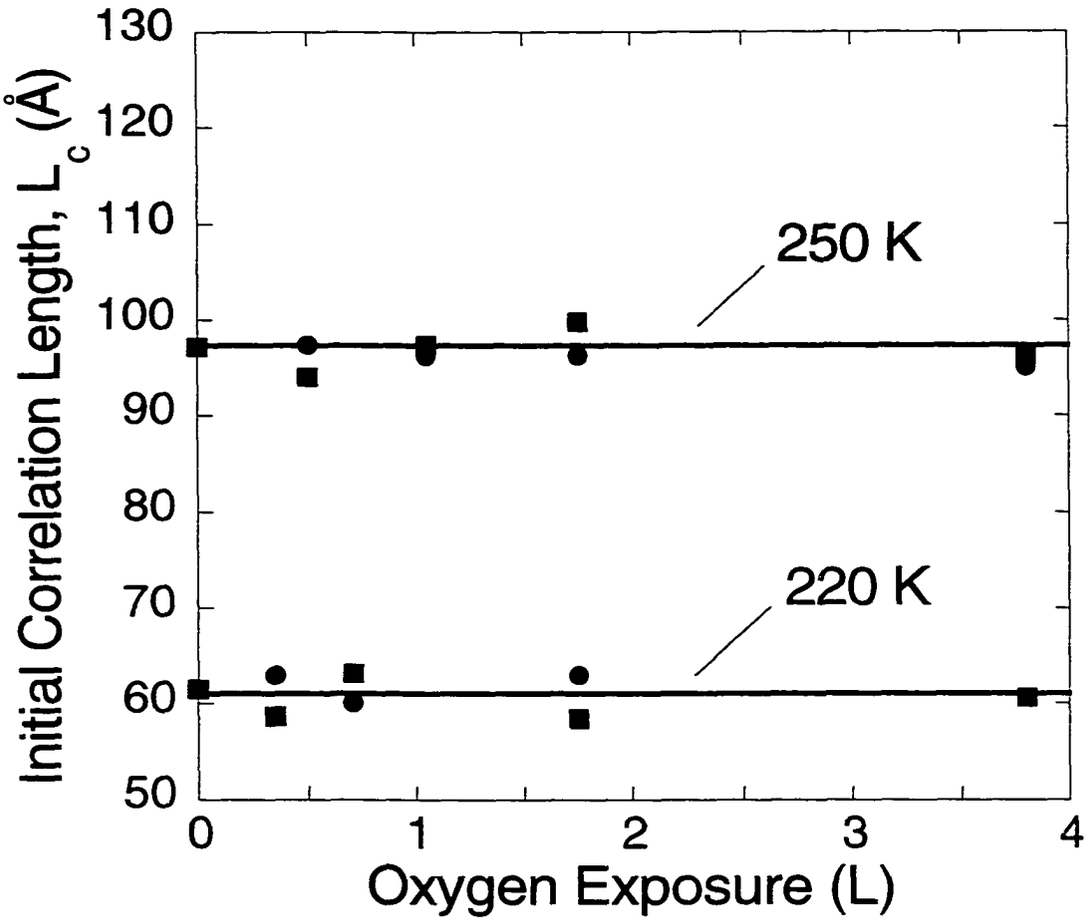
Initial Correlation Length, L_c (Å)
130
120
110
100
90
80
70
60
50
0
1
2
3
4
Oxygen Exposure (L)
250 K
220 K

Figure 1

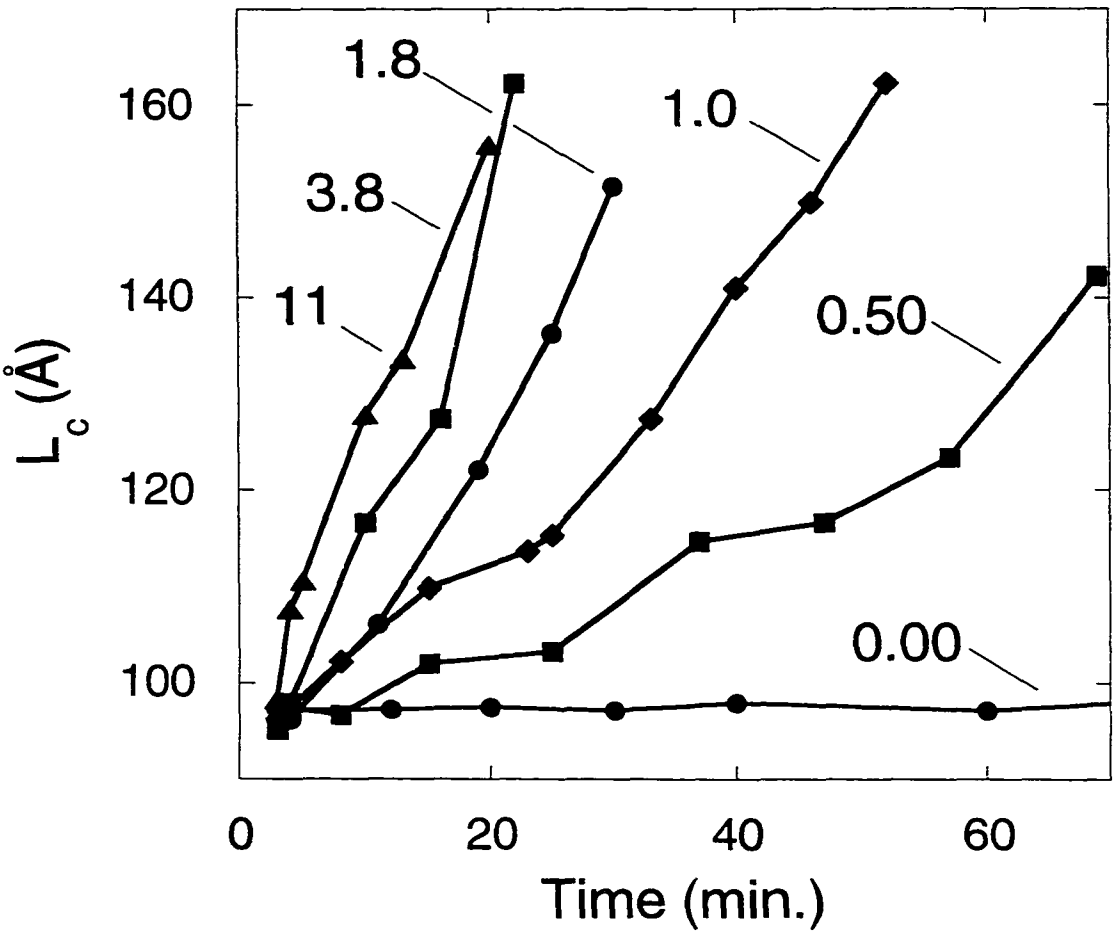

Figure 2

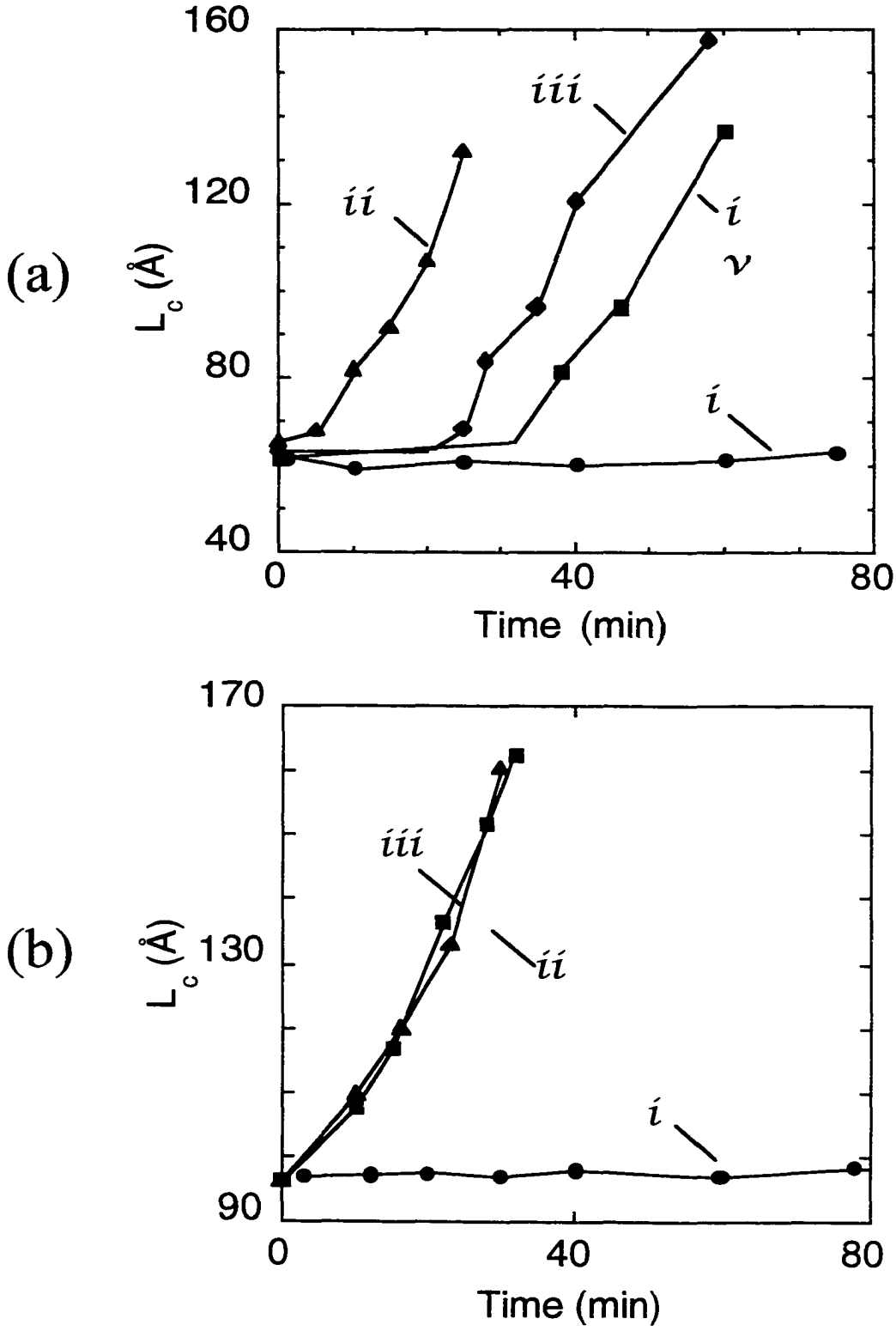
(a)
160
120
80
40
L_c (Å)
0
40
80
Time (min)
iii
ii
i
v
i
(b)
170
130
90
L_c (Å)
0
40
80
Time (min)
iii
ii
i

Figure 3

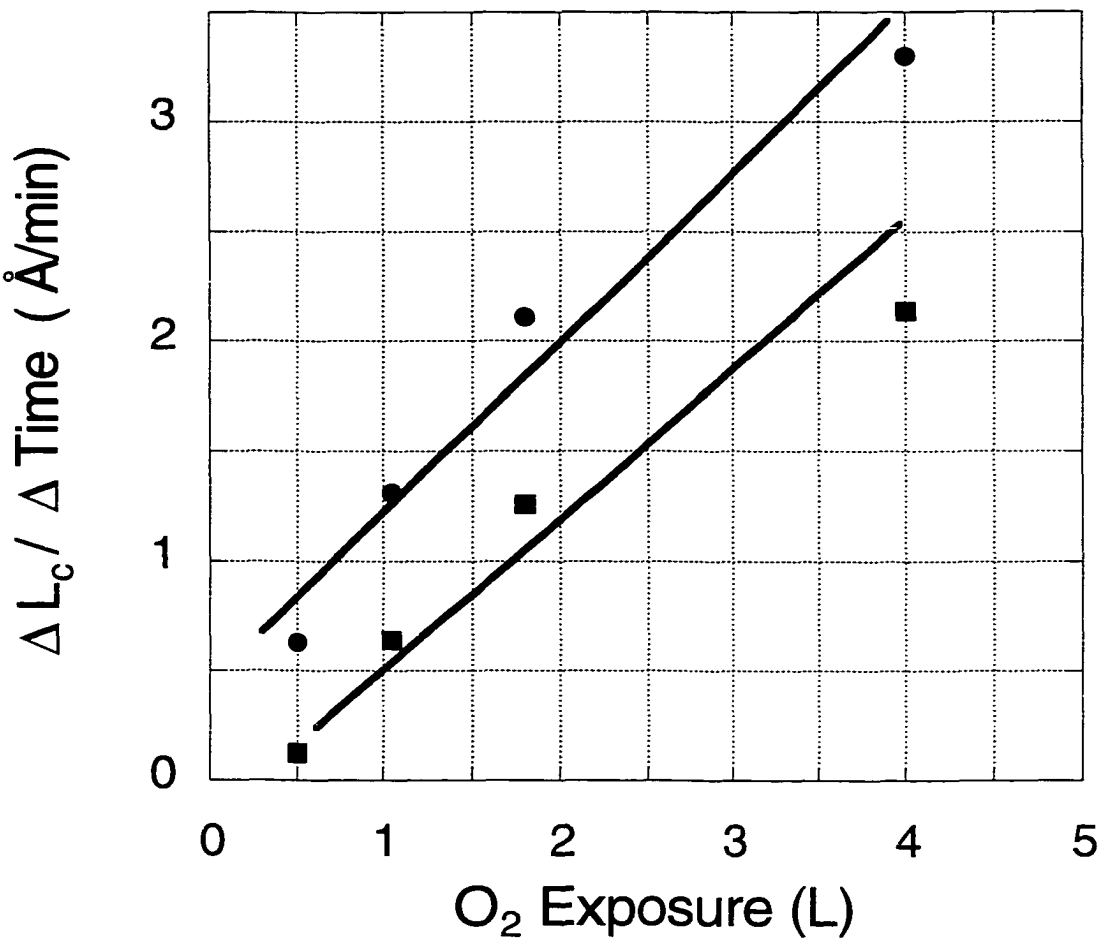

Figure 4

III. ADDITIVE-ENHANCED COARSENING AND SMOOTHENING OF METAL FILMS: COMPLEX MASS-FLOW DYNAMICS UNDERLYING NANOSTRUCTURE EVOLUTION

A paper submitted to PRL

A.R. Layson, J.W. Evans, and P.A. Thiel

PACS: 68.35.Fx, 68.35.Md, 68.43.-h

Abstract

Exposure of Ag/Ag(100) thin films to molecular oxygen (O_2) at 220-250K is shown to activate low-temperature coarsening of submonolayer island distributions, and smoothening of multilayer films with "mounded" morphologies. Dissociation of O_2 at kink sites populates step edges with atomic oxygen (O), modifying the step-edge energetics, and facilitating Ostwald ripening of film nanostructures, which we propose is mediated by "easy" detachment and terrace diffusion of an Ag_nO species. Cluster diffusion does not play a significant role, contrasting the O-free system.

The presence of even minute amounts of adsorbates or "additives" can have a significant effect on the formation and post-deposition relaxation of nanostructures in thin films. One example of considerable technological significance is the use of surfactants to control the growth mode in semiconductor heteroepitaxy, e.g., converting 3D Volmer-Weber

growth of Ge/Si to quasi-layer-by-layer growth [1]. Surfactants can also produce smoother interfaces in the fabrication of superlattice heterostructures (e.g., spin valves) in thin metal films [2]. Naturally, there have also been many theoretical proposals for detailed mechanism of surfactant action [3].

Numerous studies have explored fundamental aspects of adsorbate effects in the growth of homoepitaxial metal films. There has been much interest in the role of Sb in converting "mounding" to smooth growth in Ag/Ag(111) [4]. Hydrogen complexation [5], and interactions with surfactants [6], can modify terrace diffusion of isolated adatoms, and thus of submonolayer island densities. Decoration by CO of monoatomic steps in Pt/Pt(111) affects step-edge energetics and transport (which control 2D island shapes), as well as interlayer diffusion [7]. Studies of several systems show that halides alter step edge energetics, and that floating oxygen adlayers modify intra- and interlayer diffusion processes, which control growth [8].

Much less studied, but just as critical, is an assessment of the effect of adsorbates on the post-deposition stability and evolution of thin film nanostructures. This impacts the operation of nanostructure devices in non-pristine environments. Here, we just mention one notable study: exposure of rough Au/Au(111) films to air activates the decay of multilayer stacks of islands, which are quite stable in ultra-high vacuum [9]. We instead consider the oxygen + Ag system has considerable technological interest, e.g., in catalysis (epoxidation of ethylene). Earlier studies focussed on the highly reactive Ag(110) surface, which displays novel surface reconstructions involving alternating -Ag-O-Ag- strings [10]. In this Letter, we consider the relatively inactive oxygen+Ag(100) system [11,12], where controlled analysis of the effect of a weak adsorbate is possible. Indeed, we show that the presence of oxygen

activates relaxation of Ag/Ag(100) films at low temperatures. It actually changes the kinetic pathway for submonolayer coarsening, and furthermore facilitates a novel study of the low-temperature smoothening of mounded morphologies. We elucidate the complex mass-flow dynamics underlying this behavior.

As background, we review previous results for growth and relaxation of Ag/Ag(100) films without oxygen. Between 190K and 300K, compact 2D islands form irreversibly during deposition in the submonolayer regime mediated by terrace diffusion. Subsequently, multilayer stacks of islands or "mounds" develop due to the presence of a small additional barrier inhibiting downward transport [13]. For ~25ML films, mounds are most pronounced at ~230K. Post-deposition coarsening of θ=0.1-0.4ML films at 300K does not occur via the expected Ostwald ripening - OR (diffusive mass transfer from smaller to larger islands), but rather via Smoluchowski ripening - SR (diffusion and coalescence of large 2D islands) [14]. For Ag/Ag(100), SR with an effective barrier of $E_{SR}\approx 0.75$eV has an energetic advantage over OR with $E_{OR}\approx 0.9$eV [15], and thus should also dominate at lower temperatures (T). Some post-deposition smoothening of multilayer films occurs at 300K [16], but smoothening of mounded 25ML films is negligible below 260K (as shown below). All these relaxation processes are driven by the tendency to minimize the free energy associated with step edges.

Our experiments were performed in a UHV chamber with base pressure $<10^{-10}$ Torr. Evaporative deposition of Ag onto the Ag(100) single-crystal surface was usually performed at $\leq$250K. The surface was also exposed to molecular oxygen (O_2) by back-filling the chamber to ~10^{-8} Torr (typically after deposition of Ag). O_2 only chemisorbs below 180K, while dissociation of (transient) O_2 to more stable atomic oxygen (O) is thermally activated only at higher T, and is inefficient occurring only at kink sites along step edges [11].

However, this process effectively populates step edges in our deposited films with O above 210K. Nanostructure evolution is monitored with an Omicron variable-temperature scanning tunneling microscope (VTSTM).

First, we present our VTSTM analysis of coarsening of island distributions in 0.3ML Ag films on broad terraces of Ag(100) at 250K. Comparing Fig.1a and 1b reveals no significant evolution in the absence of oxygen. This might be expected since an effective barrier for SR of $E_{SR} \approx 0.75$eV [15] implies coarsening is slower by a factor of 330 than at 300K (where it occurs only over tens of minutes). However, dramatic evolution after exposure to oxygen is apparent comparing Fig.1a and 1c (and also Fig.s 1d,e,f). Detailed analysis reveals no significant island diffusion and coalescence, but rather dissolution of small islands, i.e., evolution is dominated by OR, not SR. Thus, exposure to oxygen not only activates coarsening at 250K, but it actually changes the dominant coarsening mechanism! A clear illustration of OR processes comes from following the evolution of several islands on a narrow terrace in Fig.2a-f: smaller islands dissolve, and larger ones (which are more isolated from the step edges) grow initially. Here, OR is somewhat enhanced by the presence of extended step edges, as is true in the clean system [16]. OR can be terrace-diffusion-limited (expected for clean metal systems) or interface-transfer-limited (due to an extra barrier for attachment at step edges, which is possible in the presence of adsorbates). The area, A, of dissolving islands decays linearly ($A \sim A_0 - kt$) for the former, and like $A \sim (t_0 - t)^{2/3}$ for the latter. Our experimental observations (not shown) for several islands consistently indicate the latter behavior.

A conventional analysis of OR considers the coarsening kinetics of island distributions on broad terraces. In Fig.3a, we show VTSTM data for the increase with time, t,

of the mean island separation, $L_{av}=1/\sqrt{N_{av}}$, where N_{av} is the mean island density. The rate of coarsening increases significantly with oxygen exposure, saturating at above 20 Langmuir (L). Perhaps surprising is the lack of apparent deceleration in the coarsening kinetics expected from the classic OR relation $L_{av} \sim L_0(1+t/\tau)^{1/3}$ [17]. However, this relation is predicated on the island size distribution having achieved its "selected" asymptotic long-time form. Although it is not viable to obtain precise statistics for this size distribution from VTSTM data, one can accurately determine lower moments such as the mean size, and the scaled width, σ (in units of the mean size – in atoms), or the variance, σ^2 [18]. We find that the initial size distributions created by the deposition process are much narrower than the predicted asymptotic forms for diffusion-limited OR properly accounting for spatial correlations in the island distribution [17]. This is an intrinsic feature of island nucleation and growth, but likely also reflects the rapid post-deposition disappearance of the smaller islands, which further narrows the distribution [18]. However, σ^2 increases with time, and after 2-3 hours achieves values roughly consistent with those from OR theory [17] (at least for 0.1-0.3ML where bigger islands enable more accurate size measurement). See Fig.3b. Thus, broadening of the narrow initial size distribution enhances the driving force for coarsening by OR. For the first few hours, this roughly counterbalances the natural deceleration in coarsening.

Submonolayer coarsening also occurs at lower T (down to 220K) after exposure to O_2. Our detailed STM analysis are consistent with LEED studies [12] which assessed only L_{av} vs. t.

Second, we examine the smoothening of 25ML Ag/Ag(100) films with mounded morphologies deposited at 250K and below. See Fig.4 for STM images of morphological

evolution. Monitoring the film roughness, W (RMS width of the film height distribution), versus time, t, reveals that smoothening at 250K is negligible without oxygen, but does become significant after exposure to oxygen, the rate increasing with exposure. See Fig.5a. The mechanism underlying smoothening is a multilayer version of OR, as seen in other metal homoepitaxial systems [19]. For fixed oxygen exposure of 17L, the smoothening rate drops quickly from 250K to 240K, then varies little down to 220K, before switching off at 210K. See Fig.5b. This does not correspond to simple Arrhenius dependence, e.g., for the activated detachment process underlying smoothening. Presumably, it also reflects the decrease in the lateral mound size, L_m (which accelerates decay –see below), and the possible increased amount of O on the surface (due to an increased kink density), as T decreases from 240K to 220K.

Again OR is expected to be terrace-diffusion-limited, and not significantly influenced by the small step edge barrier in this system. Indeed, this is consistent with our observations of non-linear decay of island areas in multilayer island stacks, analogous to submonolayer behavior. A thermodynamic formulation (based on line tension reduction for curved steps) as well as simulations of the smoothening of a bi-periodic array of mounds predicts roughly linear decay of the mound height over a characteristic time scaling like $(L_m)^3$ [20]. This theory may describe the initial stages of decay, particularly at 240K and below. Of course, we do not have a perfect bi-periodic array of mounds which produces non-linear decay [20]. Furthermore, W cannot vanish for non-integral ML films (for a half-integral ML films, $W \geq 0.5 \times$ interlayer spacing), as reflected in the 250K data. In general, precise description of the evolution of "smaller" far-from-equilibrium nanostructures must be based on system-specific kinetic rather than thermodynamic considerations. One can draw upon studies of the

decay of individual islands and island stacks, from which we find an additional enhancement in decay in lower layers (for a given island size).

Next, we discuss the key atomistic mechanism underlying evolution. We propose that this involves the detachment of an Ag_nO species from step edges, and present supporting evidence. Recall that the effective activation barrier for OR has the form $E_{OR}=E_d+\delta E$, where E_d is the diffusion barrier, and δE is the energy difference between the (typical) attached and detached configurations of the diffusing species.

(i) If OR were mediated by terrace-diffusion of Ag adatoms, then coarsening would be no faster than in the O-free system (E_d and δE would be unchanged from the O-free system). It is quite possible that O at the step edge could increase the microscopic detachment rate for Ag, but the reverse attachment rate would also be increased (according to detailed balance). The effective detachment rate would be unchanged from the O-free system, consistent with unchanged E_{OR}.

(ii) Since coarsening is actually enhanced by the presence of O, we conclude that OR must occur via transfer of a species containing both Ag and O (likely Ag_nO with n=1 or 2), rather than just Ag. The effective detachment barrier for Ag_nO must be lower than for Ag due to a lower δE (consistent with strong Ag-O bonding lowering the energy of the detached species), or lower E_d. We note that mobile -M-O- units are believed to mediate formation of domains of oxygen-induced reconstructions on M(110) surfaces, where M=Ag, Cu, and Ni [21].

(iii) The proposed role of Ag_nO in coarsening is consistent with the strong dependence of coarsening rate on O_2-exposure: the process is limited by the amount of O at the step edge.

(iv) For low O_2-exposure, it is conceivable that a small island could be depleted of O before completely dissolving, thus inhibiting further evolution. There is no clear evidence of this

effect, so we argue that O can also detach from step edges, and diffuse across terraces and steps to repopulate depleted islands (see below).

Finally, we present some observations from additional experiments tailored to further elucidate behavior in this system, and to explore the above proposals. The first explores changes in step edge energetics due to preferential attachment of O, changes which would be compatible with the presence of a readily detaching Ag_nO species. One could imagine a lowering of the energy of open or kinked [100] oriented step edges (where O is more likely to be attached), relative to the energy of close-packed [110] orientations. Indeed, in observations of large islands coarsened over very long times (>40 hrs), one does see a change in shape from the near-square configuration with primarily [110] step edges (familiar in the O-free system), to a more rounded or even diamond-shaped "equilibrium" configuration with a preference for [100] orientations. See Fig.1d-f. Extended step edges bounding broad terraces also take on a different structure from the O-free system (analogous to the observed effect of halides and oxygen in other systems [8]).

Second, we determine the effect on film growth of pre-dosing with oxygen. Suppose that only step edge detachment of Ag (and not of O or Ag_nO) is active. Then, pre-dosing an Ag(100) surface to populate extended step edges with O should have no significant impact on subsequent film growth: the density of detaching Ag adatoms would be overwhelmed by the supersaturation density of depositing Ag adatoms. In fact, we find that pre-dosing with 20L O_2 reduces the island density of 0.3ML of Ag/Ag(100) films deposited at 250K by a factor of ~20 relative to the O-free system. The large flux scaling exponent of ~0.9 is inconsistent with irreversible island formation seen in the O-free system [16]. Thus O or an O-containing species must be detaching from step edges, and either interacting with depositing Ag to form

a more mobile species, or attaching to small Ag-islands and destabilizing and/or mobilizing them.

In summary, exposure to oxygen of Ag films on the unreactive Ag(100) surface activates coarsening and smoothening processes at low temperature. Atomic oxygen decorating step edges allows for more complex mass flow dynamics: an Ag_nO species is created which can more readily detach from step edges than Ag, facilitating transport Ag metal adatoms. This work was supported by NSF Grant CHE-0078596, and performed at Ames Laboratory, which is operated for the USDOE by Iowa State University under Contract No. W-7405-Eng-82.

References

1. M. Copel *et al.*, Phys. Rev. Lett. **63**, 632 (1989); D.J. Eaglesham *et al.*, *ibid*, **70**, 966 (1993); I.-S. Hwang *et al.*, *ibid*, **80**, 4229 (1998).
2. W.F. Egelhoff *et al.*, J. Appl. Phys. **79**, 2491 (1996) and ref.s therein.
3. B.-G. Liu *et al.*, Phys. Rev. Lett. **83**, 1195 (1999) and ref.s therein.
4. J. Vrijmoeth *et al.*, Phys. Rev. Lett. **72**, 3843 (1994); V. Fiorentini *et al.*, J. Appl. Phys. A **60**, 399 (1995).
5. G.L. Kellogg, Phys. Rev. Lett. **79**, 4417 (1997); Phys. Rev. B **55**, 7206 (1997).
6. S. Liu, L. Bonig, and H. Metiu, Phys. Rev. Lett. **74**, 4495 (1995).
7. M. Kalff, G. Comsa, and T. Michely, Phys. Rev. Lett. **81**, 1255 (1998).
8. E. Kopatzki *et al*, Surf. Sci. **284**, 154 (1993); S. Esch *et al.* Phys. Rev. Lett. **72**, 518 (1994); E.R. Frank and R.J. Hamers, J. Catal. **172**, 406 (1997); A. Steltenpohl and N. Memmel, Phys. Rev. Lett. **84**, 1728 (2000).

9. B.H. Cooper *et al.*, MRS Proc. 280, 37 (1993).

10. J.S. Ozcomert *et al.*, Phys. Rev. Lett. 72, 258 (1994).

11. F. Buatier de Mongeot et al., Chem. Phys. Lett. 270, 345 (1997); G. Constantini *et al.*, J. Chem. Phys. 112, 6840 (2000).

12. A.R. Layson and P.A. Thiel, Surf. Sci. Lett., in press (2001).

13. C.R. Stoldt *et al.*, Phys. Rev. Lett. 85, 800 (2000); K.J. Caspersen *et al.*, Phys. Rev. B, 63, 085401 (2001).

14. J.-M. Wen *et al.*, Phys. Rev. Lett. 76, 652 (1996); W.-W. Pai *et al.*, *ibid*, 79, 3210 (1997).

15. For Ag/Ag(100), the diffusion barrier is $E_d \approx 0.4$eV across terraces, $E_e \approx 0.25$eV along [110] steps, and $E_r = E_e + E_{kse}$ around kinks. Since $E_{kse} < J$ (adatom pair interaction)≈ 0.26eV, so $E_{OR} = E_d + 2J$ exceeds $E_{SR} = E_r + J < E_e + 2J$.

16. P.A. Thiel and J.W. Evans, J. Phys. Chem. B 104, 1663 (2000).

17. A.J. Ardell, Phys. Rev. B 41, 2554 (1990); T.M. Rogers and R.C. Desai, *ibid*, 39, 11956 (1989).

18. C.R. Stoldt *et al.*, J. Chem. Phys. 111, 5157 (1999); the density of islands of s atoms satisfies $N_s \sim \theta(s_{av})^{-2} f(s/s_{av},t)$, where $s_{av}(t) = \theta/N_{av}(t)$ is the mean size, $\int_0^\infty dx\, f(x,t) = \int_0^\infty dx\, xf(x,t) = 1$, and $\int_0^\infty dx(x-1)^2 f(x,t) = \sigma^2$.

19. M. Giesen and H. Ibach, Surf. Sci. 431, 109 (1999); M.S. Hoogeman *et al.*, J. Phys. Cond. Matt. 11, 4349 (1999); K. Morgenstern *et al.*, Phys. Rev. Lett. 80, 556 (1998).

20. A. Rettori and J. Villain, J. Physique 49, 257 (1988); M.V. Ramana Murty, Phys. Rev. B 62, 17004 (2000).

21. M. Kiskinova, Chem. Rev. 96, 1431 (1996).

Figure Captions

1. Evolution of 0.3ML Ag/Ag(100) films at 250K: (a) just after deposition without O; (b) after 160 min. without O; (c) after 167 min. with 20L O_2. Evolution of 0.3ML films deposited at 300K, exposed to 20L O_2, then cooled to 250K after: (d) 44 min.; (e) 8 hrs; (f) 44 hrs. Image sizes are 100x100 nm^2.
2. (a)-(f) Evolution over about 15 min. of Ag islands on a narrow terrace at 250K after exposure to 20L O_2. Image sizes are 35x35 nm^2.
3. (a) Change in L_{av}, versus time, t, for 0.3ML Ag/Ag(100) films at 250K with various oxygen exposures (shown). (b) Evolution of the scaled variance of the size distribution, σ^2, versus t for Ag/Ag(100) films with various coverages (shown) at 250K with 12-17L O_2. Asymptotic ($t\rightarrow\infty$) theoretical OR values are σ^2 =0.273, 0.243, 0.224, for θ=0.3, 0.1, 0.05ML, respectively (shown), decreasing to 0.119, as $\theta\rightarrow 0$.
4. Smoothening of 25ML Ag/Ag(100) films at: (a) 250K, (b) 230K, after exposure to 17L O_2. STM images are 154×154 nm^2.
5. Smoothening of 25ML Ag/Ag(100) films. (a) Decay of the roughness, W (in units of interlayer spacing) at 250K with various oxygen exposures (shown). (b) Temperature dependence of W-decay for fixed oxygen exposure of 17 L.

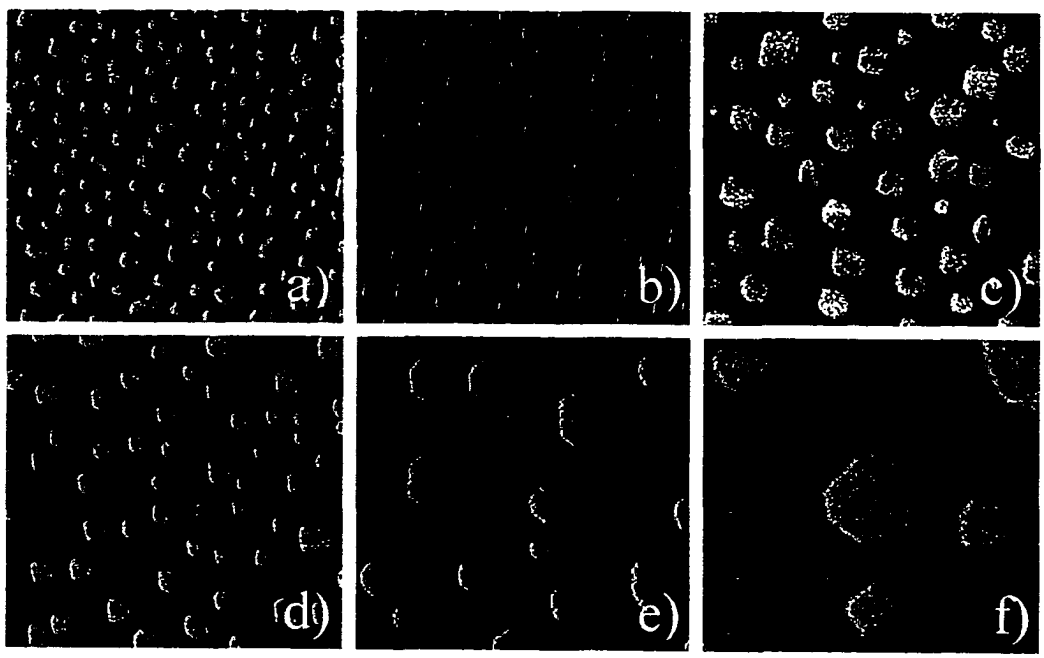

Figure 1

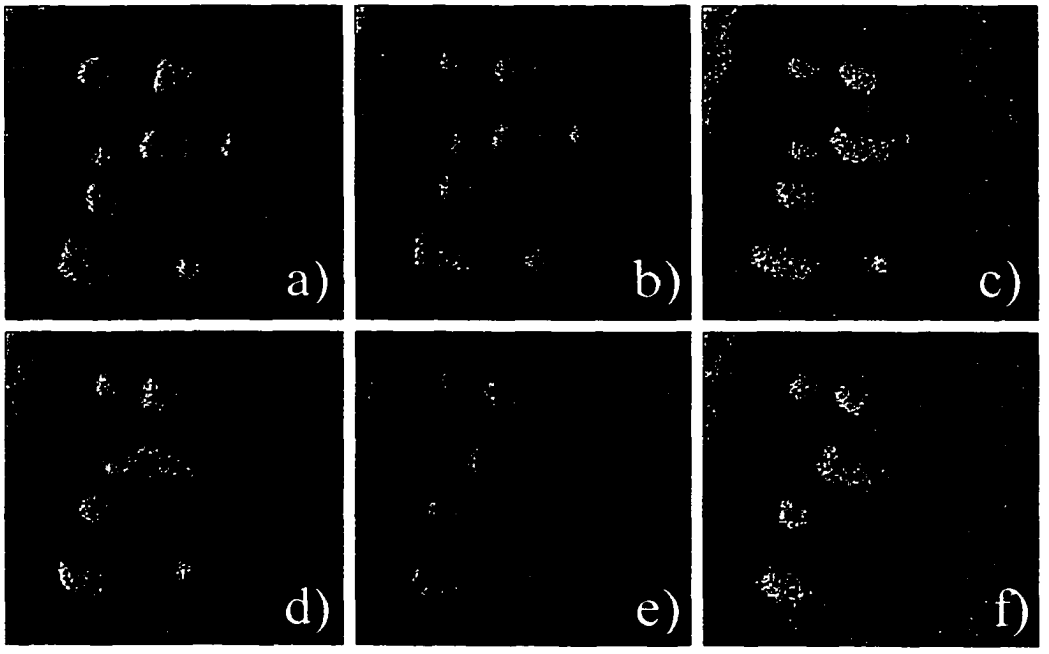

Figure 2

(a)

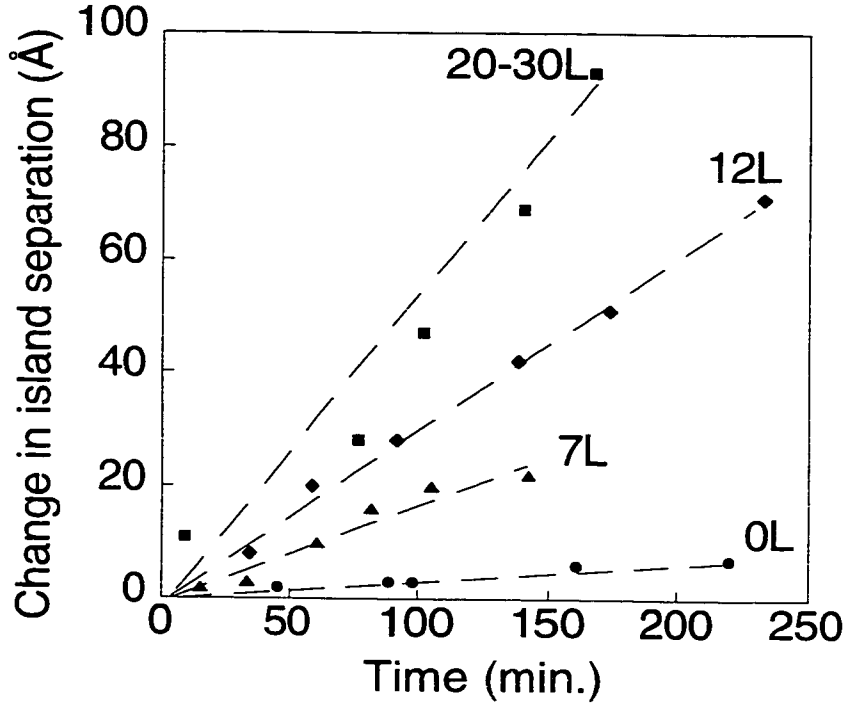
Change in island separation (Å)
100
80
60
40
20
0
0
50
100
150
200
250
Time (min.)
20-30L
12L
7L
0L

(b)

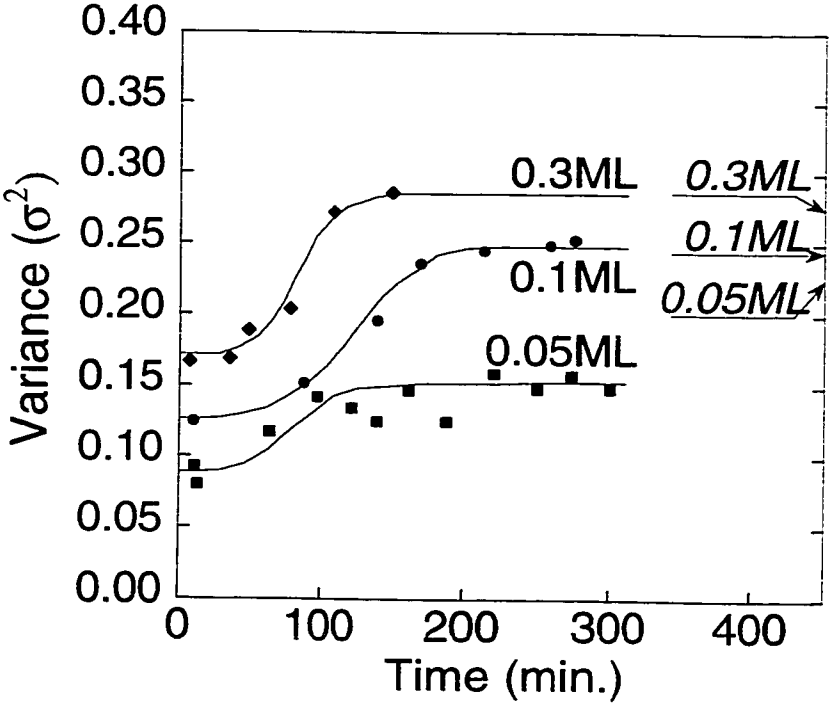
Variance (σ^2)
0.40
0.35
0.30
0.25
0.20
0.15
0.10
0.05
0.00
0
100
200
300
400
Time (min.)
0.3ML
0.1ML
0.05ML
0.3ML
0.1ML
0.05ML

Figure 3

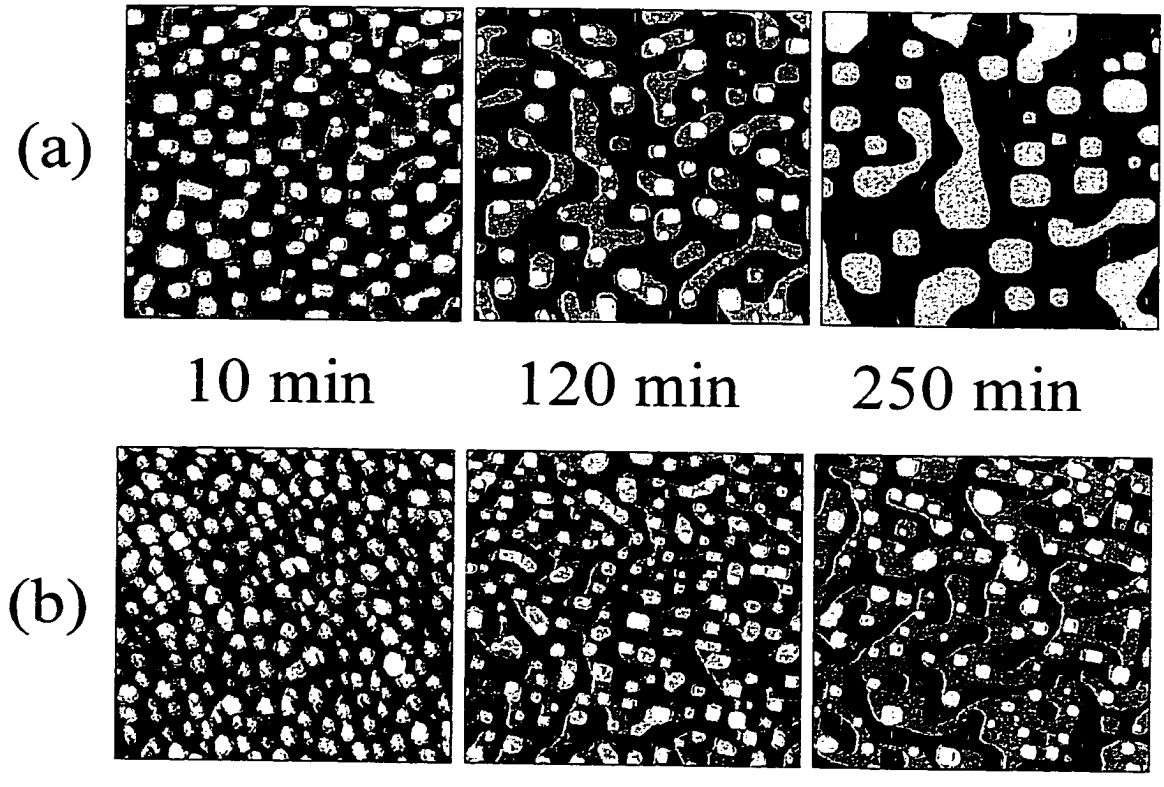

Figure 4

(a)

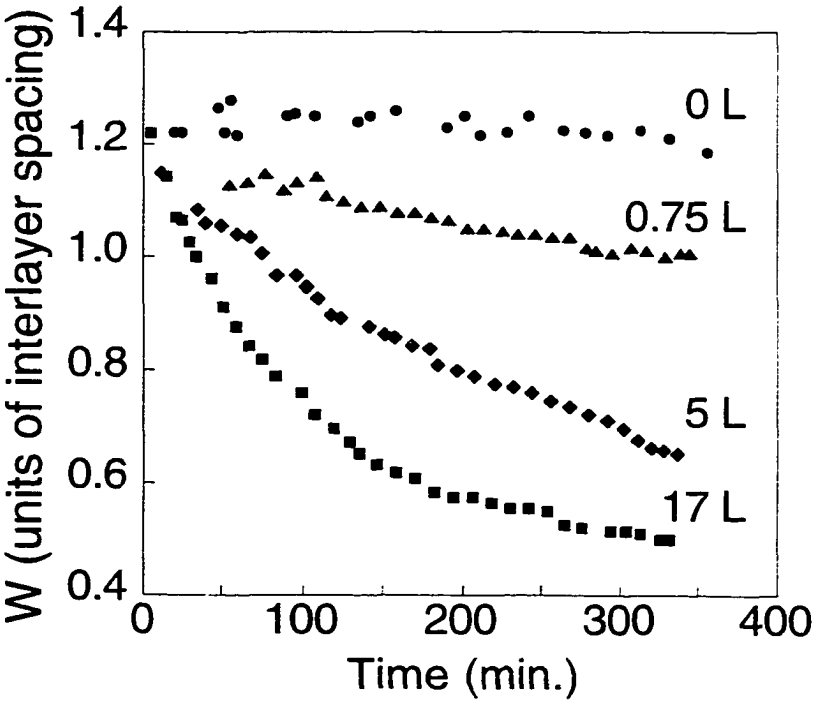
W (units of interlayer spacing)
1.4
1.2
1.0
0.8
0.6
0.4
0
100
200
300
400
Time (min.)
0 L
0.75 L
5 L
17 L

(b)

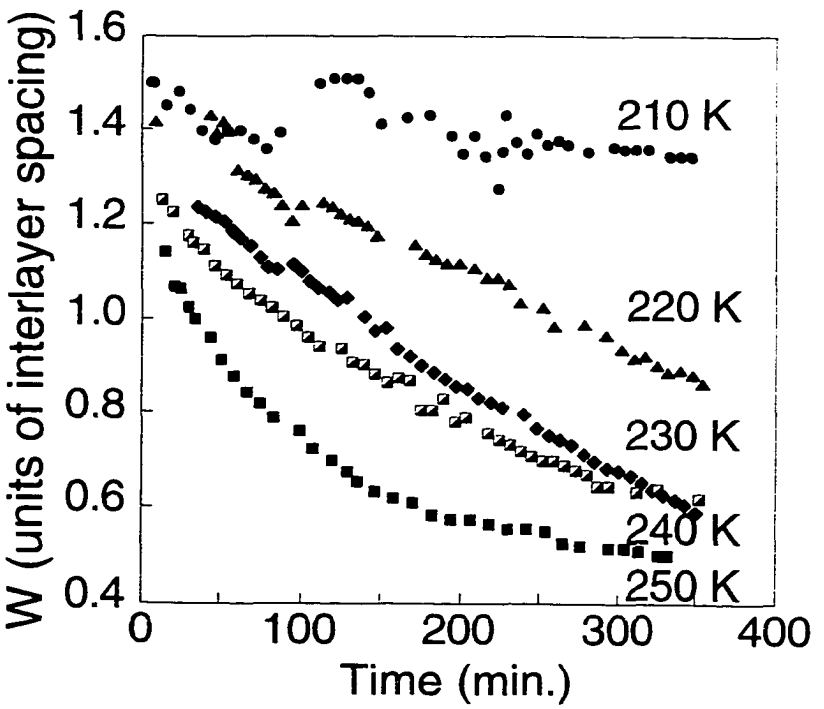
W (units of interlayer spacing)
1.6
1.4
1.2
1.0
0.8
0.6
0.4
0
100
200
300
400
Time (min.)
210 K
220 K
230 K
240 K
250 K

Figure 5

IV. USE OF ADSORBATES TO MANIPULATE NANOSTRUCTURE FORMATION: O+Ag/Ag(100)

A paper submitted to Surface Science

A.R. Layson, J.W. Evans and P.A. Thiel

ABSTRACT

We examine the effects on the initial nucleation and growth of Ag islands on an oxygen pre-exposed Ag(100) surface at 250 K. The presence of O-atoms on the surface prior to Ag deposition results in a decrease in the initial density of surface islands. An increase in the flux scaling exponent, from 0.28 for the O-free surface to 0.9 for the pre-exposed surface, is observed which indicates an increase in the critical size for island nucleation. Multi-deposition experiments provide evidence that supports the possibility that mobile O and AgO diffuse across terraces and interfere in the nucleation of depositing Ag atoms. O may also affect nucleation by destabilizing small Ag clusters and/or makes these clusters mobile.

---

1. Introduction

The ability to control the growth of metal thin films and surface structures continues to be of considerable interest. The use of Sb in the growth of Ag/Ag(111) is one of numerous examples in the use of foreign metal atoms as a surfactant to induce smooth layer-

by-layer growth in homoepitaxy [1-5]. The use of gases as surfactants has also been studied in both homo and heteroepitaxy. For example the use of fluorine on Fe/Cu(100) [6] and oxygen (O_2) on Cu/Ru(0001) [7] both improve smooth film formation in their respective heteroepitaxial systems. The use of O_2 as a surfactant in homoepitaxy has been studied in metal systems including Pt(111) [8] and Cu(100) [9]. Surfactants are only one example in the use of foreign atoms in metal film growth. It's long been known that contamination from residual gas can affect the morphology of films grown from vapor deposition[10]. Recently, the study of adsorbates has attracted some interest in their effects on nanostructure growth and equilibration. It has been shown that the presence of CO affects the size, shape and density of islands during the deposition of Pt/Pt(111) [11]. Ni deposition on an O_2 pre-covered Ni(100) surface results in the rotation and elongation of Ni islands[12]. O_2 has also been shown to affect the post deposition relaxation of Ag islands on Ag(100) [13]. As trends in technology advance to ever-smaller scales, the production and control of nanoscale structures becomes increasingly more important. Contamination, such as adsorbate gas, can never be entirely eliminated, even in the cleanest environments.

Due to this circumstance, much the same way surfactants are used in the growth of smooth films, it may be possible to use adsorbates in the creation of nanostructures. In this paper we show that exposing Ag(100) to O_2 prior to Ag deposition changes the initial nucleation and growth of Ag islands. As a result, the regulated use of oxygen allows a means to control the initial size and density of nanostructures during deposition from the vapor phase. We also examine the underlying processes by which oxygen interacts with depositing Ag atoms.

2. Experimental Details

Our experiments were performed in a UHV chamber with base pressure $<10^{-10}$ Torr. The sample was cleaned by repeated cycles of Ar^+ sputtering (20min, 500 V, T ≈ 300 K) followed by annealing at 700 K. Oxygen treatments (500L, 700 K) were performed periodically and were useful in removing the last bit of remaining contamination from the surface. No residual oxygen was found to exist as a result of these treatments. This was confirmed through the reproduction of known experimental results on the oxygen-free surface. Evaporative deposition of Ag onto the Ag(100) single-crystal surface was usually performed at ≤250K. The surface was exposed to oxygen (O_2) by back-filling the chamber to $\sim 10^{-8}$ Torr in continuous flow. All exposures were conducted at the same temperature as Ag deposition. The temperature of the sample is within +/- 5K of reported values. Temperature variations were minimal with fluctuations of no more than +/- 1 K throughout the duration of the experiment. Nanostructure evolution is monitored with an Omicron variable-temperature scanning tunneling microscope (VTSTM).

3. Background on O + Ag/Ag(100)

The Ag(100) surface is quite unreactive to O_2 adsorption with a sticking probability of 10^{-4} at 300 K [14]. It has been shown that O_2 will dissociatively adsorb at specific step sites identified as kinks[15-17]. Upon dissociation, O-atoms are quite stable on the (100) surface and do not recombine and molecularly desorb [15].

Previous experiments examining the effects of O_2 on the nucleation and growth of Ag/Ag(100) were conducted by exposing the samples to O_2 in one of two ways. The first

was to expose the surface after the deposition (post-deposition) of Ag to see how O would affect preexisting surface structures (ie. submonolayer islands) and observe any changes in post-deposition events as compared to the O-free surface. The second was to expose O_2 simultaneously with the deposition of Ag. This was done to see if the presence of O during the deposition process had any effect on Ag island nucleation and the initial stages of growth.

HRLEED results for the post-deposition studies showed that the rate of submonolayer-island coarsening increased with O_2 exposure [13]. More dramatic results were revealed by STM which showed that the coarsening mechanism for Ag/Ag(100) changed from Smoluchowski ripening - SR (diffusion and coalescence of large 2D islands) on the O-free surface, to Oswald ripening- OR (diffusive mass transfer from smaller to larger islands) in the presence of O[18] . It is speculated that a Ag_nO species (heretofore AgO where n=1,2), rather than atomic Ag, is the diffusing species in island coarsening [18].

It was shown that O_2 dissociation was slightly higher in experiments where the O_2 exposure and Ag deposition were simultaneous, as compared to exposures that were performed after Ag deposition. The simultaneous exposure results in an increased O density, which in turn further increases the rate of island coarsening [13,18]. However, the presence of O_2 during deposition had *no effect* on the initial nucleation and growth of submonolayer Ag islands.

The lack of any change in surface structure during the initial growth stage in the presence of O_2 is not surprising for several reasons. First, the previously mentioned low reactivity of O_2 on Ag(100) limits the amount of O-atoms that are on the surface. The time for Ag deposition (~0.2 ML) is on the order of a few tens of seconds. It is probable that the deposition time is too short for the O density to increase to a point where it can have any

significant effect on the initial island growth. Second, due to the short deposition time, it is reasonable to suspect that the supersaturation density of depositing Ag adatoms would overwhelm the much smaller density of O-atoms, diminishing the possibility for change during the deposition process.

Any effect O may have on island nucleation and growth of Ag islands appears to be limited by the time for Ag deposition. This suggests that if conditions were altered to so that (i) the time scale for Ag-O interactions during Ag deposition are long enough and/or (ii) the density of O-atoms is allowed to become large enough, O could affect the initial stages of growth.

4. Results and discussion

4.1 Submonolayer Deposition Studies

To test the above hypothesis an experiment was performed where the Ag surface is pre-exposed to O_2. By exposing the surface prior to Ag deposition, the O density can be adjusted simply by changing the exposure time. A pre-existing density of O on the surface also increases the Ag-O interaction time by eliminating the O_2 dissociation step during Ag deposition.

Fig. 1 shows a series of images where a clean Ag(100) surface was exposed to various amounts of O_2 prior to the deposition of 0.2 ML Ag. The images show that the presence of O prior to Ag deposition affects the nucleation and growth of Ag islands. Increasing the O preexposure results in a decrease in island density (or the complimentary increase in island size).

The above results strongly suggest that O or O-containing AgO, is mobile on the terrace. It is possible that O-adatoms and AgO particles diffusing on the surface interact with depositing Ag-atoms which impedes island nucleation. An equally strong possibility is that the addition of O or AgO to small island clusters may destabilize and/or make these clusters mobile. Recent calculations on Cu(111) support this possibility through the enhanced diffusion of Cu trimers decorated with sulfur atoms[19].

The decrease in island density due to the presence of O is significant because it shows that the presence of small amounts of an adsorbate species can dramatically affect the initial growth process. On the O-free surface, manipulation of the size and density of islands during the nucleation process was controlled through the sample temperature and the deposition flux of Ag atoms. Alternately, pre-treating the Ag surface with O_2 prior to Ag deposition may also give a means to control the initial island size and density. By pre-exposing the surface, O_2 dissociation no longer has to compete on the same time scale as Ag deposition. O_2 dissociating at terrace kink sites, can populate the surface with O-atoms which then in turn can interact with Ag atoms during the deposition process.

4.2 Comparisons with O-free Ag/Ag(100)

Comparisons in the nucleation and growth of 2D islands in the presence of oxygen can be made against the clean Ag/Ag(100) system. The study of nucleation and growth of Ag/Ag(100) has been extensively studied. For detailed analysis the reader is referred to [20,21]. In the clean Ag(100) system island growth is described in terms of a critical size, i, above which islands are stable against dissociation. Mean field rate equations predict the following:

$$N_{av} \approx (R/\nu)^{\chi} \exp[E/(k_B T)] \text{ , where } \chi = i / i+2 \text{ and } E \approx \chi (E_d + E_i / i) \qquad (1)$$

Where N_{av} is the average island density, R is the deposition flux, E_d is the activation barrier for adatom diffusion and ν is the attempt frequency. For clean Ag/Ag(100) island nucleation is irreversible up to room temperature. The critical size (i = 1) results in an exponent χ of 1/3. If small clusters, such as dimers, where mobile on the surface in the time scale of the deposition process, the value of χ would increase to around 0.4 [20,21]..

Fig. 2 shows the flux-dependence of the average island density at 250K for (a) O-free and (b) 30L O_2 preexposure, as determined by STM. Data for Fig. 2 are summarized in Table I. The value of 0.275 for the O-free surface is consistent with prior results [21]. For the O-exposed surface, however, there is a noticeably large increase in the flux exponent, to about 0.9. It is possible that the large increase in the flux exponent reflects an increase in the critical size. The increase could support the claims for O-induced mobility of small clusters and/or the destabilization of small clusters by O or AgO, which results in the apparent transition to reversible-island formation.

The temperature dependence of the nucleation and growth process can also be observed with STM. Fig. 3 shows an Arrhenius plot for the average island density. Data for Fig. 3 is summarized in Table II. Curve (a) in Fig. 3 corresponds to the data collected previously on O-free surface [22]. The values for the data were adjusted to compensate for differences in deposition flux between the O-free and O-preexposed experiments. Curve (b) in Fig. 3 corresponds to a surface exposed to 30L of O_2 prior to the deposition of 0.2ML of Ag, for each temperature. In the temperature range of 300-220K the Arrhenius slope of E ≈

0.104 eV is found. This value is similar to the result (E = 0.13eV) on the O-free surface for temperatures between 300-200 K. At about 210 K there is a transition region where the island density rapidly increases to about 180 K. Below this temperature, island densities values approach those of the O-free results. Dissociation of molecular oxygen is not active below 180 K, which explains the similar island densities on the O-free and O pre-exposed surfaces at these low temperatures. It seems possible then that the presence of oxygen or AgO may indeed destabilize small Ag clusters or at least inhibit island formation resulting in the lower island densities at higher temperatures. These processes begin to slow down around 210 K and then become inactive below 180K.

The above results show that when O is introduced on the surface, the atomic interactions become more complex. Therefore, it is appropriate to adjust the theory in equation (1) to reflect the presence of O. The simplest approach is to assume that in the beginning stages of Ag deposition, O is sufficiently mobile to immediately attach to deposited Ag. The predominant diffusing species will therefore become AgO, with hop rate h', as compared to hop rate h on O-free surface. The AgO makes weakly bonded (unstable) small islands, so there is a large critical size i to nucleate stable islands. The energy barrier for adatom diffusion (E_d) now becomes E_d', the barrier for diffusion of AgO. There will also be a small binding energy (E_b) for the critical (AgO)i cluster. The equation, adjusted for the presence of O thus becomes:

$$E \approx \chi (E_d' + E_b / i) \qquad (2)$$

Substituting in the flux exponent value of 0.9, and the Arrhenius slope of

0.104 eV, it is found that Ed' < 0.12 eV. This compares to the value E_d = 0.4 eV on the O-free surface. The barrier for for AgO diffusion is markedly lower than for Ag on Ag(100). This picture is probably a bit too simplistic. It is possible that some deposited Ag (diffusing at rate h) could form islands which are later destabilized by O. It becomes more difficult to develop appropriate treatments for such cases.

4.3 Multilayer Deposition Studies

Fig. 4 shows the results from a multi-deposition experiment, where the final surface films are created through two distinct Ag deposition steps. Fig. 4a is a clean Ag(100) surface after deposition of ~0.2 ML of Ag at 300 K, which results in large islands homogeneous in shape and size. An O-free experiment (Fig. 4b) was performed as a basis for comparison. In the O-free example the sample is cooled to 250 K prior to the second deposition of Ag (~0.2 ML) which increases the nucleation density of secondary islands. The flux for the second deposition was also increased (see Fig. 4) to further enhance the nucleation density. Fig. 4b shows the nucleation of small islands on the terrace regions between as well as on top of the previously created large islands. This type of surface structure is expected and is similar to other double-deposition type experiments, free from adsorbate interactions [23]. Fig.4c shows a surface which was exposed to 30 L of O_2 prior to the second deposition of ~0.2 ML of Ag at 250 K. No additional island nucleation occurs on the O-exposed surface. With O present prior to the second Ag deposition, all Ag atoms appear to have diffused to preexisting islands or steps. There is also a noticeable lack of island nucleation on top of preexisting

islands. Interestingly, these observations are exactly the opposite to those found for similar experiments for oxygen on Pt(111) [8].

The lack of island nucleation on the large islands shows that O must populate the top of these islands, and provides further evidence for the mobility of O-atoms on the Ag terraces. The tops of the initially formed large islands can be thought of as individual terraces. If O were not able to populate these terraces, the island surface would appear no different to incident Ag atoms than the O-free surface. The result would be the nucleation of small islands on top of the larger ones, regardless of the presence of O. The absence of small islands indicates that O must be present on the large island surface. There are several ways in which this may happen. O could populate the island terrace as a result of O_2 dissociation. HREELS data showed that oxygen molecules are able to adsorb in kink sites in an end-down arrangement [24]. It may be possible that as O_2 dissociates, one of the O-atoms hops up and populates the island or terrace. A more probable explanation is that mobile O-atoms are simply able to ascend/descend Ag steps. In this way the large islands are continuously being populated with O which can then interact with depositing Ag atoms.

An alternative interpretation of the multilayer data could be made where O-atoms are not able to ascend or cross surface steps, however when present at a step, could lower the Ehrlich-Schwoebel (ES) barrier for Ag interlayer diffusion. On clean Ag(100), due to the ES barrier, Ag atoms approaching a step are reflected back on the terrace where they can collide with another Ag atom to nucleate an island. A decrease in the ES barrier could inhibit the nucleation of second layer islands by allowing diffusing atoms to hop over a step before they can nucleate new islands. While the presence of O at the step may indeed affect the ES barrier, it does not fully account for the observations of this experiment. The order of

magnitude increase in the deposition flux, as well as the lower temperature for the second deposition result in islands with a very small separation distance (on the O-free surface). Even if the ES barrier is lowered, the deposition conditions are such that second layer nucleation would still be expected on the O_2 preexposed surface. For this reason it is reasonable to suspect that mobile O-atoms, which are able to ascend/descend steps, are responsible for the observed changes in island nucleation.

A final interesting result was obtained in the deposition of 25 ML of Ag, while simultaneously exposing the surface to O_2 during the deposition process at 260 K. The deposition and exposure time was approximately 10 minutes. In contrast to the submonolayer experiments where simultaneous Ag deposition and O_2 exposure resulted in no significant change in the initial island density (see section 3), the multilayer films exhibited a measurable decrease in the initial surface roughness when the films were deposited in the presence of O_2. While seeming to contradict former results, the observations validate the suggestions posed at the end of section 3. The increased deposition time for the multilayer films made it possible to increase the O-atom density during the deposition process. The longer deposition time also increased the time for O to interact with the Ag. The increase in the number of O-atoms as well as the increase in interaction time results in smoother initial surface films.

5. Conclusion

In summary, preexposing Ag(100) with O_2 changes the nucleation and growth of Ag islands deposited at 250 K. It was demonstrated that the O_2 preexposure can be used as a

means to control the initial size and density of the resultant nanostructures during the deposition of Ag. VTSTM data shows that the initial island nucleation is impeded by the presence of mobile O-atoms and possibly AgO, which interact with depositing Ag atoms or small islands during the nucleation process. Analysis of nucleation events as a function of deposition flux reveals an increase in the flux exponent (χ) from 0.3 on the O-free surface, to about 0.9 for a surface preexposed to 30 L O_2. The temperature dependence for island nucleation, after a 30 L preexposure, gives an activation energy (E) of 0.104 eV between 300-220 K. Assuming that all diffusing species during the Ag deposition process are AgO, the activation energy for AgO diffusion (E_d') is calculated to be < 0.12 eV as compared to $E_d \approx 0.4$ eV for Ag/Ag(100). The assumption that all diffusing species are AgO, however, is an oversimplification therefore actual values may differ.

Multi-deposition experiments clearly support the claim that O and AgO particles are mobile on the terraces and are able to ascend/descend terrace steps. The lack of small islands after the second Ag deposition verifies that the O or AgO disrupts island nucleation. This is accomplished either through direct interaction of O with depositing Ag atoms, or the through the addition of O to small island clusters which destabilizes and/or makes the clusters mobile. The multi-deposition experiment demonstrates a second clear example in which the growth of nanostructures can be controlled through the use of an adsorbate precursor.

This work was supported by NSF Grant CHE-0078596, and performed at Ames Laboratory, which is operated for the USDOE by Iowa State University under Contract No. W-7405-Eng-82.

References

1. J. Vrijmoeth J. Vrijmoeth, H. A. van der Vegt, J. A. Meyer, E. Vlieg, and R. J. Behm, Phys. Rev. Lett. 72 (1994) 3843;
2. V. Fiorentini, S. Oppo, M. Schleffler, Appl. Phys. A 60 (1995) 399
3. H.A. van der Vegt, H.M. van Pinxteren, M. Lohmeier, E. Vlieg, J.M.C. Thornton, Phys. Rev. Lett. 68 (1992) 3335
4. K. Fukutani, Surf. Sci. 281 (1993) 285
5. H. A. van der Vegt, J. Alverez, X. Torrellas, S. Ferrer, E. Vlieg, Phys. Rev. B 52 (1995) 17443
6. W.F. Egelhoff Jr. Surf. Sci. 402-404 (1998) 32
7. H. Wolter, M. Scmidt, K. Wandelt, Surf. Sci. 298 (1993) 173
8. S. Esch, M. Hohage, T. Michely, G. Comsa Phys. Rev. Lett. 72 (1994) 518
9. M. Yata, H. Rouch, K. Nakamura, Phys. Rev. B 56 (1997) 10579
10. E. Bauer, Thin Solid Films 12 (1972) 167
11. M. Kalff, G. Comsa, T. Michely, Phys. Rev. Lett. 81 (1998) 1255
12. E. Kopatgzki, S. Gunther, W. Nichti-Pecher, R.J.Behm, Surf. Sci. 284 (1993) 154
13. A.R. Layson and P.A. Thiel, Surf. Sci. Lett. 472 (2001) L151
14. F. Buatier de Mongeot, M.Rocca, U. Valbusa, Surf. Sci. 363 (1996) 68
15. F. Bauatier de Mongeot, A. Cupolillo, U. Valbusa, M. Rocca, Chem. Phys. Lett. 270 (1997) 345
16. F. Bauatier de Mongeot, M. Rocca,A. Cupolillo, U. Valbusa, H.J. Kreuzer, S.H. Payne, J. Chem. Phys. 106 (1997) 711

17. G.Constantini, F. Bauatier de Mongeot,S.Rusponi, C. Boragno, U.Valbusa, L.Vattuone, U.Burghaus, L.Savio, M.Rocca, J. Chem. Phys. 112 (2000) 6840

18. A.R. Layson, J.W. Evans, P. A. Thiel (submitted to PRL) (2001)

19. P.J. Feilbelman, Phys. Rev. Lett. 85 (2000) 606

20. P.A. Thiel, J.W. Evans J.Phys. Chem. 104 (2000) 1663

21. C.-M. Zhang, M.C. Bartelt, J.-M. Wen, C.J. Jenks, J.W. Evans, P.A.Thiel Surf. Sci. 406 (1998) 178

22. S. Frank, H. Wedler, R.J. Behm, J. Rottler, P. Maass, K.J. Caspersen, C.R. Stoldt, P.A. Thiel, and J.W. Evans, Phys. Rev. B., submitted (2001)

23. K.J. Caspersen, A.R. Layson, C.R. Stoldt, P.A. Thiel, J.W. Evans, S. Frank, H. Wedler, and R.J. Behm, (to be submitted to Surf. Sci.)

24. F. Buatier de Mongeot, A. Cupolillo, M. Rocca, U.Valbusa, Chem. Phys. Lett. 302 (1999) 302

Table Captions

1. Numerical data corresponding to the curves in Figure 2. Island density versus deposition flux for 0.2 ML Ag/Ag(100) at 250 K
2. Numerical data corresponding to the curves in Figure 3. Island density versus temperature for 0.2 ML Ag/Ag(100) at 250 K.

Figure Captions

1. Ag islands on a Ag(100) surface exposed to various amounts of oxygen prior to deposition at 250K. Exposures in units of Langmuirs (L): (a) OL (clean) (b) 1 L (c) 5 L (d) 15 L (e) 30 L. The deposition flux for all images was 0.002 ML/sec. All images 125 x 125 nm^2
2. Island density versus deposition flux for 0.2 ML Ag/Ag(100) at 250 K for (a) O-free surface and (b) surface preexposed to 30 L O_2.
3. Arrhenius plot for 0.2 ML Ag/ Ag(100) for (a) the O-free surface and (b) surface preexposed to 30 L O_2.
4. Image (a) taken after deposition of 0.2 ML Ag/Ag(100) at 300 K. Image (b) taken after a second deposition of 0.2 ML Ag at 250 K, on the surface shown in (a). Image (c) taken after the surface in (a) was exposed to 30L O_2, followed by a second deposition of 0.2 ML of Ag at 250 K. The flux for the first and second depositions were, 0.002 ML/sec. and 0.02 ML/sec. respectively. All image 175 x 175 nm^2.

Experiment	Flux (ML/sec.)	log (Flux) (ML/sec.)	Island Density (island/nm^2	log (island Density) (island/nm)
O-Free	0.0008	-3.10	0.00924	-2.03
	0.0020	-2.70	0.01400	-1.85
	0.0100	-2.00	0.02385	-1.62
	0.1000	-1.00	0.03126	-1.51
30 L O_2	0.0008	-3.10	0.00019	-3.72
	0.0020	-2.70	0.00054	-3.26
	0.0100	-2.00	0.00119	-2.92
	0.0200	-1.70	0.00766	-2.12
	0.1000	-1.00	0.01307	-1.88

Table 1

Experiment	Temp. (K)	1000 / T (K)	Island Density (island/nm^2	ln (island Density) (island/nm)
O-Free	295	3.39	0.00359	-5.63
	284	3.52	0.00438	-5.43
	250	4.00	0.01291	-4.35
	225	4.44	0.03175	-3.45
	200	5.00	0.05558	-2.89
	180	5.56	0.10861	-2.22
	162	6.17	0.18637	-1.68
30 L O_2	295	3.39	0.00018	-8.62
	270	3.70	0.00021	-8.48
	250	4.00	0.00050	-7.60
	220	4.55	0.00069	-7.29
	200	5.00	0.01076	-4.53
	170	5.88	0.10150	-2.29

Table 2

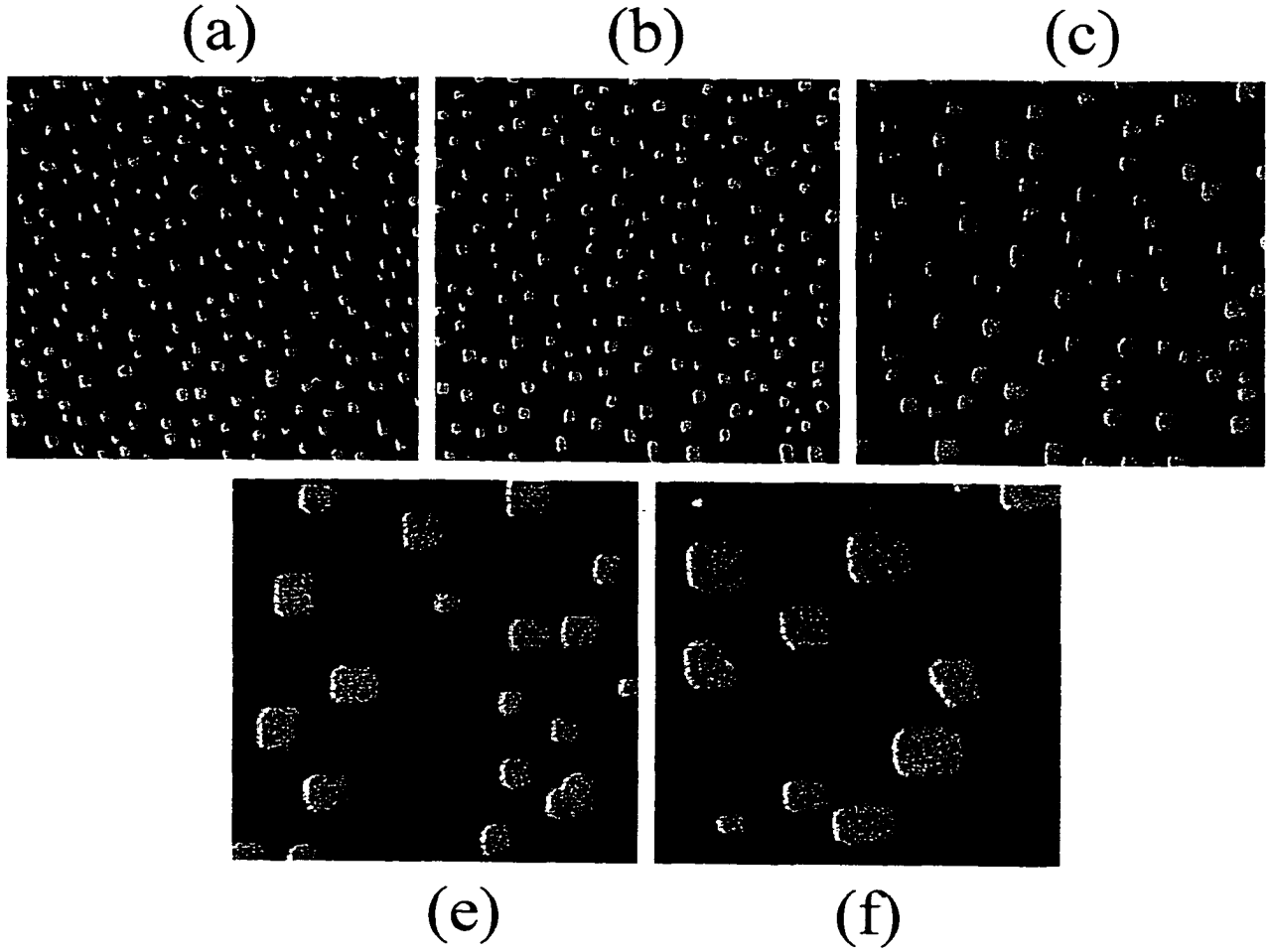

Figure 1

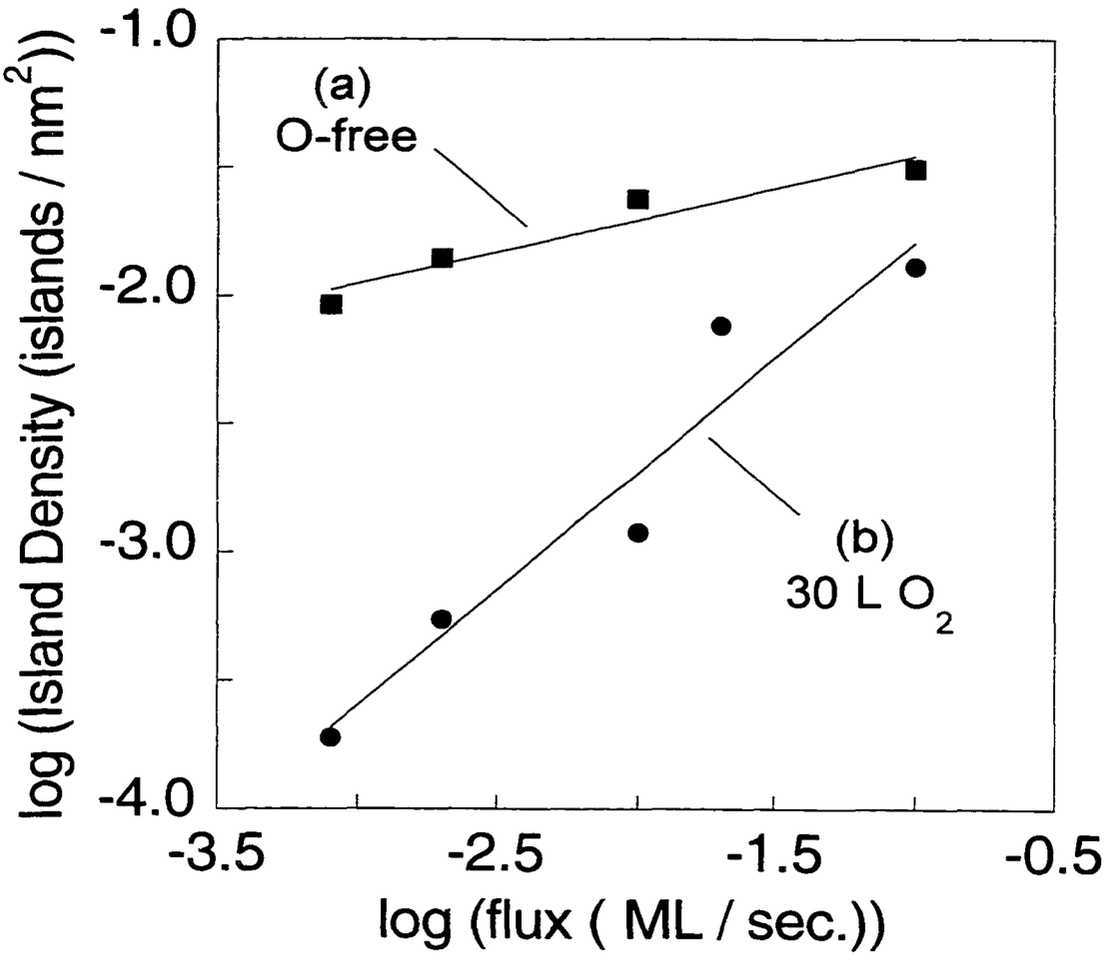
-1.0
-2.0
-3.0
-4.0
log (Island Density (islands / nm^2))
(a)
O-free
(b)
30 L O_2
-3.5
-2.5
-1.5
-0.5
log (flux (ML / sec.))

Figure 2

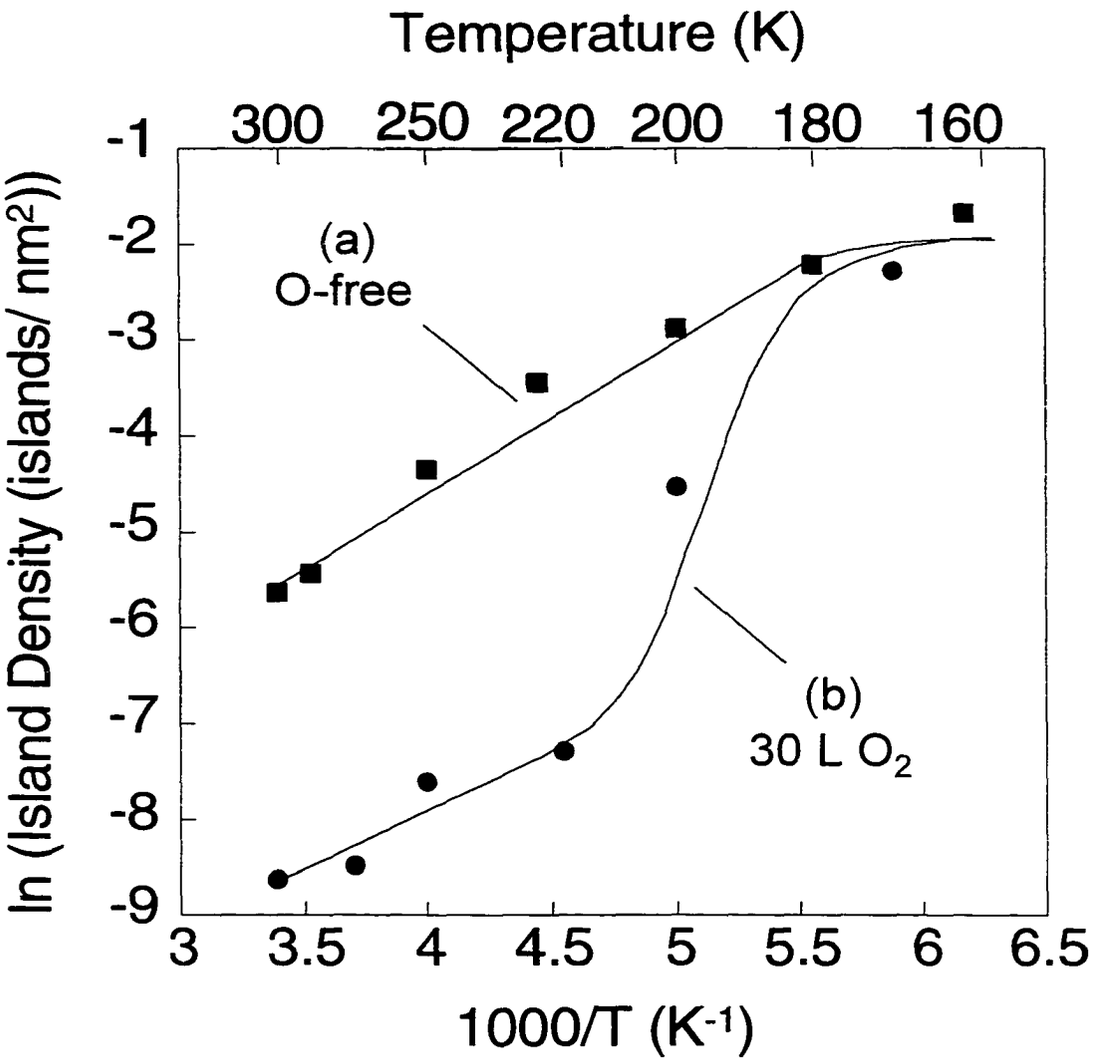
Temperature (K)
300 250 220 200 180 160
-1
-2
-3
-4
-5
-6
-7
-8
-9
ln (Island Density (islands/ nm²))
(a)
O-free
(b)
30 L O2
3 3.5 4 4.5 5 5.5 6 6.5
1000/T (K-1)

Figure 3

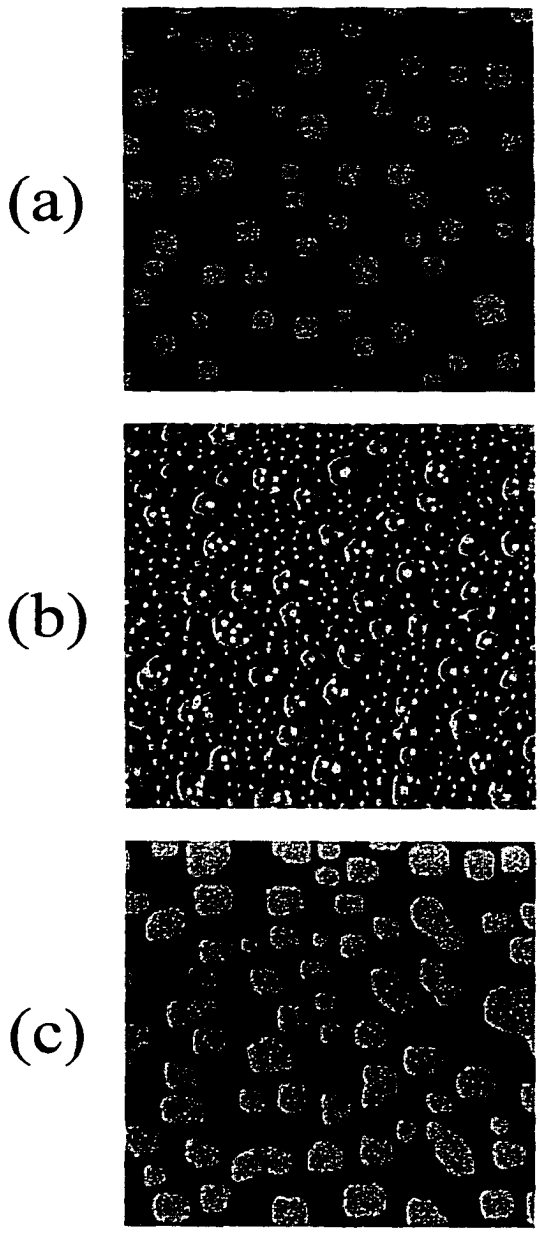

Figure 4

V. THE INFLUENCE OF OXYGEN ON ISLAND SHAPES AND RESTRUCTURING DYNAMICS ON Ag(100)

A paper to be submitted to Surface Science

A.R. Layson, J.W. Evans and P.A. Thiel

Abstract

Results from scanning tunneling microscopy reveal the effects of oxygen on the evolution and restructuring of Ag islands and steps on Ag(100) at 250 K. The presence of O-atoms at the island edge results in the change in equilibrium shape and stabilization of the open [100] arrangement of atoms at the surface steps. Observations of oxygen induced island-island and island-step coalescence events gives insight into the mechanisms for atomic mass transport during island restructuring.

---

1. Introduction

Adsorbed species have long been known to influence film morphology during metal film growth [1-4]. For example, islands formed by Ni deposition on an oxygen pre-covered Ni(100) surface were rotated and elongated relative to the clean surface [5]. The orientation

and shape of Pt islands as well as the morphology of multilayer films on Pt(111) change when Pt is deposited in the presence of minute amounts of CO [6].

Adsorbate exposures after deposition and film formation can also dramatically affect the structure of the film. The stability and structure of surface steps, such as adsorbate induced step bunching on vicinal surfaces [7-11] or step structure evolution on low-index metal surfaces [9,12-14] are but a few examples of restructuring due to adsorbed species at surface steps.

The stability of surface nanostructures can also be compromised when exposed to adsorbates. Au island-stacks on Au(111), which are stable in vacuum, decay rapidly when exposed to air [15,16]. More recently we found that submonolayer coarsening and multilayer smoothing of Ag on Ag(100) is enhanced after exposure to oxygen [17,18]. In this paper we examine the effects of oxygen ($O_{2(g)}$) on the structure and evolution of Ag islands and steps on Ag(100).

To better understand the role oxygen plays in the island restructuring, we here give a brief summary of Ag(100) and the interactions of oxygen on the surface. Fig. 1(a) shows the typical step and island structure on a Ag(100) surface. The islands are square with island edges oriented in the close-packed [110] orientation. Typical terrace step configurations are also shown in Fig 1(a), with the close-packed [110] step orientation being favored over the open [100] orientation. Upon deposition of Ag on Ag(100), square islands and steps with a close-packed arrangement of atoms will predominate on the observed surface.

Ag(100) is quite unreactive to $O_{2\,(g)}$ adsorption, with a dissociative sticking probability on the terraces of approximately 4×10^{-3} at 300 K [19]. While the adsorption probability on the terraces is low, above 180 K oxygen adsorption and dissociation is

favorable at kink sites along the surface steps [20-22]. Bautier de Mongeot *et al.* showed that upon $O_{2\,(g)}$ dissociation, O-adatoms (O_{ad}) diffuse from the kink sites, thereby leaving them open for further $O_{2\,(g)}$ dissociation [20]. For the clean Ag(100) surface, terrace steps are the only available source of kink sites that can contribute to the production of O_{ad}. Therefore for low $O_{2\,(g)}$exposures the O_{ad} concentration is quite small.

Nanostructure formation as a result of Ag deposition may also contribute to the overall kink density. While the equilibrium shape of Ag islands is square, most islands exhibit rounding of the corners (see Fig. 1b). The rounded corners of the square submonolayer islands are comprised primarily of kinks. Depending on deposition conditions (flux and temperature) the initial island density can be quite high. Hence, the contribution of Ag islands in the creation of O_{ad} cannot be disregarded. This is supported by HRLEED, which showed that the coarsening rate of Ag islands increased when $O_{2\,(g)}$ is present during as opposed to after the formation of the islands [17]. The rate change is the result of increased $O_{2\,(g)}$ dissociation during the deposition process.

2. Experimental section

Our experiments were performed in a UHV chamber with base pressure $<10^{-10}$ Torr. The sample was cleaned by repeated cycles of Ar^+ sputtering (20min, 500 V, $T \approx 300$ K) followed by annealing at 700 K. Oxygen treatments (500L, 700 K) were performed periodically and were useful in removing the last bit of remaining contamination from the surface. No oxygen remains as a result of these treatments. This was confirmed through the reproduction of known experimental results on the oxygen-free surface. Ag was deposited onto the Ag(100)

single-crystal surface using an Omicron EFM3 UHV evaporator. Silver was usually deposited at temperatures ≤250K. The surface was exposed to molecular oxygen ($O_{2\,(g)}$) by back-filling the chamber to ~10^{-8} Torr in continuous flow. All oxygen exposures were performed after the deposition of Ag. All exposures were conducted at the same temperature as Ag deposition. Temperature variations were minimal with fluctuations of no more than +/- 1 K throughout the duration of an experiment. Nanostructure evolution is monitored with an Omicron variable-temperature scanning tunneling microscope (VTSTM). Typical tunneling conditions were I_{tunnel} = 1.0-5.0 nA and V_{sample} = 1.00 V.

3. Results and Discussion

3.1 Equilibrium shapes

Fig. 2 shows the island evolution of 0.2 ML of Ag after exposure to 30 L $O_{2\,(g)}$ at 250K. Cartoons inset in the upper corners indicate the nominal island shape at that time in island evolution. Fig. 2a) was taken 45 minutes after $O_{2\,(g)}$ exposure. The nearly square shape is typical of islands on the O-free Ag/Ag(100) surface, with island edges of the close packed [110]-type orientation. After roughly four hours (Fig. 2b) the islands have increased in size through the process of island coarsening [18]. However, rather than maintaining the square equilibrium shape, the island shape begins to change. The larger islands have adopted an octagonal geometry where the corners of the initially square islands have been removed, while several of the smaller islands have a slightly rounder appearance. 45 hours after the oxygen exposure (Fig. 2c) a noticeable change in island shape and orientation has

occurred. The three tiles in Fig 2(c) show the nominal island shapes after long evolution times. The left tile shows an island with an even more pronounced octagonal shape, with steps of the more open (100)-type orientations clearly evident. The extended (100) step is more easily observed in the large island in the center tile of Fig. 2(c). Smaller islands, such as the one observed in the lower half of left tile, are often rotated entirely by 45-degrees. More common, however, are the extremely round island shapes like those observed in the right tile of Fig 2(c). While extended steps of the (100)-type do persist for some period of time, the round geometry appears to be more stable. Given enough time, the extended (100)-type steps will reshape and also adopt the round geometry. O-induced restructuring also occurs at the terrace steps. Fig. 3 shows the typical terrace step structure after extended evolution (45 hours) of 0.2ML after exposure to $O_{2\,(g)}$, at 250 K. In contrast to the O-free Ag(100) surface where terrace steps are straight and smooth, the steps after $O_{2\,(g)}$ exposure are rough and uneven with a round scalloped shape.

Fig. 2 clearly shows that O-induced coarsening of Ag islands has a profound effect on the island shape. On the O-free surface, the near-square equilibrium island shape is reached shortly after Ag deposition and is maintained throughout the coarsening process. However, when O_{ad} is introduced to the system, the near-square shape is no longer favorable. A more appropriate comment is to say that the close packed [110]-type step is no longer the preferable arrangement for atoms at an island or terrace step. After $O_{2\,(g)}$ exposure, island coarsening simultaneously results in the reshaping of the islands, as the system strives to achieve some new equilibrium state where the [100]-type orientation is favored for atoms at a surface step.

Recent experiments show that the mechanism for island coarsening on Ag(100), changes from island diffusion/coalescence on the O-free surface, to Ostwald ripening in the presence of O_{ad} [10]. We recently proposed that the diffusing species in the ripening process is Ag_nO (n=1,2) where O_{ad} residing at kink sites causes the detachment of Ag_nO of from the island step. The lower number of Ag-Ag nearest neighbor bonds in a kink site, as well as the O_{ad} affinity for these sites, suggests that the removal of Ag-atoms from an island or terrace step most likely occurs at kink sites. As discussed in the next section, Ag_nO diffusion along the surface steps also occurs, however, as observed by the lack of island diffusion in the coarsening studies, much more probable is the direct detachment of Ag_nO from the kinks. The O-atoms themselves are able to freely diffuse along the surface steps and are also able to detach from the island step where they can diffuse to other islands and further aid in the detachment of additional Ag-atoms [23].

In the initial stages of coarsening, where island steps are predominantly of the [110]-type, detachment of Ag_nO results in the erosion of the straight [110] steps, while the reattachment of Ag_nO to other islands results in the roughening of the [110] steps. Repeated over time, the coarsening process increases the number of kinks on the surface. This kink creation is readily observed in the shape of islands and steps, as they strive to achieve equilibrium. Extended step edges of the [100]-type orientation are essentially a linear chain of kinks. Rounded island features are multiple kink sites oriented in a random fashion. Therefore, while the [110] step orientation is energetically favored for islands on O-free Ag(100), in the presence of O_{ad}, the open [100] arrangement of atoms at the surface steps becomes favored in achieving equilibrium.

When comparing the surface just after the $O_{2\,(g)}$ exposure and then again after extensive coarsening, reshaping of the islands and terrace steps clearly results in an increases the number of kinks on the surface. Initially, with the majority of the surface steps being of the [110]-type, the kink density on the surface will be quite low. As the islands coarsen in an effort to attain their equilibrium shape, kinks are continually being created. However, the O_{ad} density does not change or at least does not increase. After long evolution times, O_{ad} has stimulated the creation of a large number of kinks, which are observed in the extended [100]-type and rounded island steps as well as the scalloped shapes of the terrace steps. A similar effect was observed on a vicinal Cu(1 1 11) surface where the number of kinks increased after adsorption of S-atoms [11]. S-adsorption also decreased the kink mobility at the surface steps, which resulted in more irregular step structure.

In these experiments, the continued evolution of the surface features shows the effect that a finite O_{ad} density can have on the surface structures on Ag(100). The restructuring of Ag islands and steps clearly demonstrates that the relative energies of the open and closed steps change in the presence of O_{ad}. The result is the non-square equilibrium shapes observed for surface structures after long evolution times.

3.2 Restructuring Dynamics

Further insight into the effects of oxygen on the restructuring of Ag islands can be garnered through analysis of the coalescence and reshaping of individual islands with other islands or terrace steps. Detailed analysis of island-island and island-step coalescence events on the clean (O-free) Ag(100) surface has been studied previously [24]. Diffusion and

coalescence events on the O-free surface show that island restructuring occurs through perimeter diffusion (PD) where mobile atoms diffuse at the edges of islands. An alternative pathway for mass transport, not observed for O-free Ag(100), is terrace diffusion (TD) where atoms can detach and reattach from the island step. On the O-free surface there is a marked energetic advantage of 0.2 eV for PD over TD. Therefore, all restructuring events occur through diffusion of atoms at the steps. Upon exposure to $O_{2\,(g)}$, it is no longer valid to assume that island restructuring occurs solely through PD. As shown above, Ag_nO particles readily detach from islands (TD). It is therefore quite reasonable to suspect that TD also plays an active role in the restructuring process.

Fig. 4(a-c) shows three examples for coalescence of two small islands on the O-free Ag surface. Fig. 4(d-f) shows the coalescence of islands that have been exposed to 12 L of oxygen. The island sizes for Fig. 4 and restructuring times are given in Table 1. Examination of Fig. 4 shows that the evolution of the island shape is similar for the O-free and O-exposed examples. The time for island reshaping, however, is quite different. Upon island connection, it takes up to an hour for the islands to reach a near rectangular shape in the O-free example, while only a few minutes are needed for the O-exposed islands to reach this same shape. It is evident that the presence of O_{ad} increases the rate of restructuring.

It is possible that island size plays a role in the time for restructuring. Simple Mullins-type evolution equations produce a decrease in restructuring rate proportional to the increase in island area [25]. Comparing island sized in table 1 shows that this relationship holds true for both the O-free and the O-exposed examples. Fig. 4(c) and 4(f) offer the closest match in island size for direct comparison between the O-free and O-exposed examples. The comparison reveals a decrease in time by a factor of about 10 for the islands exposed to $O_{2\,(g)}$.

Therefore, regardless of island size, O_{ad} has a profound effect on island restructuring. It should be stated, however, that the magnitude of increase is proportional to the $O_{2\,(g)}$ exposure. A smaller exposure will result in slower restructuring rates, while higher exposures will increase the restructuring rate, presumably up to some limit where $O_{2\,(g)}$ dissociation sites at the surface steps become saturated.

Close examination of the island evolution offer clues into the mechanism for restructuring when O_{ad} is present. Islands exposed to $O_{2\,(g)}$ clearly evolve through detachment of particles from the island edge (TD) [18]. However, there is a strong indication that PD also plays a role in island reshaping in the presence of O_{ad}. Fig. 5 shows two examples of island coalescence with a step edge after exposure to 12 L $O_{2\,(g)}$ at 250K.

At the onset of coalescence (Fig. 5a) there is a noticeable concave feature at the terrace step, created as atoms diffuse from the step, into the neck between the island and the terrace. Similar behavior, on the O-free surface, occurs through diffusion of Ag-atoms along the step (PD) [24]. The concave step formation implies that even though TD is dominant in the presence of O_{ad}, PD is still observed in the event of island coalescence.

Upon $O_{2\,(g)}$ exposure at 250K, the lack of island diffusion indicates that diffusion of Ag-atoms or Ag_nO at the island edge is very slow. This is not surprising, for even on the O-free surface where PD dominates, island diffusion is negligible at 250 K [17]. However, even at 250 K, after exposure to $O_{2\,(g)}$, PD is readily observed through the increased restructuring rate during island coalescence events. Therefore, both TD and PD appear to be active in the evolution of Ag islands in the presence of O_{ad}. TD dominates island coarsening up to the onset of coalescence, at which time PD become active during island restructuring.

In the course of these $O_{2\,(g)}$ studies numerous coalescence events have been observed. Examination of these events show that O-exposed islands coalesce primarily in a corner-to-corner fashion or in a related manner in which the island corners are slightly adjacent to each other, as shown in Fig. 4(f) and 4(e) respectively. Islands that do not have corners closely adjacent to other more often will decay and disappear through Ostwald ripening rather than coalesce with the nearby islands. This behavior offers further insight into the atomic processes at the island edge when O_{ad} is present.

Under the experimental conditions, island diffusion is inactive due to the extremely slow diffusion of atoms at the island edge. Therefore, the initial connection between the islands must occur through the *detachment* of atoms (Ag_nO) from the island edge. (Because islands themselves do not diffuse, they cannot 'collide', therefore the word connect is chosen.) As discussed in section 3.1, detachment of Ag_nO most easily occurs at the island corners where there is a high density of kink sites. If the corners of two adjacent islands are in close proximity to each other, the possibility exists that the detachment and diffusion of Ag_nO between the islands forms a bridge connecting them. Once this bridge is formed, a pathway for rapid restructuring is opened. Bridge formation can only occur in the regions where atom detachment is favorable. Therefore, if the island separation is too large or the island corners are not appropriately positioned with respect to nearby islands, the islands will continue to coarsen but a bridge between the islands will not form and connection will not occur.

Support for the idea of bridge formation can be found in examples for other metal systems. Experiments examining the decay of Cu(111) [26] and Ag(111) [27] island stacks revealed an increased decay rate for the top layer, when the island diffused to within a few

nanometers of the edge of the island below. It was determined that the close proximity of the island edges lead to a bypass of the normal atom detachment barriers in that region. This resulted in diffusion processes with lower activation barriers. It is possible that a similar effect occurs for O-exposed islands on Ag(100) resulting in bridge formation.

Similar behavior is observed for vacancy island coalescence on Ni(100) [28]. As two vacancies diffuse to with close proximity of each other, the islands "snap" together, forming a bridge. Connection through bridge formation is faster than the process where the islands would have to collide through diffusion. Interestingly, both Ni(100) vacancy islands and O-exposed Ag(100) islands decay through the Ostwald ripening process. Therefore, it is reasonable to suspect that Ag islands could behave in a similar manner to the Ni vacancies by "snapping" together and forming a bridge.

It is still not clearly understood what role O_{ad} plays in the dramatic rate increase for island restructuring after island connect with other islands or steps. The presence of O_{ad} at the island edge may have a localized effect, lowering the barrier for surrounding Ag atoms to diffuse at the edge. The presence of O_{ad} does not increase the *overall* PD rate of Ag atoms. This is manifest in the lack of island diffusion. However, it does appear to increase PD on a *localized* level, such as the island edge in the event of island connection and coalescence.

4. Conclusions

We have examined the effects of $O_{2\,(g)}$ exposure on the restructuring and dynamics of Ag islands on Ag(100) at 250K. The size and shape of submonolayer Ag islands were followed after exposure to $O_{2\,(g)}$. As a result of island coarsening, a change in the near-

square equilibrium shape for islands on the O-free surface is observed. With the addition of O_{ad}, islands and terrace steps adopt a scalloped or rounded geometry, with some exhibiting extended steps of the open [100]-type. The rounded features and extended [100] steps are essentially comprised of kink sites. Therefore, the presence of O_{ad} increases the kink density on the surface and stabilizes surface steps with the energetically less favorable [100] orientation.

Submonolayer island coalescence events, after $O_{2\,(g)}$ exposure, were monitored and compared to similar events on the O-free Ag(100) surface. Upon island connection, islands exposed to $O_{2\,(g)}$ reshape 5–10 times faster than O-free islands. It is speculated that when O_{ad} is present, the early stages of island coalescence occur through TD of Ag_nO particles detaching from island corners. If the neighboring island positions are favorable, a bridge can form between the islands. Once this bridge is formed, restructuring of the islands to achieve equilibrium is rapid and is dominated by PD of Ag atoms at the island edge. While the exact mechanism is not known, the presence of O_{ad} at the island edge appears to increase the local rate of PD resulting in the rapid island restructuring.

5. Acknowledgments

The work performed here was supported by NSF Grant CHE-0078596, and performed within the facilities of Ames Laboratory, which is operated for the USDOE by Iowa State University under Contract No. W-7405-Eng-82.

References

1. E. Bauer, Thin Solid Films 12, 167 (1972)
2. W. F. Englehoff and D.A. Steigerwald, J. Vac.Sci. Technol. A 7 (1989) 2167
3. J. Schröder, C. Günther, R.Q. Hwang, and R.J. Behm, Ultramicroscopy 42-44 (1992) 475
4. R.Q. Hwang, C. Günther, J. Schröder, S. Günther, E. Kopatzki, and R.J.Behm, J. Vac. Sci. Technol. A 10 (1992) 1970
5. E. Kopatgzki, S. Gunther, W. Nichti-Pecher, R.J.Behm, Surf. Sci. 284 (1993) 154
6. M. Kalff, G. Comsa, T. Michely, Phys. Rev. Lett. 81 (1998) 1255
7. J.S. Ozcomert, W.W. Pai, N.C. Bartlet, J.E. Reuett-Robey, Phys. Rev. Lett. 72 (1994) 258
8. E. Hahn, H. Schief, V. Marsico, A. Fricke, K. Kern, Phys. Rev. Lett. 72 (1994) 3378
9. C.Y. Nakakura, E.I.Altman, Surf. Sci. 424 (1999) 244
10. H.E. Dorsett, E.Go, J.E. Reutt-Robey, N.C. Bartelt, Surf. Sci. 342 (1995) 261
11. L. Masson, L. Barbier, J.Cousty, B. Salanon, Surf. Sci. 338 (1995) 60
12. Frank, J.Catal. 172 (1997) 406
13. C.Y. Nakakura, G.Zheng, E.I.Altman, Surf. Sci. 401 (1998) 173
14. T. Matsumoto, R.A. Bennett, P. Stone, T. Yamada, K. Domen, M. Bowker, Surf. Sci. 471 (2001) 225
15. B.H. Cooper, D.R. Peale, J.G. McLean, R. Phillips, E.Chason, Mat. Res. Soc. Symp. Proc. 280, 37 (1993).
16. D.R. Peale, B.H. Cooper, J. Vac. Sci. Technol. A 10 (1992) 2210
17. A.R. Layson and P.A. Thiel, Surf. Sci. Lett. 472 (2001) L151

18. A.R. Layson, J.W. Evans, P.A. Thiel, submitted to PRL (2001)

19. F. Buatier de Mongeot, M.Rocca, U. Valbusa, Surf. Sci. 363 (1996) 68

20. F. Bauatier de Mongeot, A. Cupolillo, U. Valbusa, M. Rocca, Chem. Phys. Lett. 270 (1997) 345

21. F. Bauatier de Mongeot, M. Rocca, A. Cupolillo, U. Valbusa, H.J. Kreuzer, S.H. Payne, J. Chem. Phys. 106 (1997) 711

22. G.Constantini, F. Bauatier de Mongeot, S.Rusponi, C. Boragno, U.Valbusa, L.Vattuone, U.Burghaus, L.Savio, M.Rocca, J. Chem. Phys. 112 (2000) 6840

23. A.R. Layson, J.W. Evans, P.A. Thiel (To be Published)

24. C.R. Stoldt, A.M. Cadilhe, C.J. Jenks, J.-M. Wen, J.W. Evans, P.A. Thiel, Phys. Rev. Lett. 81 (1998) 2950

25. W.W. Mullins, J. Appl. Phys. 30 (1959) 77

26. M. Geisen, G.Schulze Icking-Konert, H. Ibach, Phys. Rev. Lett. 80 (1998) 552

27. K. Morgenstern, G. Rosenfeld, G. Comsa, M.R. Sørensen, B. Hammer, E. Laegsgaard, F. Besenbacher, Phys. Rev. B 63 (2001) 045412

28. M.S. Hoogeman, M.A.J. Klik, R. van Gastel, J.W.M. Frenken, J. Phys. Cond. Matter. 11 (1999) 4349

Table Caption

1. The initial island size and the time for island restructuring for images in Fig. 3. Sizes are indicated for islands in the first image in each restructuring sequence. Islands are labeled as Left (L) and Right (R) corresponding to their relative position in the image. The first image in any sequence is designated time 0 min. The middle and last images are designated as the midpoint and final restructuring times respectively.

Figure Captions

1. Island and step structure on Ag(100). (a) shows the two distinct terrace steps typical of Ag(100), the close packed [110]-type, also observed for the 2D island, and open [100]-type steps. (b) An enhanced view of a 2D island showing the typical 'near-square' equilibrium shape. Notice the kink structure in the rounded corners. The ideal Ag(100) island shape is indicated by the dashed square. (c) Typical step structure of Ag(100) after extended evolution in the presence of O_{ad}. The straight [100] step is comprised of a linear chain of kinks. The curved or 'scalloped' shape step is comprised of a random arrangement of kinks. Dashed lines are provided to guide the eyes.
2. The evolution of island shape for 0.2ML Ag/Ag(100) at 250K after exposure to 30 L of O_2. The images are: (a) 45 min. (b) 4 hrs. (c) 45 hrs. after O_2 exposure. Cartoons inset in the upper left corners show typical island shapes at that point in island evolution. All images are scaled the same to reflect true island size. (a) and (b) are 100 x 100 nm^2. Each frame in (c) is 100 x 68 nm^2.

3. Terrace step structure for 0.2 ML of Ag/Ag(100) 45 hours after exposure to 30 L O_2 at 250 K. The dashed square shows a straight [100]-type step bounded on either end by the rounded 'scalloped' shape step structure. The image size is 200 x 125 nm^2.
4. Island restructuring for small Ag islands on Ag(100) at 250 K. Images (a-c) are islands on the O-free surface. Images (d-f) are islands that have been exposed to 12 L O_2. The initial island sizes and the time for island restructuring are given in Table 1. Image sizes for (a-c) are 13x13 nm^2. Images (d-f) are 14x14 nm^2.
5. Ag island-step coalescence and restructuring on Ag(100) after exposure to 12 L of O_2 at 250 K. The time for the restructuring is (a) 6 min. (b) 10 min. All images are 25 x 25 nm^2.

Image	Island size (nm^2)		Restructuring time (min)		
Fig. 3(-)	Left island	Right island	Initial	Midpoint	Final
a	12	20	0	21	46
b	21	23	0	30	57
c	13	25	0	14	36
d	27	48	0	2	3
e	29	35	0	2	5
f	13	31	0	2	5

Table 1

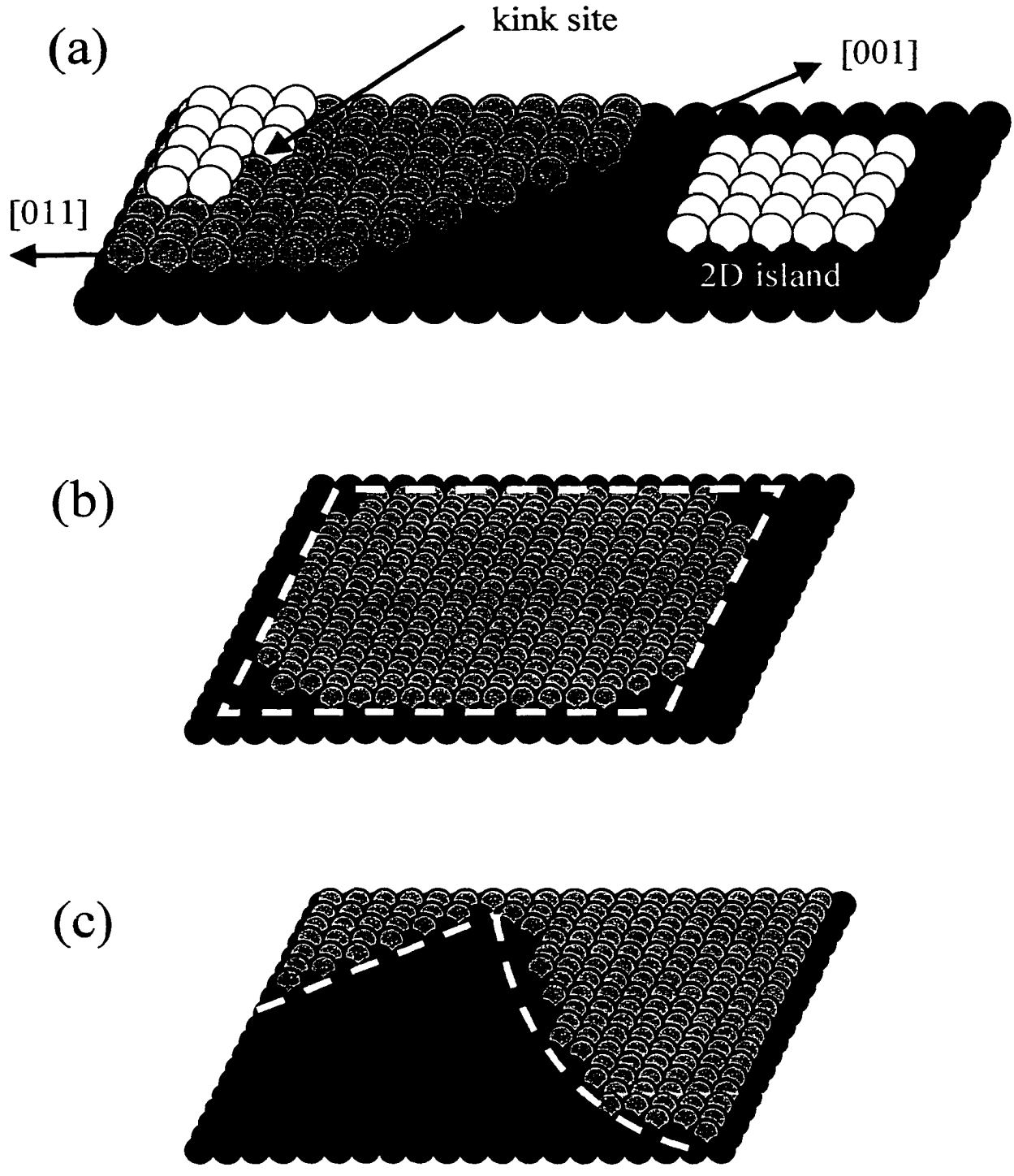

Figure 1

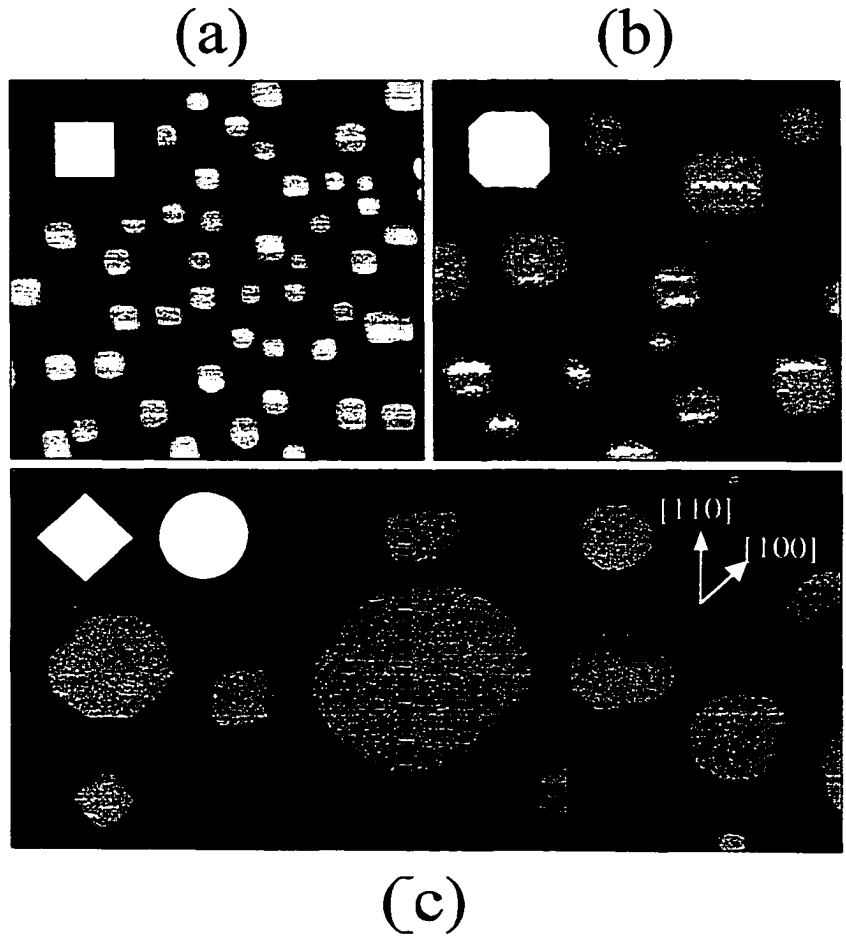

Figure 2

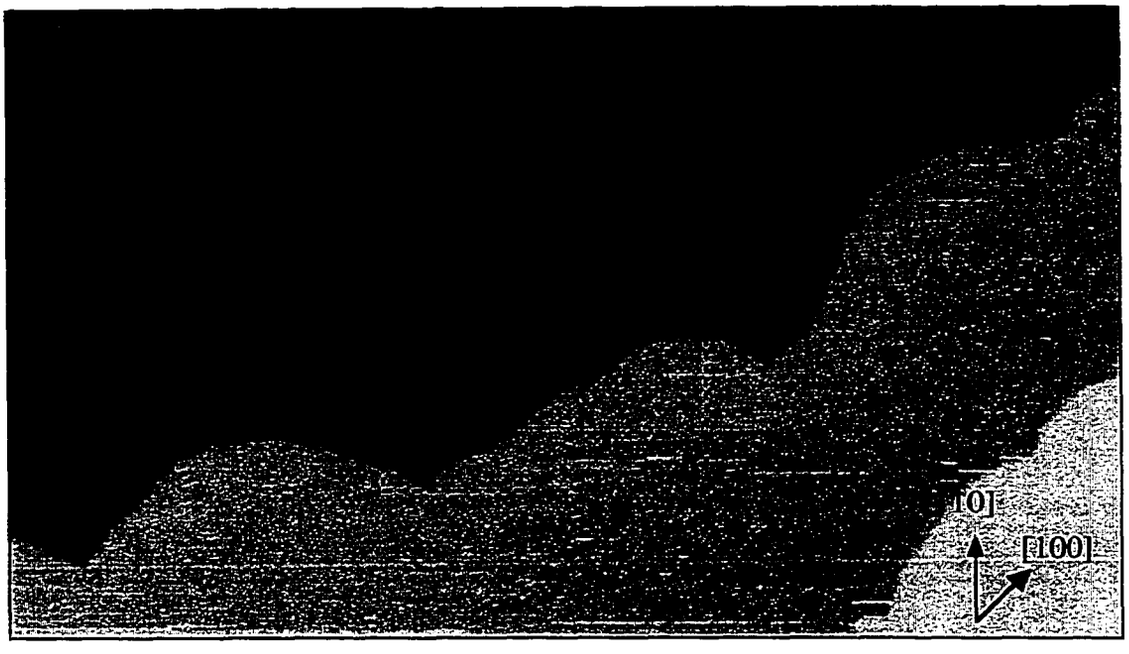

Figure 3

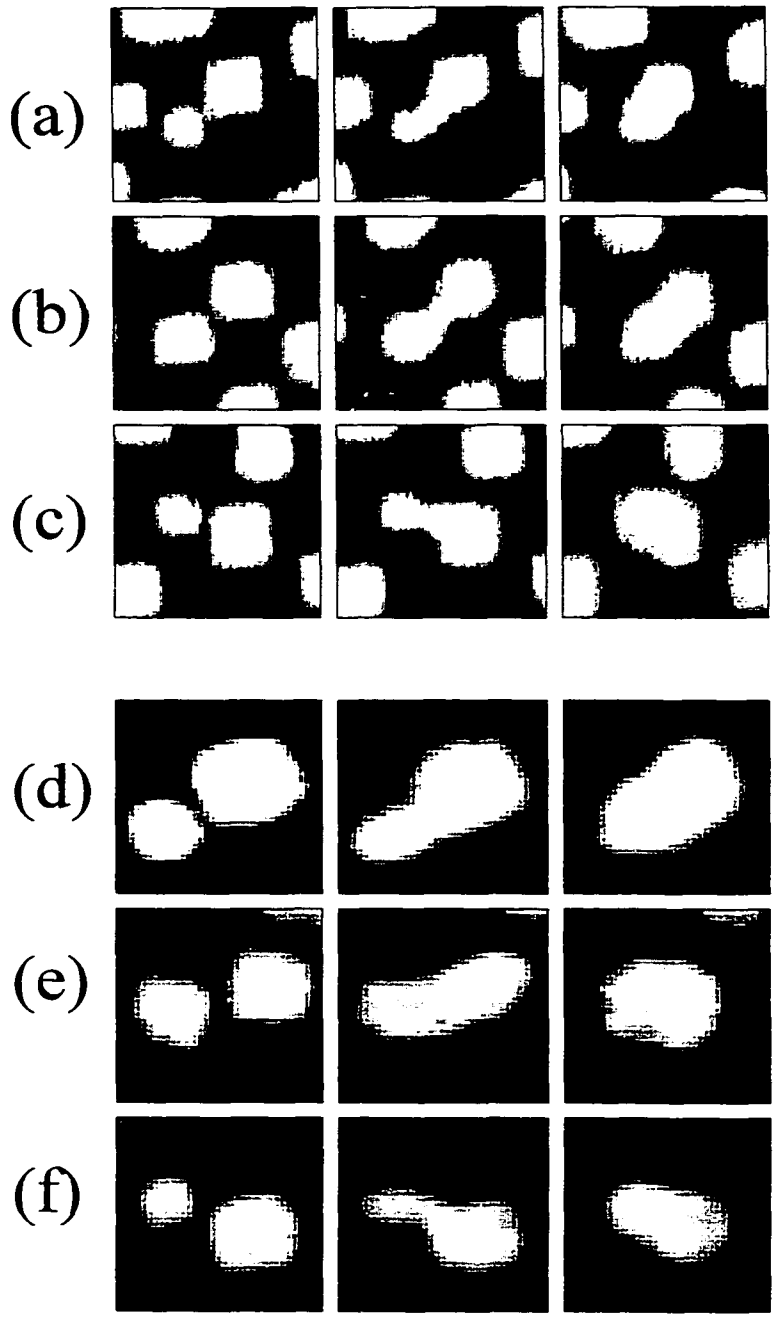

Figure 4

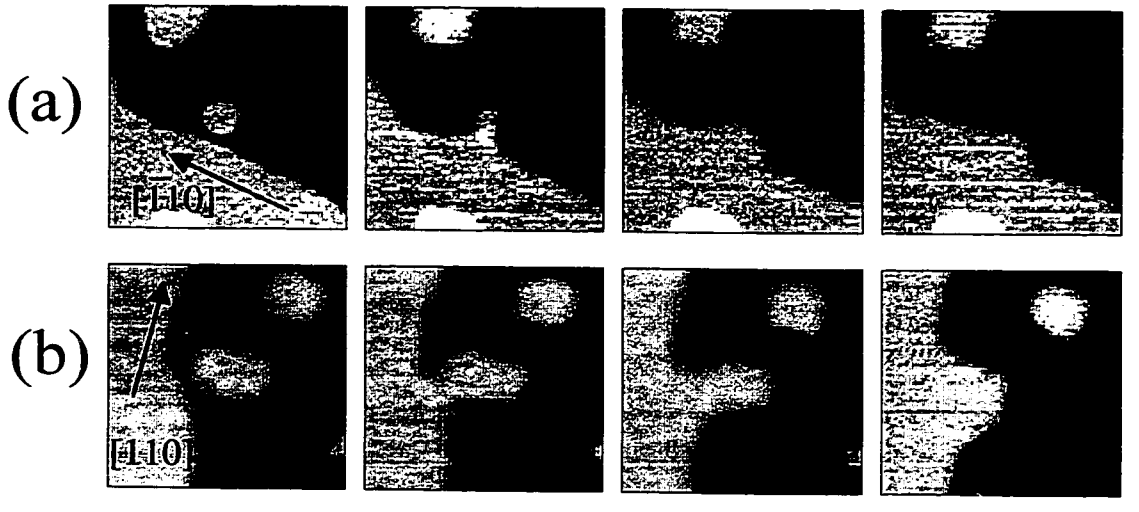

Figure 5

VI. GENERAL CONCLUSIONS

The work presented in this dissertation clearly shows that the presence of oxygen on Ag/Ag(100) homoepitaxy, affects nearly every aspect of the nucleation, growth and relaxation of surface films and nanostructures. The main observations and conclusions are summarized as follows:

a) The presence of O_{ad} accelerates the rate of submonolayer island coarsening and multilayer mound smoothing. HRLEED and STM show that increasing the amount of O_{ad} on the surface, by increasing the exposure time, results in a corresponding increase in the rate of coarsening or smoothing. This demonstrates that careful manipulation of the oxygen exposure provides a method to control the rate of surface structure evolution.

b) STM reveals that the mechanism for submonolayer coarsening changes in the presence of O_{ad} from Smoluchowski ripening (island diffusion/coalescence) on the clean Ag(100) surface, to Ostwald Ripening on the oxygen exposed surface. Smoothing of multilayer films exposed to oxygen also evolve through Ostwald ripening of the surface mounds.

c) The presence of O_{ad} increases the number of kink sites on the surface and stabilizes the less energetically favored [100] surface step orientation. The increased kink density results in a change in equilibrium shape and orientation for surface structures and steps on the (100) surface. After long evolution times, the initially square surface structures adopt a rounded geometry, with some exhibiting extended steps in the [100] orientation.

d) It is speculated that the diffusing Ag species on the surface is Ag_nO (n=1,2). O_{ad} residing at a kink site lowers the Ag-Ag bond strength at the step allowing the detachment of an

Ag_nO particle. The Ag-O bond may also decrease the bond strength with the surface atoms thereby enhancing the diffusion of this species on the terraces.

e) Island-island and island-step-restructuring events provide detail into the dynamics of surface step evolution. Terrace diffusion dominates the initial stages of restructuring through detachment of Ag_nO from the island corners, which in turn may form a bridge between the islands (or island and step). Once a bridge is formed, restructuring of the islands to achieve equilibrium is rapid and is dominated by periphery diffusion of Ag atoms at the island edge. The time for restructuring events is accelerated in the presence of O_{ad} as compared to restructuring events on O-free Ag(100).

f) Decay analysis for submonolayer islands and multilayer island stacks reveal that O_{ad} is mobile on the Ag terraces as well as along the terrace steps, and is able to freely ascend and descend the surface steps. Multi-deposition experiments verify this result through the lack of second layer nucleation events when O_{ad} is present.

g) The presence of mobile O_{ad} or Ag_nO on the surface prior to Ag deposition, impedes the island nucleation process. It is possible that the direct interaction of O_{ad} (or Ag_nO) with depositing Ag atoms inhibits island nucleation. Equally probable is that the addition of O_{ad} (or Ag_nO) to small island clusters destabilizes the cluster, causing it to break it apart, or possibly allows the cluster itself to become mobile.

h) Pre-exposure of the Ag(100) surface demonstrates that the use of oxygen as an adsorbate precursor provides further means to control the initial size and density of nanostructures deposited on the surface.

APPENDIX A. SUBMONOLAYER COARSENING AND MULTILAYER SMOOTHING OF O + Ag/Ag(100)

Data presented in chapters 1 and 2, show that the rates for submonolayer coarsening and multilayer smoothing of Ag nanostructures on Ag(100) increases after exposure to oxygen. STM analysis also shows that the dominant mechanism for coarsening changes from Smoluchowski ripening on oxygen-free Ag(100), to Ostwald Ripening (OR) after exposure to oxygen. Here we present additional data in the analysis of coarsening events on oxygen exposed Ag(100) surfaces.

Fig. 1(a) shows the evolution of several small islands on a narrow terrace. Consistent with OR, smaller islands dissolve, and larger ones (which are more isolated from the step edges) initially grow. Here, OR is somewhat enhanced by the presence of the extended step edges, which act as a sink for diffusing adatoms [1].

The observed evolution can mimicked by analysis of diffusion equations with the appropriate Gibbs-Thompson boundary conditions for adatom densities at step edges. Fig. 1(b) shows the numerical evaluation of diffusion mass flow for the configuration in image (i) of Fig. 1(a), for an assumed step edge energy of 0.1 eV/atom. Diffusive flux arrows indicate the flow of adatoms from the small islands to the larger islands as well as the surface steps. This simulated example does a very good job at predicting the evolution of the islands.

A conventional analysis of OR considers the coarsening kinetics of island distributions on broad terraces. Fig. 2 shows a sequence of images illustrating island coarsening on broad terraces for several coverages after exposure to oxygen. In Fig. 3(a) we show VTSTM data for the increase with time, t, of the mean island separation, $L_{av}=1/\sqrt{N_{av}}$, where N_{av} is the mean island density. The rate of coarsening increases significantly with

oxygen exposure, saturating at above 20 Langmuir (L). Perhaps surprising is the lack of apparent deceleration in the coarsening kinetics expected from the classic OR relation $L_{av} \sim L_0(1+t/\tau)^{1/3}$ [17]. However, this relation is predicated on the island size distribution having achieved its "selected" asymptotic long-time form. Initial and final island size distribution curves for the STM data are plotted in Fig. 4. It should be noted, however, that precise statistics for the size distributions are difficult to obtain from VTSTM data. One can more accurately determine lower moments such as the mean size, and the scaled width, σ (in units of the mean size – in atoms), or the variance, σ^2 (Fig. 5) [18]. We find that the initial size distributions created by the deposition process are much narrower than the predicted asymptotic forms (see Fig. 6) for diffusion-limited OR properly accounting for spatial correlations in the island distribution [17]. This is an intrinsic feature of island nucleation and growth, but likely also reflects the rapid post-deposition disappearance of the smaller islands, which further narrows the distribution [18]. However, σ^2 increases with time, and after 2 -3 hours achieves values roughly consistent with those from OR theory [17] (at least for 0.1–0.3ML where bigger islands enable more accurate size measurement. See Fig. 5). Thus, broadening of the narrow initial size distribution enhances the driving force for coarsening by OR. For the first few hours, this roughly counterbalances the natural deceleration in coarsening.

We also examined the smoothing of 25 ML Ag/Ag(100) films with mounded morphologies. Fig. 7 shows the evolution or decay of the mounded surfaces for films deposited at three different temperatures. Monitoring the film roughness, W (RMS width of the film height distribution), versus time, t, reveals that smoothing at 250K is negligible without oxygen, but does become significant after exposure to oxygen, the rate increasing

with exposure (see Fig 8a). The mechanism for smoothing can be considered a mulitlayer version of OR. Fig. 8(b) shows the smoothing of 25 ML films deposited at different temperatures after a fixed oxygen exposure of 17L. The smoothing rate drops quickly from 250K to 240K, then varies little down to 220K, before switching off at 210K. This does not correspond to simple Arrhenius dependence, e.g., for the activated detachment process underlying surface smoothing. This may reflect the decrease in the lateral mound size, L_m (which accelerates decay) which a result of deposition at lower temperatures. The increase in smoothing may also be a result of an increased O density on the surface. As observed in Fig. 8(b) surfaces created at colder temperatures have a higher initial surface roughness. Increased roughness (higher step and kink site density) increases the amount of O on the surface, increasing the rate of smoothing even at colder temperatures.

References:

[16] P.A. Thiel and J.W. Evans, J. Phys. Chem. B **104**, 1663 (2000).

[17] A.J. Ardell, Phys. Rev. B **41**, 2554 (1990); T.M. Rogers and R.C. Desai, *ibid,* **39**, 11956 (1989).

[18] C.R. Stoldt *et al.*, J. Chem. Phys. **111**, 5157 (1999)

Figure Captions:

1. (a) Evolution over about 15 min. of Ag islands on a narrow terrace at 250K after exposure to 20L O_2. STM images are 35x35 nm^2. (b) The numerical evaluation of adatom diffusion for the configuration in image (i). A step edge energy of 0.1 eV/atom is assumed.
2. Evolution of (a) 0.05 ML (b) 0.3 ML Ag/Ag(100) films at 250 K, after exposure to 20L oxygen. Evolution times are indicated. All images are 100 x 100 nm^2.
3. (a) Change in L_{av}, versus time, t, for 0.3ML Ag/Ag(100) films at 250K with various oxygen exposures (shown). (b) L_{av} versus time for 0.3 ML, 0.1 ML and 0.05 ML (shown) films at 250 K.
4. Island size distributions from STM data, determined (a) just after deposition (b) after extended evolution times for 0.05 ML, 0.1 ML and 0.3 ML.
5. Evolution of the scaled variance of the size distribution, σ^2, versus t for Ag/Ag(100) films with various coverages (shown) at 250K with 12-17L O_2. Asymptotic ($t\rightarrow\infty$) theoretical OR values are σ^2 =0.273, 0.243, 0.224, for θ=0.3, 0.1, 0.05ML, respectively (shown), decreasing to 0.119, as $\theta\rightarrow 0$.
6. Predicted asymptotic form of the island size distribution for diffusion-limited OR. The distributions correspond to the asymptotic values shown in Fig. 5.
7. Smoothening of 25ML Ag/Ag(100) films at: (a) 250K, (b) 230K, and (c) 210K after exposure to 17L O_2. STM images are 154×154 nm^2.
8. Smoothening of 25ML Ag/Ag(100) films. (a) Decay of the roughness, W (in units of interlayer spacing) at 250K with various oxygen exposures (shown). (b) Temperature dependence of W-decay for fixed oxygen exposure of 17 L.

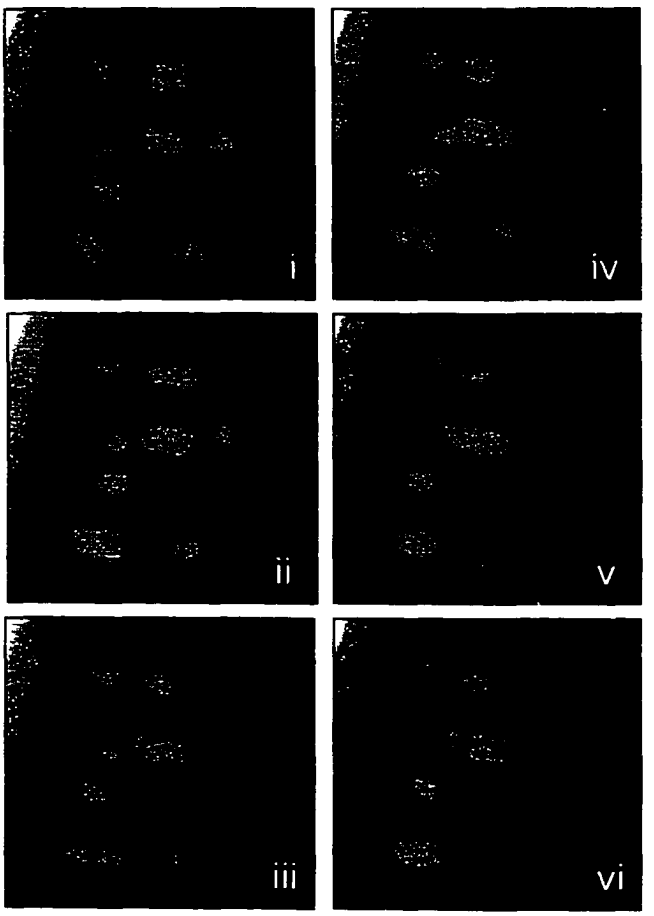

(a)

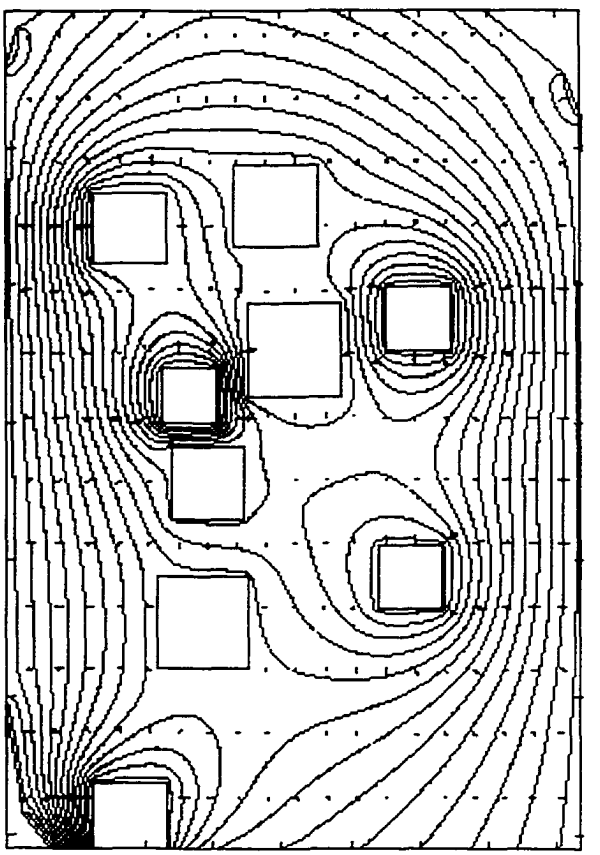

(b)

Figure 1

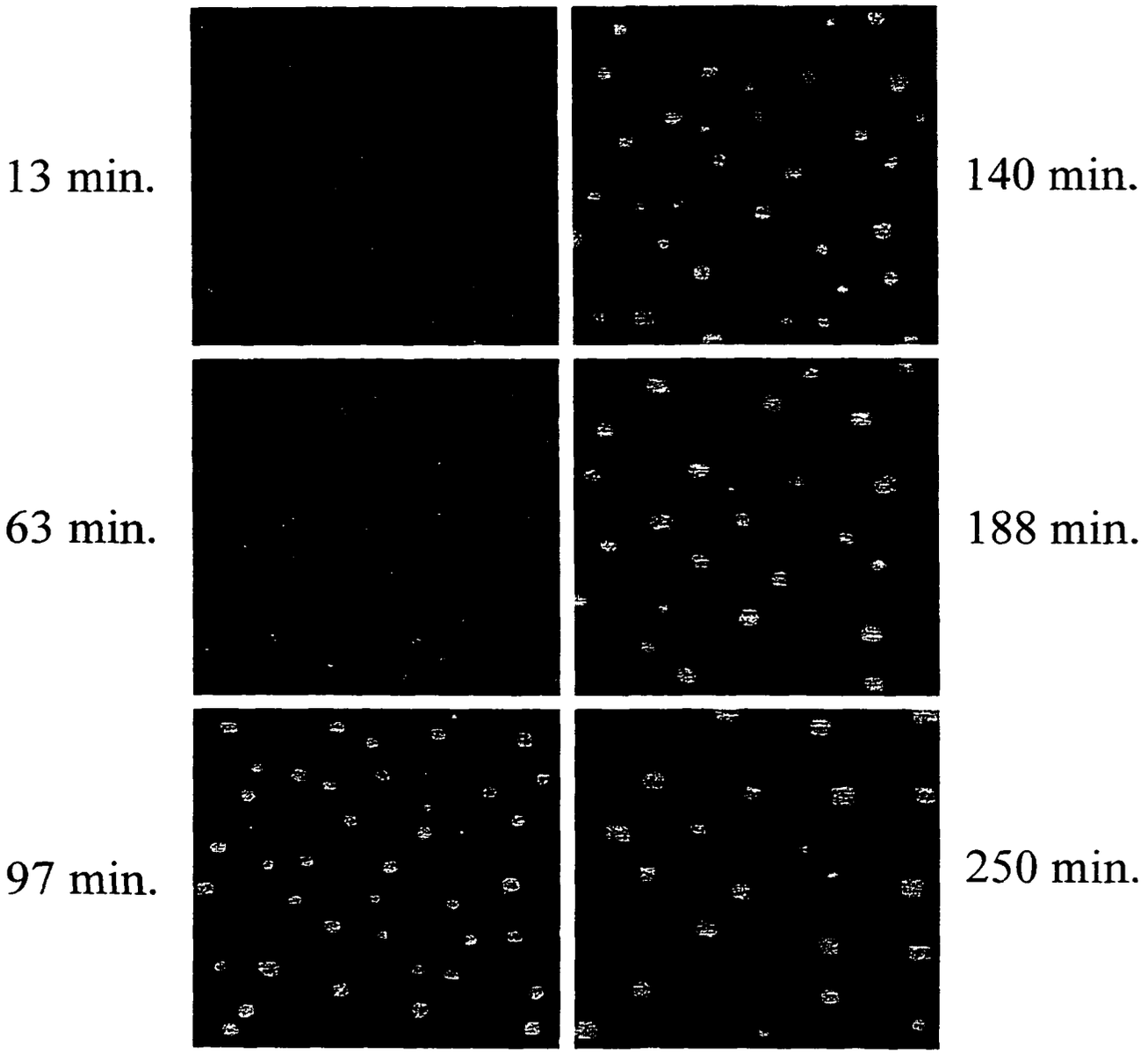

(a)

Figure 2

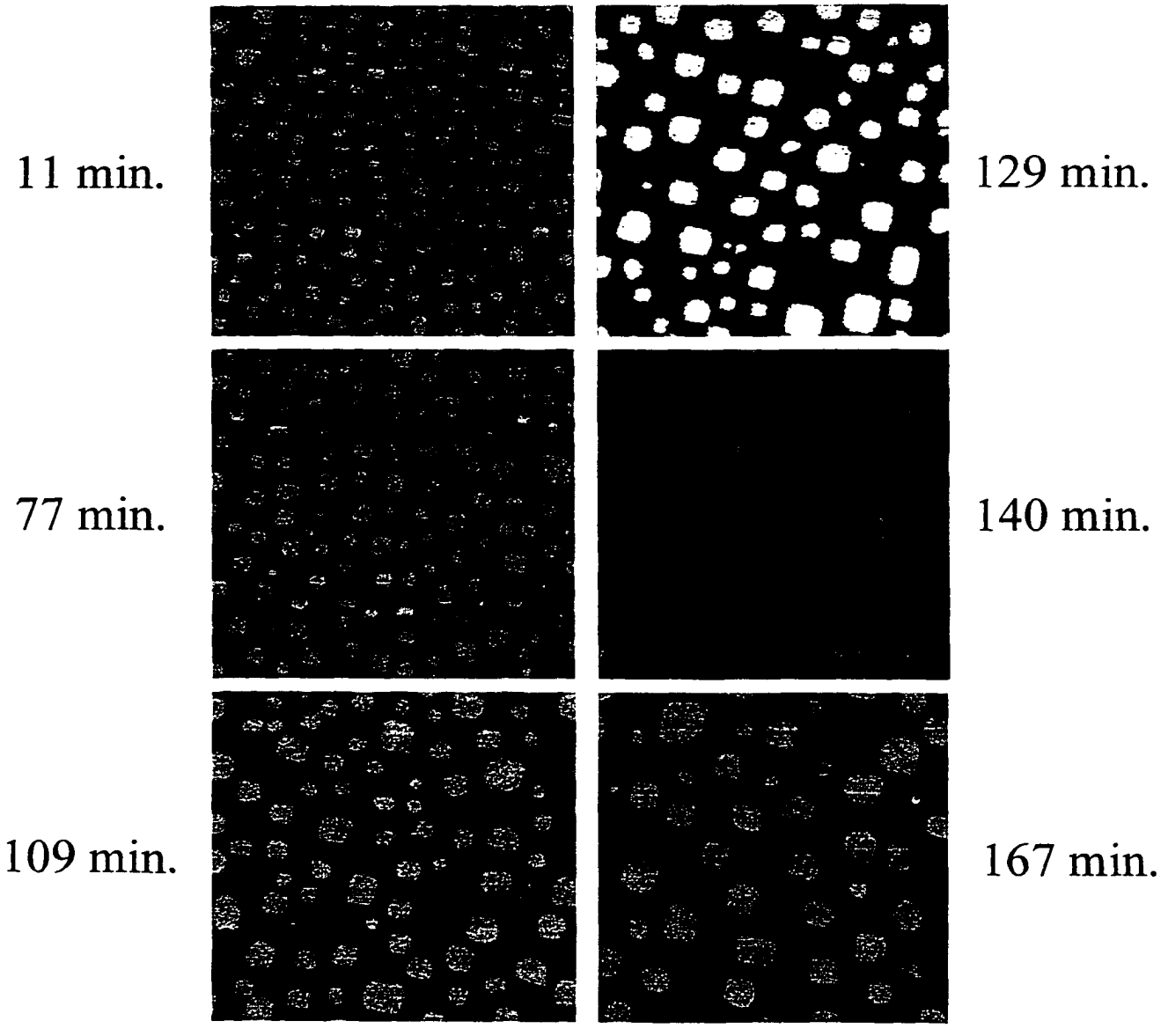

(b)

Figure 2

(a)

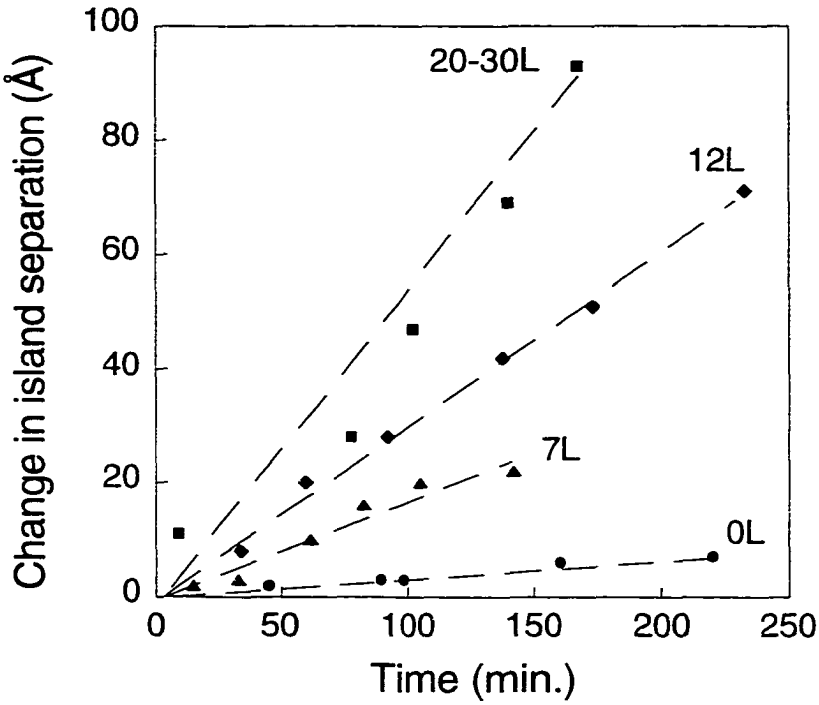
Change in island separation (Å)
Time (min.)
20-30L
12L
7L
0L
0
20
40
60
80
100
0
50
100
150
200
250

(b)

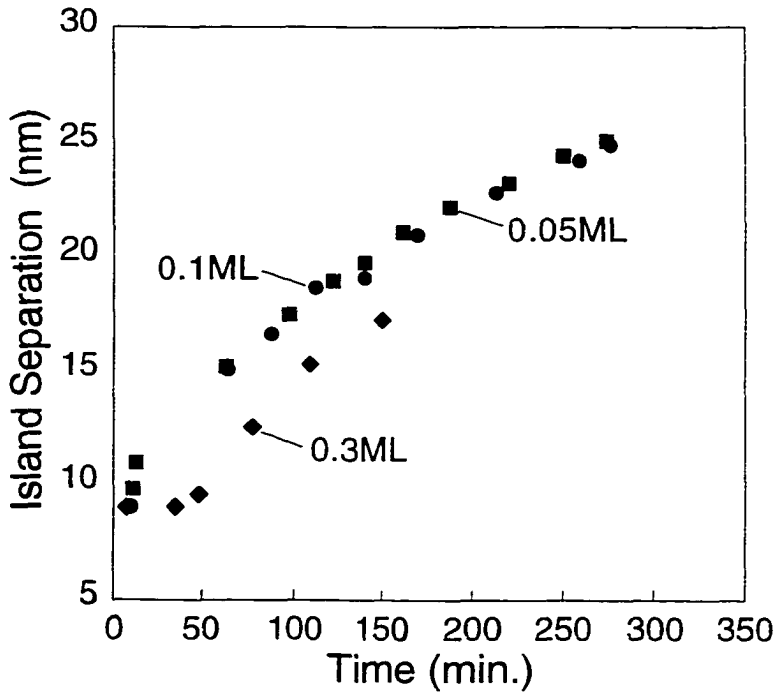
Island Separation (nm)
Time (min.)
0.05ML
0.1ML
0.3ML
5
10
15
20
25
30
0
50
100
150
200
250
300
350

Figure 3

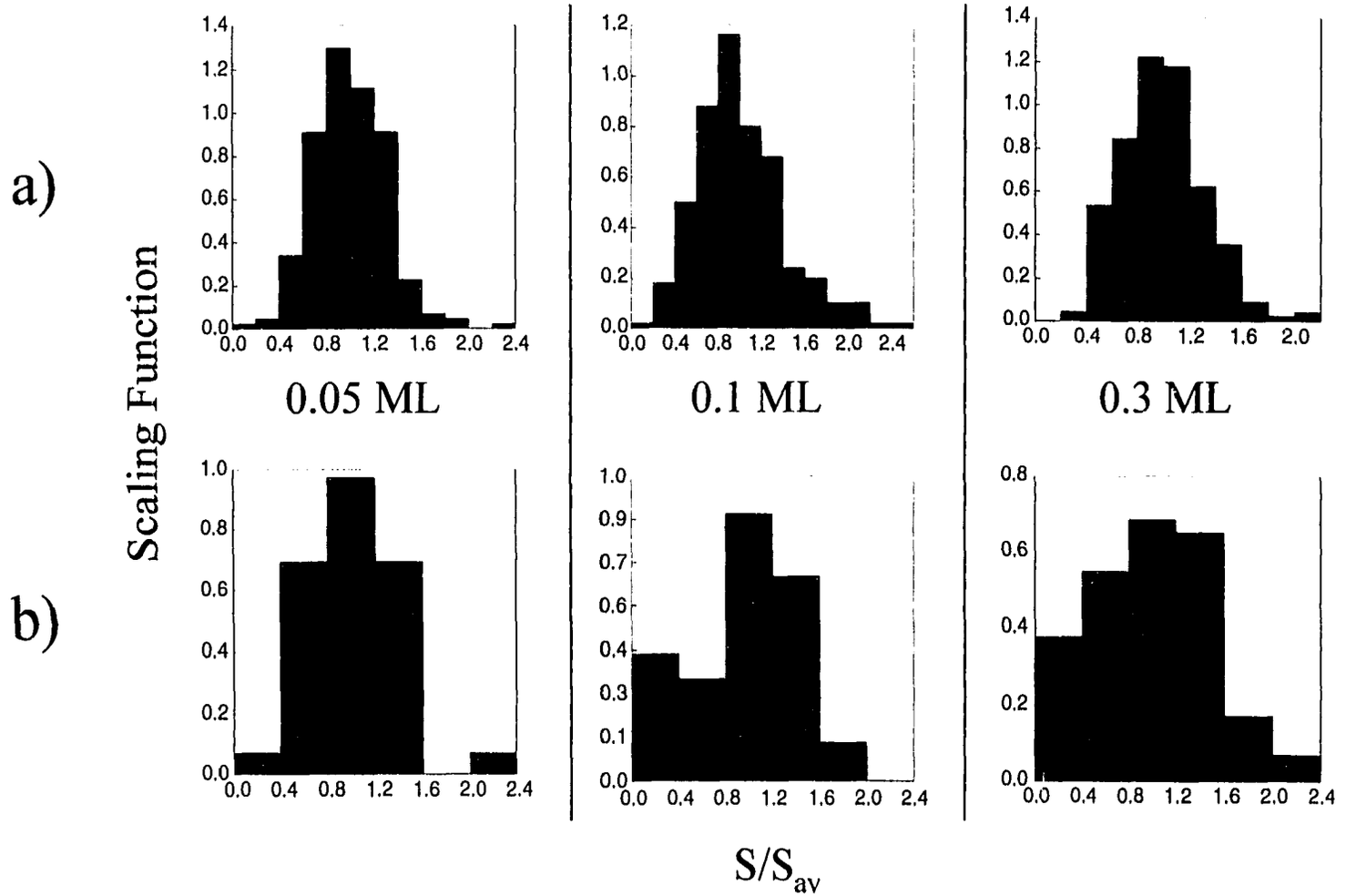

Figure 4

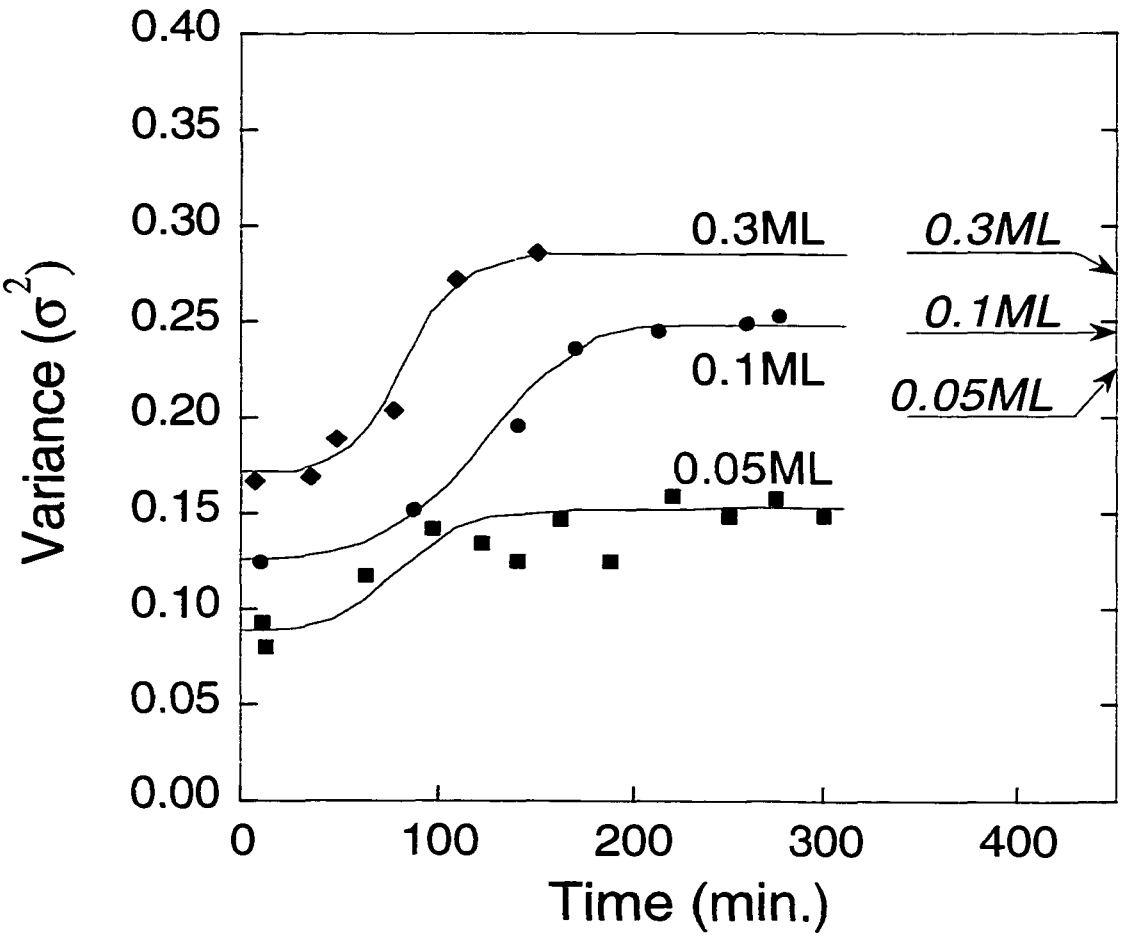
0.40
0.35
0.30
0.25
0.20
0.15
0.10
0.05
0.00
Variance (σ^2)
0
100
200
300
400
Time (min.)
0.3ML
0.1ML
0.05ML
0.3ML
0.1ML
0.05ML

Figure 5

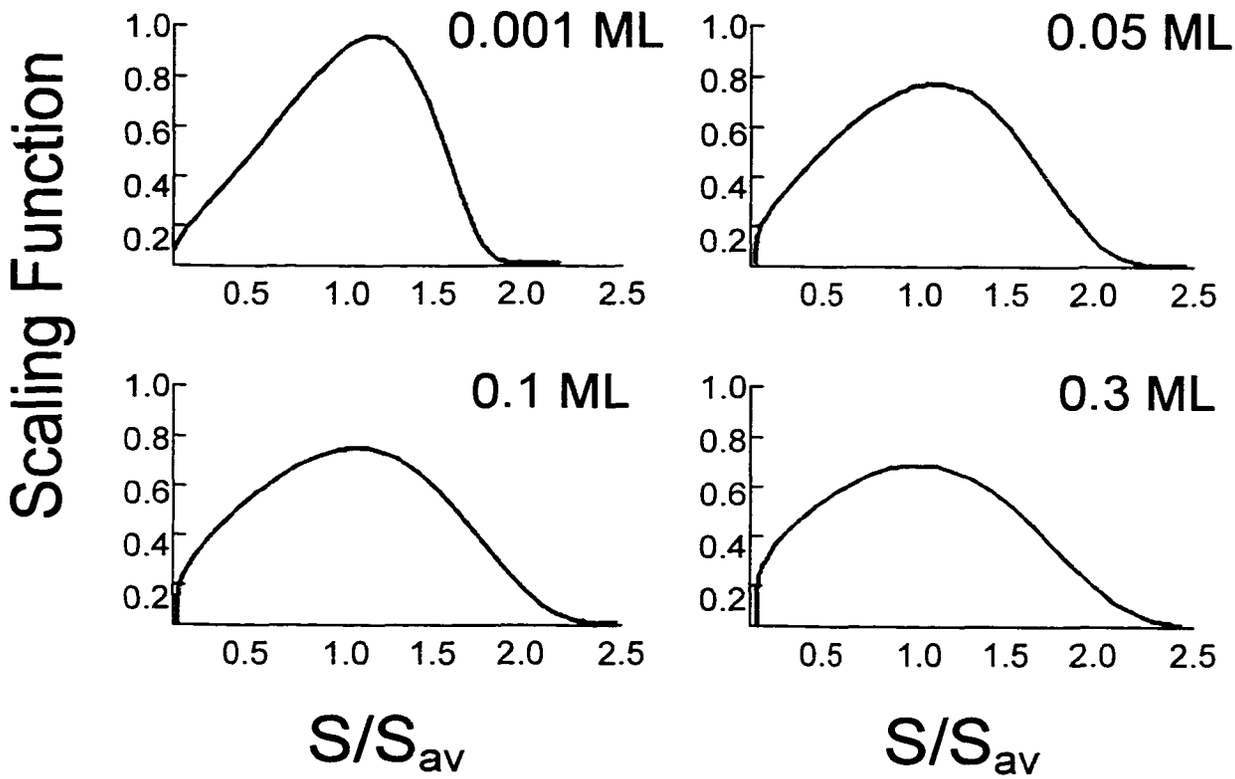
Scaling Function
0.001 ML
0.05 ML
0.1 ML
0.3 ML
1.0
0.8
0.6
0.4
0.2
0.5
1.0
1.5
2.0
2.5
S/S_av
S/S_av

Figure 6

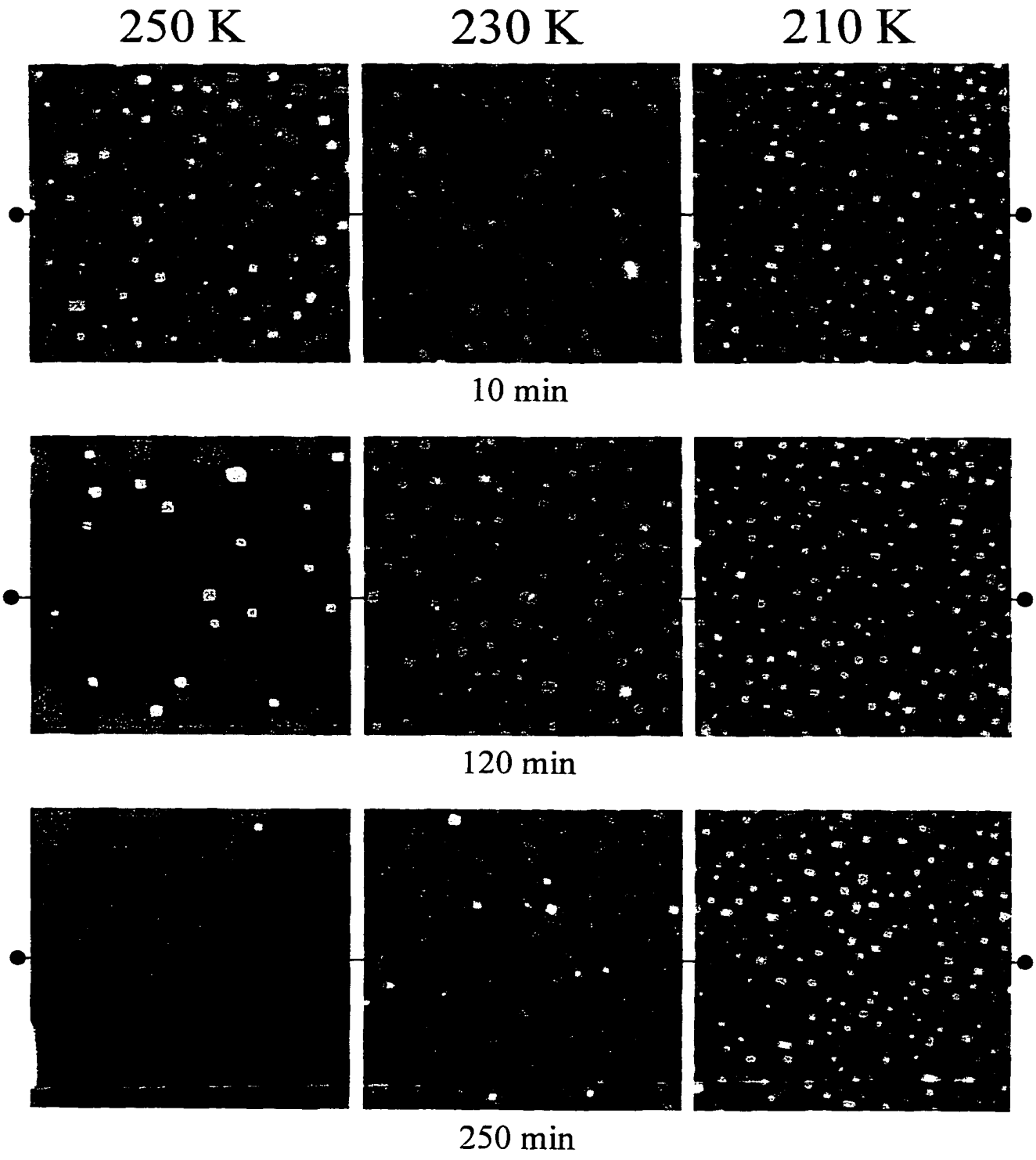

Figure 7

(a)

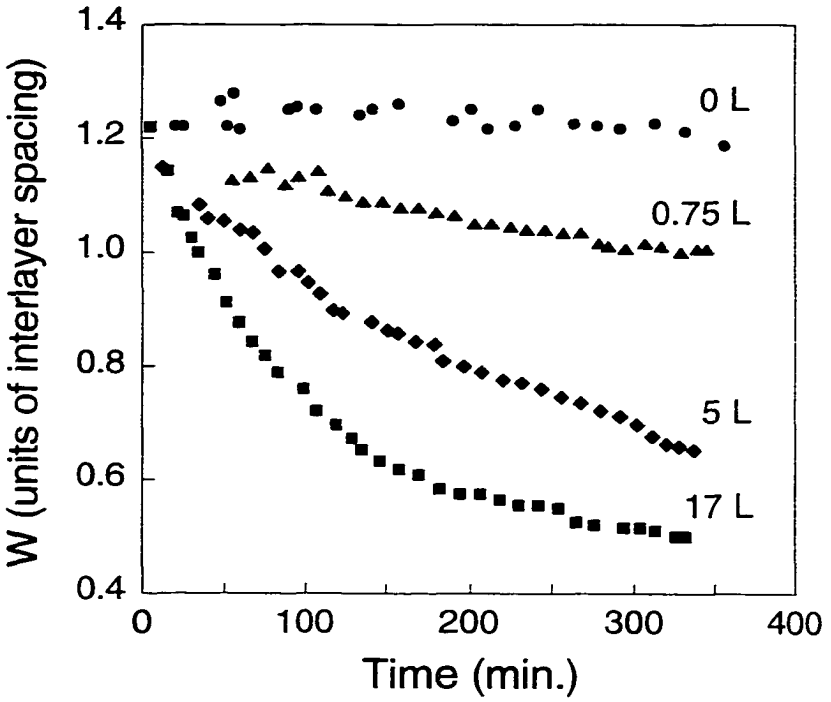
W (units of interlayer spacing)
Time (min.)
0 L
0.75 L
5 L
17 L
1.4
1.2
1.0
0.8
0.6
0.4
0
100
200
300
400

(b)

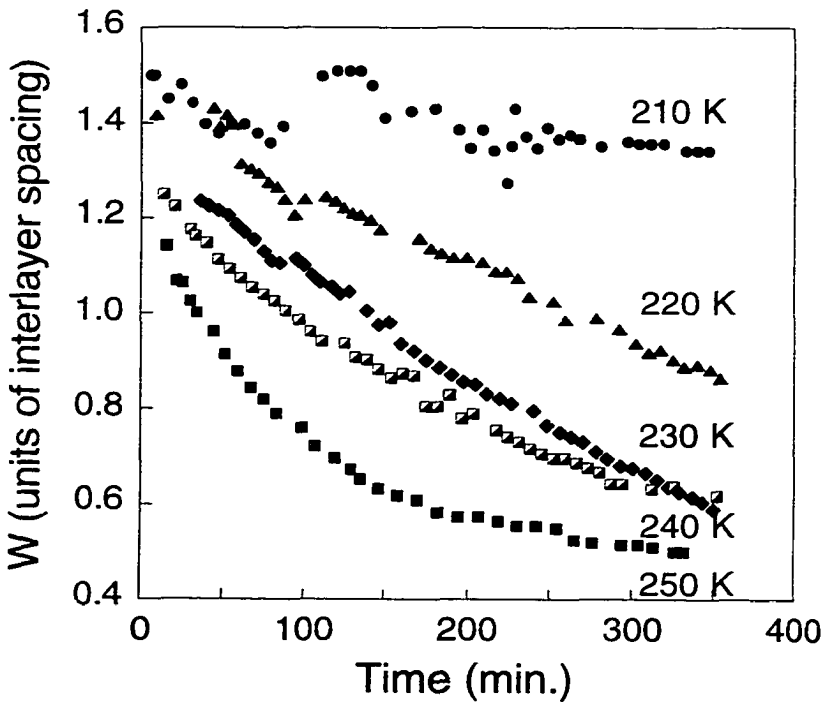
W (units of interlayer spacing)
Time (min.)
210 K
220 K
230 K
240 K
250 K
1.6
1.4
1.2
1.0
0.8
0.6
0.4
0
100
200
300
400

Figure 8

APPENDIX B. O + Ag/Ag(100) DECAYANALYSIS: SUBMONOLAYER ISLAND AND MULTILAYER ISLAND STACKS

Decay analysis of nanostructures on metal surfaces offers a complimentary method in determining how an adsorbate interacts with the surface atoms. As discussed in Chapter 2, for systems where coarsening proceeds through Ostwald Ripening (OR- the detachment and diffusion of atoms from an islands edge), there are two limiting cases for the evolution of these structures with time. If the detachment rate of adatoms from the island edge is rapid compared to the rate of diffusion, then the diffusion of adatoms is the rate-determining step. This is referred to as the terrace-diffusion-limited (TDL) case. If the detachment rate of adatoms from the island is slow compared to the rate of diffusion, then detachment of adatoms is the rate- determining step. This is referred to as the interface-transport-limited (ITL) case [1]. Surface islands decay in size with a power-law scaling in time: $A \alpha (t_o - t)^n$, where A is the island area, t_o is the time at which the feature disappears and n = 2/3 or 1 for TDL and ITL respectively [1,2].

Fig. 1(a) shows the decay of several small Ag islands on Ag(100) after exposure to 17 L $O_{2\,(g)}$ at 250 K. All islands appear to decay at approximately the same average rate, which is determined to be $\approx$ 10 atoms/min. for a 17 L exposure. Closer examination of an individual decay event (Fig. 1(b)) shows that the decay is not linear with time. This indicates that coarsening is terrace-diffusion-limited under the experimental conditions. Fig. 2(a) shows an STM image of 25 ML Ag/Ag(100) immediately after exposure to 17 L $O_{2\,(g)}$. Fig. 2(b) shows the layered island structure for a multilayer island stack (mound). Decay analysis for mulitlayer mounds reveals similar behavior to submonolayer islands. Fig. 3(a) shows

typical curves for three-layer mound decay. Decay for both the top and middle layer islands is non-linear, once again indicating TDL behavior.

Further analysis of the decay curves for the multilayer stacks provides information on atomic interactions between the adsorbate and surface atoms. In this analysis, we examined several types of surface structures: three-layer mound, two-layer mound (equivalent to submonolayer islands) and multilayer vacancy islands, after exposure to 17 L $O_{2\,(g)}$. For both two and three-layer mounds, decay is non-linear and resembles data plotted in Figs. 1 and 3. For all cases, however, island decay begins to dramatically increase, as the island size becomes very small. Observations for several mounds reveal that the rate of decay begins to increase when islands reach a size of approximately 200-300 atoms (S_m), as indicated by the dashed arrows in Fig 3(a). More intriguing results appear when these increased decay rates for successive layers are compared to each other. While not obvious from Fig. 3(a), upon reaching size S_m, the decay rate for the middle-layer is faster than the rate for the corresponding top-layer when it had reached S_m.

Data summarizing mound decay rates are shown in Fig. 4, which plots the rates for several mounds and vacancies. The data points that lie below the lower dashed line (which indicates S_m) show decay rates for islands larger than S_m. For all islands larger than S_m, the decay rate is 3-7 atoms/min. Upon decaying to size S_m, their average decay rate increases, as indicated by the vertical arrows. For two-layer mounds, as well as the top-layer of the three-layer mounds, the decay rate increases to 10-12 atoms/min. (the area between the two dashed lines). As previously stated however, upon reaching S_m, the decay rate for the middle layer of the three-layer mound, increases to 13-17 atoms/min.

It is precisely this difference in the top and middle decay rates that offers clues into the atomic interaction of oxygen with Ag. For decay to occur, O_{ad} must decorate the surface steps and aid in detachment of Ag atoms. For decay of an individual island to continue, there must be a mechanism for O_{ad} to return to the island edge. If this were not so, we would expect to see decay of upper-level islands eventually stop as the O_{ad} is depleted. Because decay does not stop, O_{ad} *must* be mobile on the Ag terrace, in order to repopulate the island. For the same reason, we suspect that O_{ad} must also be able to easily ascend and descend island steps. The difference in top and middle-layer mound decay rates provides evidence to support this claim. Once the top island has fully disappeared, there will be a buildup of O_{ad} at the edge of the lower island. This increased density of O_{ad} leads to the enhanced decay rate when the middle layer reaches S_m. This increase shows that O_{ad} must be able to descend the steps in order to observe any enhancement. The lack of equilibration of the O-edge population implies some limitations on the rates for detachment of O_{ad}.

For all vacancy islands, the rate of decay falls in the range of 3-7 atoms/min. In contrast to mound decay, vacancy decay is linear with time and no enhancement of the decay rate is observed as island size decreases (see Fig. 3b). This is easily explained, as the processes for vacancy and mound decay slightly differ. Mound decay entails removal of Ag atoms from island steps. Vacancy decay relies on the addition of Ag, filling the vacancy. If we consider the surface in Fig.2, the majority of the surface structures can be thought of as terraces and large islands and mounds. As shown previously, large structures decay with a rate of 3-7 atoms/min. Therefore, the rate to fill vacancies should be no greater than the rate at which Ag atoms are provided. The observed vacancy decay rate is consistent with this explanation.

References

1. B.H. Cooper, D.R. Peale, J.G. McLean, R. Phillips, E.Chason, Mat. Res. Soc. Symp. Proc. 280 (1993) 37

2. J.G. McLean, B. Krishnamachari, D.R. Peale, E. Chason, J.P. Sethna, B.H. Cooper, Phys. Rev. B, 55 (1997) 1811

Figure Captions:

1. Submonolayer island decay analysis for 0.05 ML Ag/Ag(100) after exposure to 17 L O_2 at 250 K. (a) The change in island size with time, for ten individual islands. Each time division is 10 minutes. (b) Expanded view for the curve outlined by the dashed rectangle in (a).
2. STM image of 25 ML Ag/Ag(100) immediately after exposure to 17 L O_2 at 250 K. (a) 154 x 154 nm^2 image showing the structure of a mounded Ag surface. The dashed squares in (a) are enhanced to show the typical structures for (b) three-layer mound and (d) mulitlayer vacancy. Image size for (b,c) are 16 x 16 nm^2.
3. Typical decay analysis curves for structures similar to those shown in Fig. 2(b,c) The graphs show the change in island size with time for (a) three-layer mound and (b) multilayer vacancy. The dashed arrows, labeled S_m in (a) signify the approximate island size at which the island decay rate dramatically increases.
4. Summary plot for the decay analysis of 25 ML Ag/Ag(100) after exposure to 17 L O_2 at 250 K. Decay for three types of surface structures is shown: three-layer mounds, two-layer mounds and multilayer vacancies. For three-layer mounds, the top and middle layers for a specific mound, are indicated by the numbers below the data points. Points below the lower dashed line signify decay rates for islands larger than S_m. Vertical arrows show the increase in decay rate after an individual island reaches S_m. The top dashed line serves to differentiate the rates for the top and middle layer decay rates for three-layer mounds.

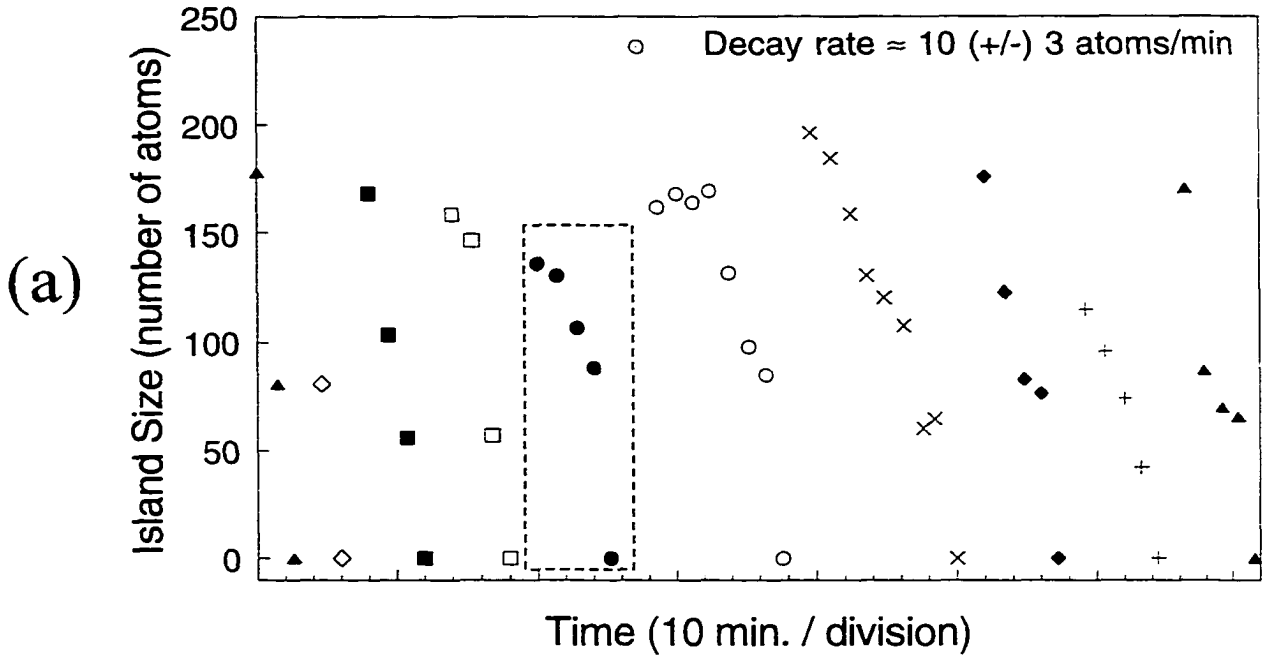
(a)
Decay rate ≈ 10 (+/-) 3 atoms/min
Island Size (number of atoms)
250
200
150
100
50
0
Time (10 min. / division)

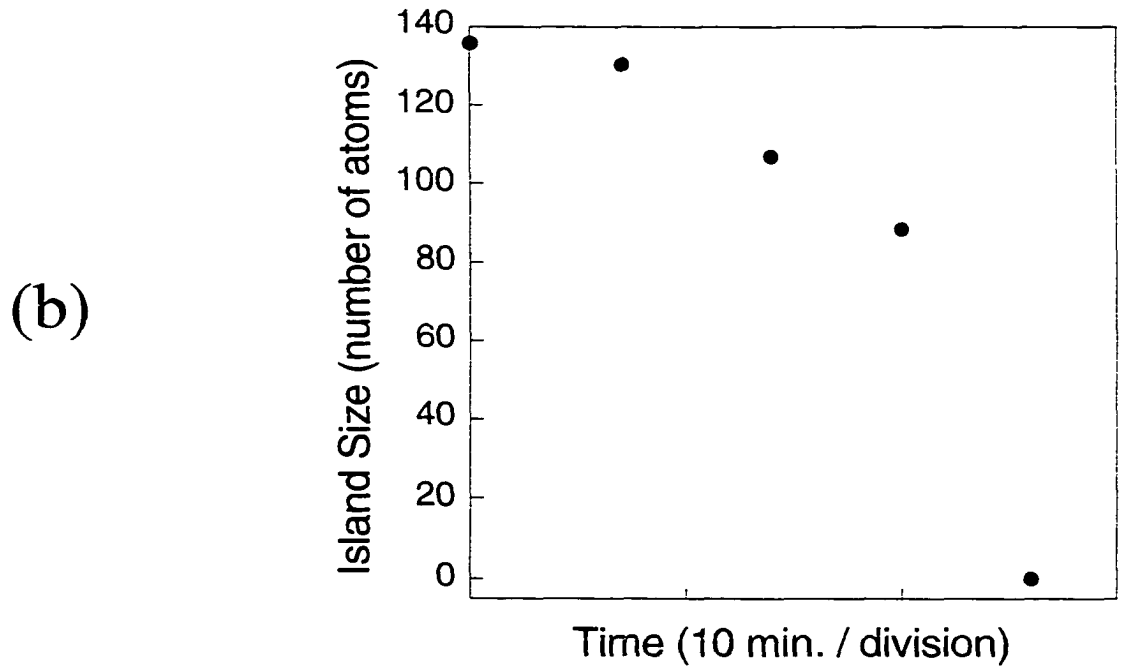
(b)
Island Size (number of atoms)
140
120
100
80
60
40
20
0
Time (10 min. / division)

Figure 1

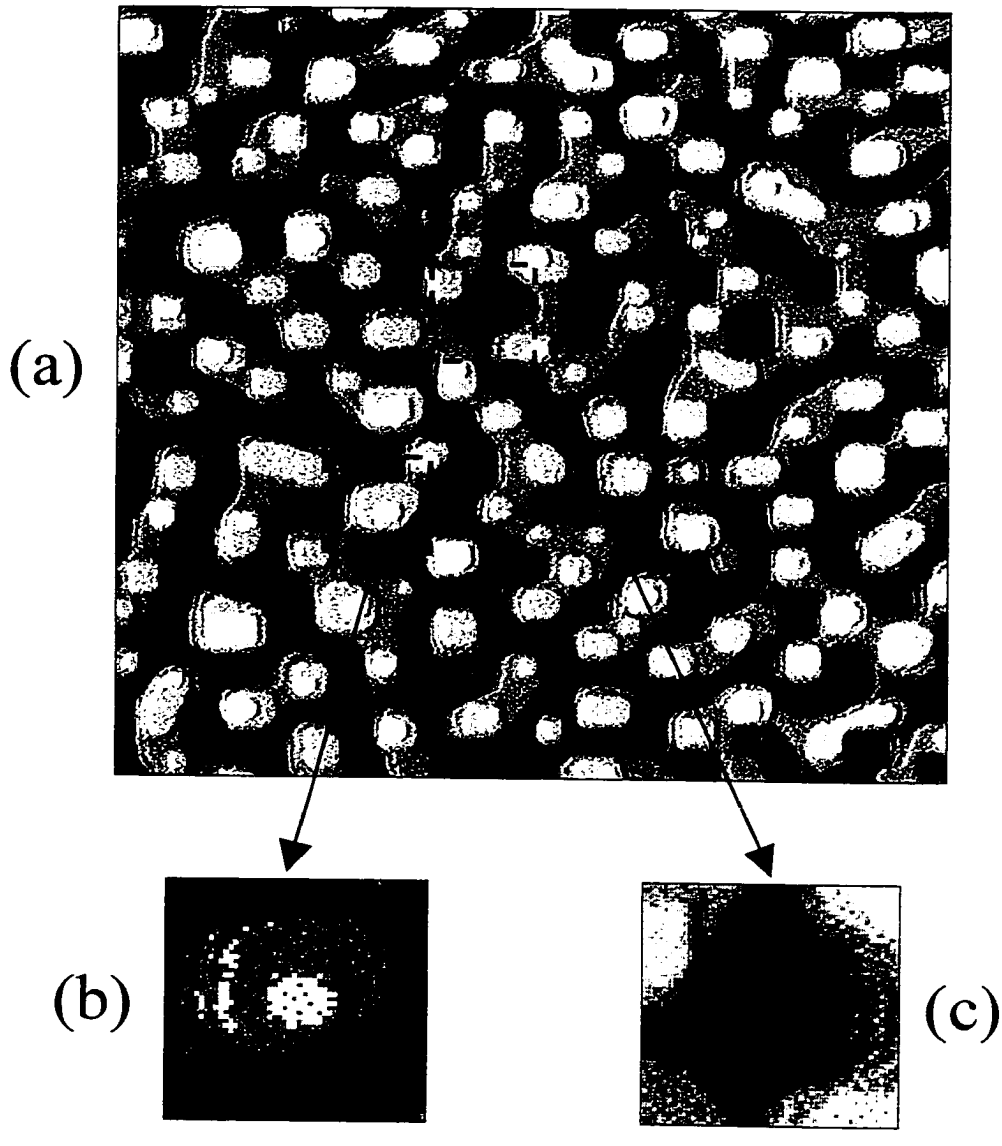

Figure 2

(a)

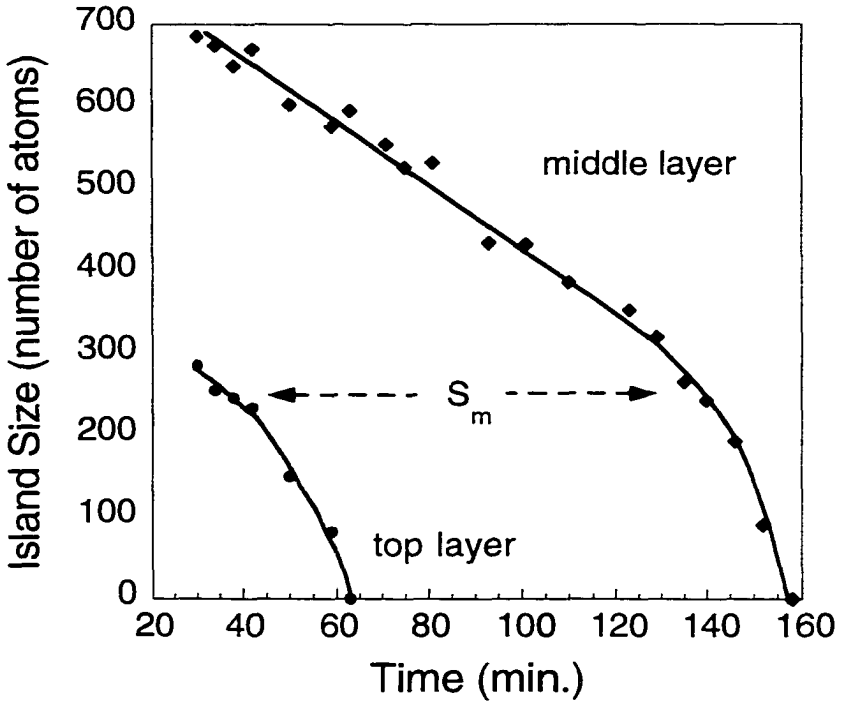
Island Size (number of atoms)
700
600
500
400
300
200
100
0
middle layer
S_m
top layer
20
40
60
80
100
120
140
160
Time (min.)

(b)

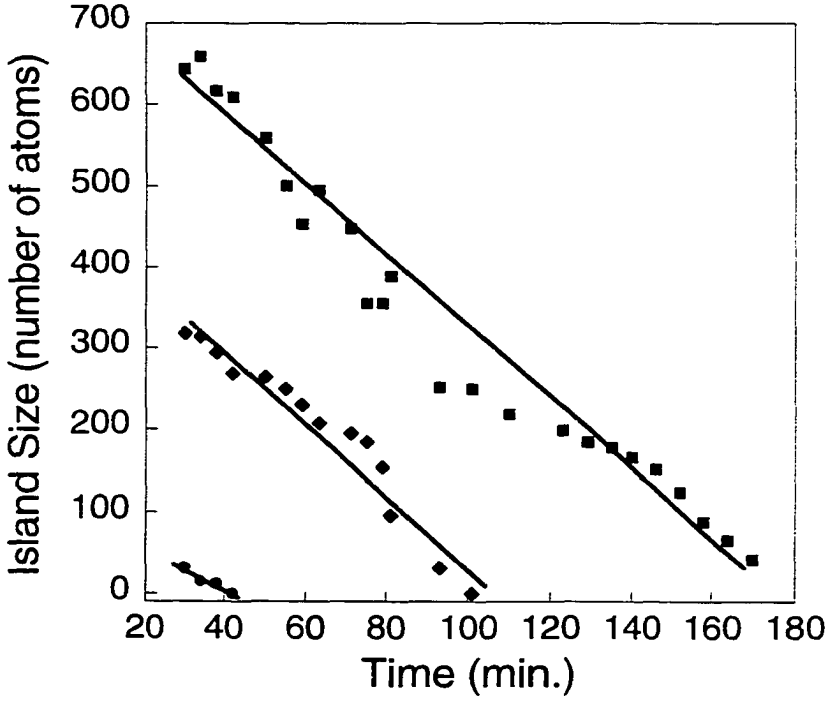
Island Size (number of atoms)
700
600
500
400
300
200
100
0
20
40
60
80
100
120
140
160
180
Time (min.)

Figure 3

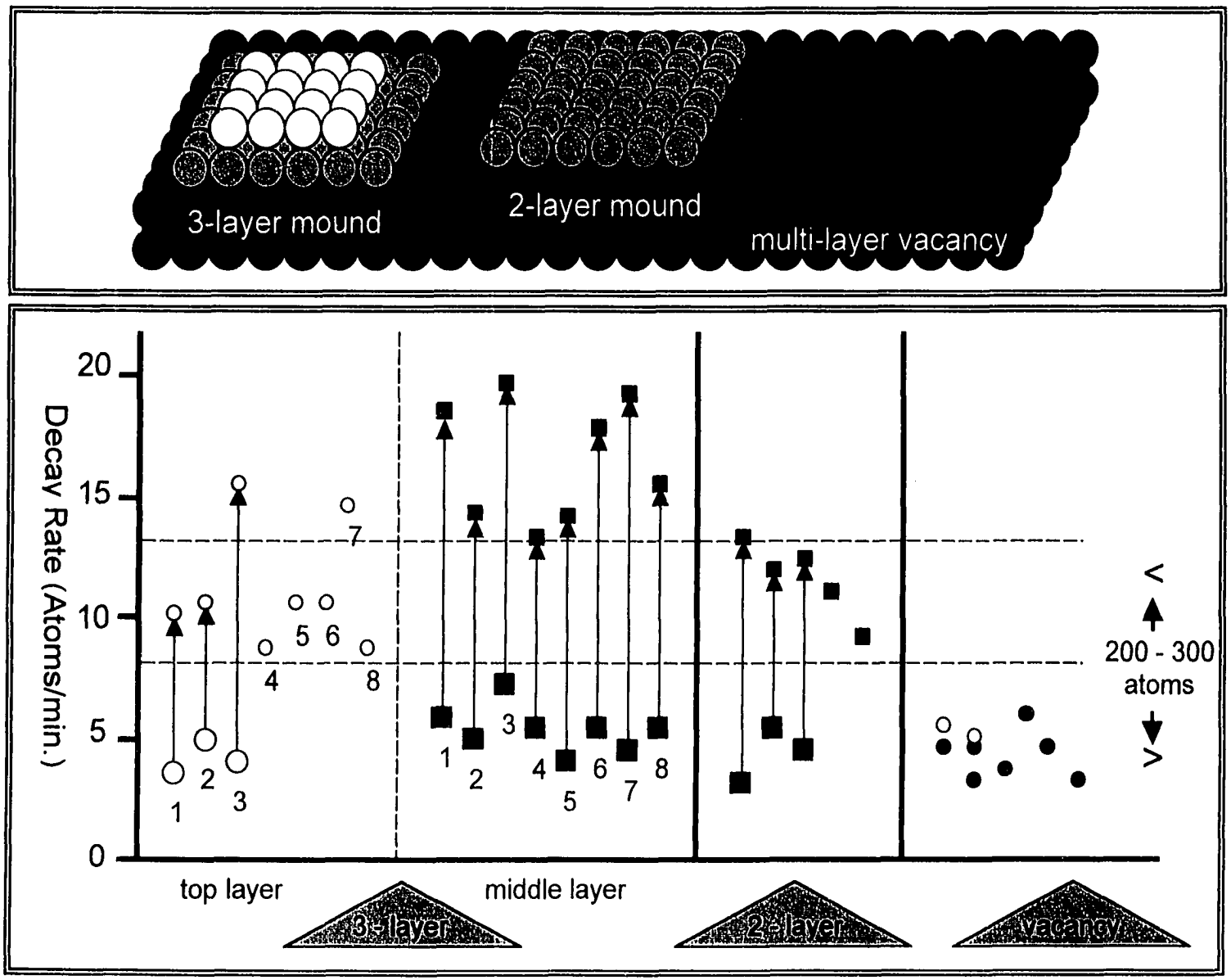
3-layer mound
2-layer mound
multi-layer vacancy
Decay Rate (Atoms/min.)
20
15
10
5
0
1
2
3
4
5
6
7
8
200 - 300
atoms
top layer
middle layer
3-layer
2-layer
vacancy

Figure 4

APPENDIX C. KINETIC ROUGHENING DURING Ag/Ag(100) HOMOEPITAXY BETWEEN 190K AND 300K

Our group has recently shown that multilayer growth of Ag films on Ag(100) is nontrivial and reasonably complex [1,2]. Ag films on Ag(100) do not grow in a layer-by-layer fashion due to the presence of a step edge barrier (Ehrlich Scwoebel barrier) that inhibits the depositing atoms from descending terrace steps. Rather, after the deposition of several ML, mounded type morphology is observed.

Characterization of the multilayer films is accomplished through examination of both the lateral and vertical morphologies of the surface. The vertical morphology provides information on the surface roughness of the films. Surface roughness (W) is characterized by the root mean square height difference between areas on the surface (see Fig. 1a). More simply stated, the roughness is a measure of the number of exposed surface layers. A simple expression relating roughness to coverage is:

$$W \sim \theta^{\beta} \qquad (1)$$

Where θ is the coverage and β is the roughening exponent with $0<\beta<1/2$.

The lateral morphology is described by the Height-Height correlation function H(r), which describes the mean-square height difference for two surface features (i.e. mounds), separated by some lateral distance (see Fig. 1b). The average distance between mounds (D_{av}) describes this lateral distance (Fig. 1c). The expression describing the lateral morphology with coverage is:

$$D_{av} \sim \theta^{n} \qquad (2)$$

Where θ is the coverage and n is the coarsening exponent.

To better understand the relationship between the vertical and lateral film morphology, direct comparisons between the two are made. For this, the idea of 'slope' is introduced (see Fig. 2a). The slope (S) of a surface mound is defined as the ratio of the roughness to the lateral distance.

$$S = W / D_{av} \tag{3}$$

Substituting equation (1) and (2) into equation (3) gives the following expression:

$$S = \theta^{\beta - n} \tag{4}$$

The slope can therefore be characterized by using the roughness and coarsening exponents. An increasing mound slope results when $\beta > n$. When $\beta \approx n$, the condition of slope selection is reached. Fig. 2(b) demonstrates slope selection behavior. When $\beta > n$, the initial mound growth is in the vertical direction, with the average distance between mounds changing very slowly. Upon achieving slope selection ($\beta \approx n$) the mounds begin to grow laterally as well as vertically.

Figs. 3(a-d) are STM images showing the change in surface morphology as the film coverage increases, for temperatures between 190 – 300 K. Roughness and coarsening analysis from the images are shown in Figs. 4(a) and (b) respectively. Roughness and coarsening exponent values are summarized in

Table I.

At 190 K it is observed that $\beta \approx n$. This signifies that at this temperature, slope selection is achieved early in the growth process. At higher temperatures, β is much larger than n. This implies that roughening proceeds faster than coarsening at these temperatures for coverages below 100 ML.. Theory describing slope selection states that when $\beta \approx 1/2$

and $n \approx 1/6$ slope selection is not active [3]. Results in Table I. are completely consistent with this statement.

References:

1. C. R. Stoldt, K. J. Caspersen, M. C. Bartelt, C. J. Jenks, J. W. Evans, P. A. Thiel, Phys. Rev. Lett., 2000, 85, 800-803.
2. K.J. Caspersen, C.R. Stoldt, A.R. Layson, M.C. Bartelt, P.A. Thiel, J.W. Evans, Phys. Rev. B **63**, 085401 (2001)
3. L.Golubovic, Phys. Rev. Lett. 78 (1997) 90

Table Caption:

I. Roughening and coarsening exponents for multilayer Ag films on Ag(100) between 190 and 260 K. Data for 300 K is not available due to poor statistical information from the STM images.

Figure Captions:

1. Descriptions for surface morphology analysis of Ag multilayer films.
   (a) Representation of the vertical morphology or roughness (W) which is described by root-mean-square of the differences in surface height.
   (b) Representation of the lateral morphology (distance between surface structures) which is described by the mean-square height difference (dh) for two surface features separated by some lateral distance (dr).
   (b) Cartoon showing D_{av}, the average distance between mounds on the surface. R_{av} is the average mound radius. $D_{av} = 2R_{av}$.
2. Mound slope selection. (a) Shows the relationship between roughness and mound size (distance) in determining the slope. $S = W / D_{av}$. (b) Cartoon depicting mound growth and eventual slope selection as the coverage (deposition time) increases. The initial lateral mound size stay fairly constant until the mound reaches the selected slope (dashed lines). Upon achieving slope selection, the lateral mound size grows as the mound increases in height.
3. STM images of multilayer Ag films on Ag(100) at (a) 190 K (b) 230 K (c) 260 K (d) 300 K. Ag coverages are shown in the figures. All images are 100 x 100 nm^2.

4. (a) Roughness versus Ag coverage for 190 – 300 K. A linear fit to the data provides the roughening exponent _. Corresponding _ values are shown in the lower right corner. (b) Mound separation (D_{av}) versus Ag coverage for 190, 230 and 260 K. A linear fit to the data provides the coarsening exponent n. Corresponding n-values are shown in the lower right corner. Data for 300 K is not available. The relatively large distance between mounds results in a low number of mounds per STM image, providing limited statistics for D_{av} at this temperature.

Temperature (K)	β	n
190	0.37	0.40
230	0.40	0.18
260	0.50	0.10

Table I

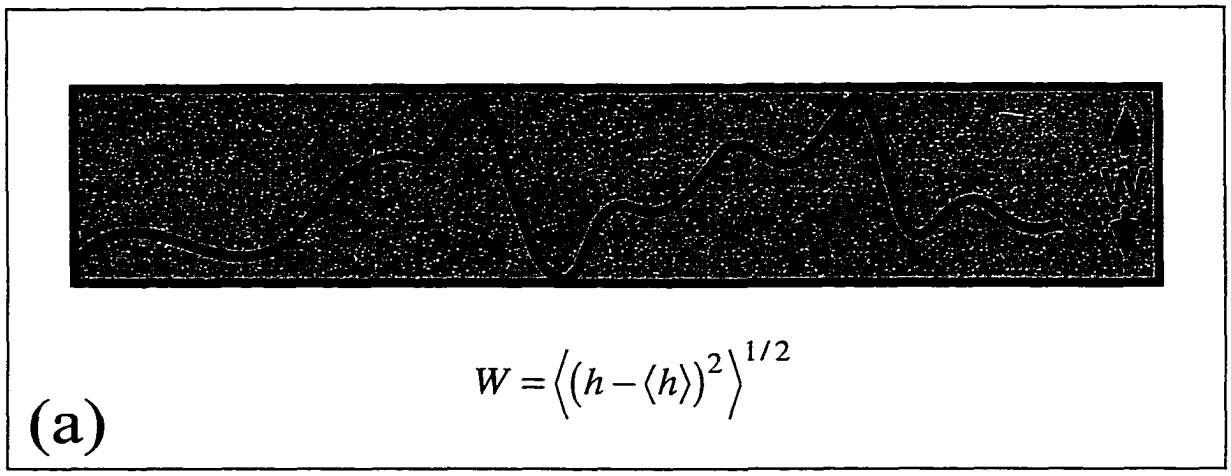

$$W = \left\langle \left(h - \langle h \rangle\right)^2 \right\rangle^{1/2}$$

(a)

$$H(dr) = \left\langle \left(h(r) - h(r+dr)\right)^2 \right\rangle$$

(b)

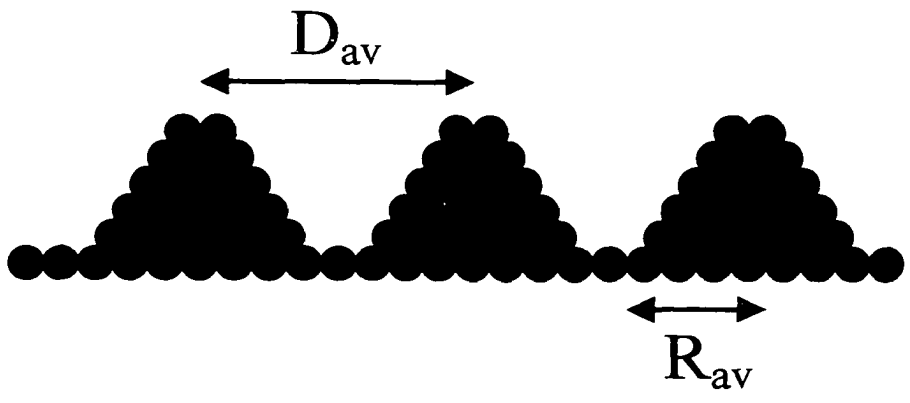

(c)

Figure 1

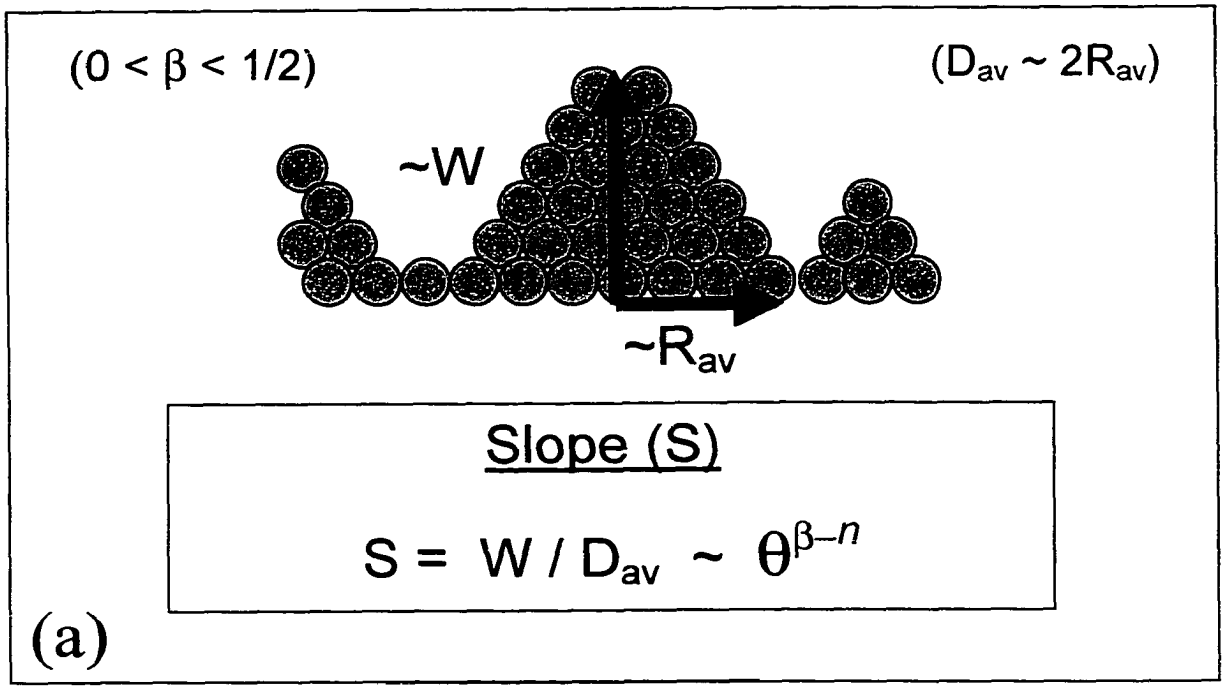
(0 < β < 1/2)
(D_av ~ 2R_av)
~W
~R_av
Slope (S)
S = W / D_av ~ θ^(β–n)
(a)

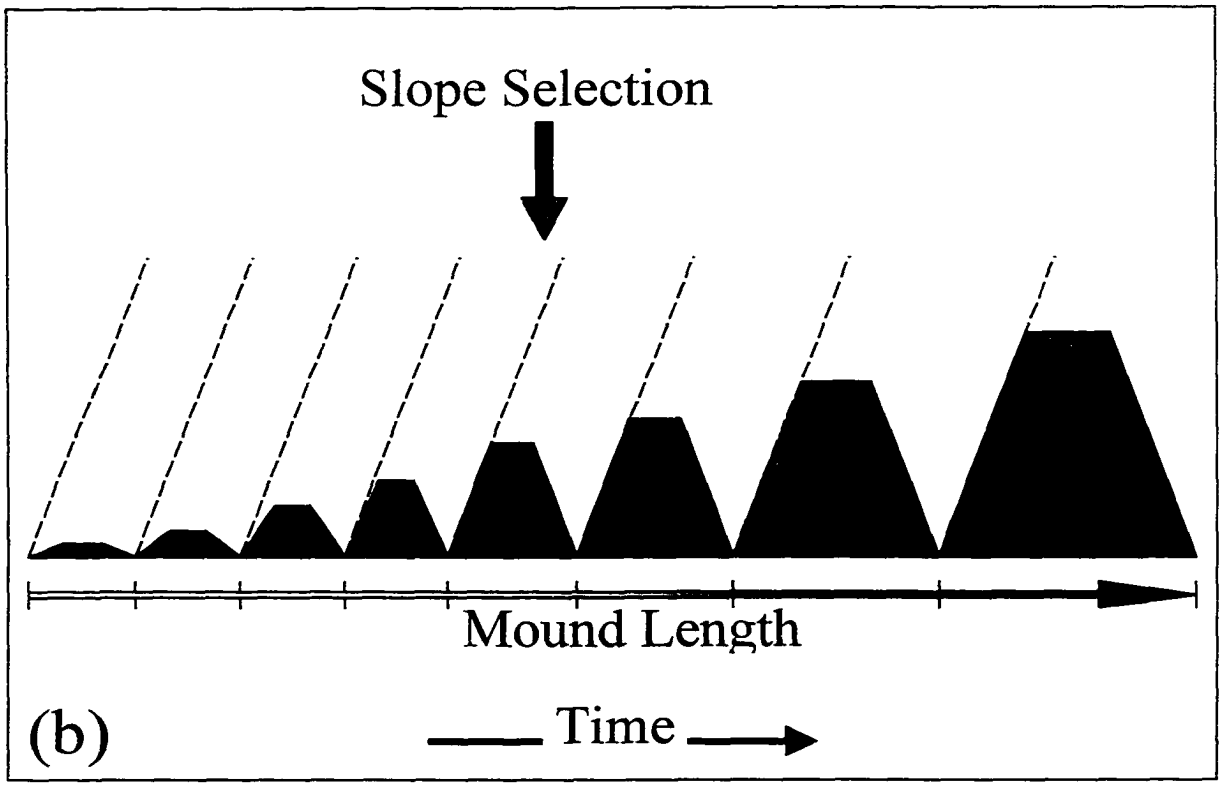
Slope Selection
Mound Length
(b)
Time

Figure 2

(a)

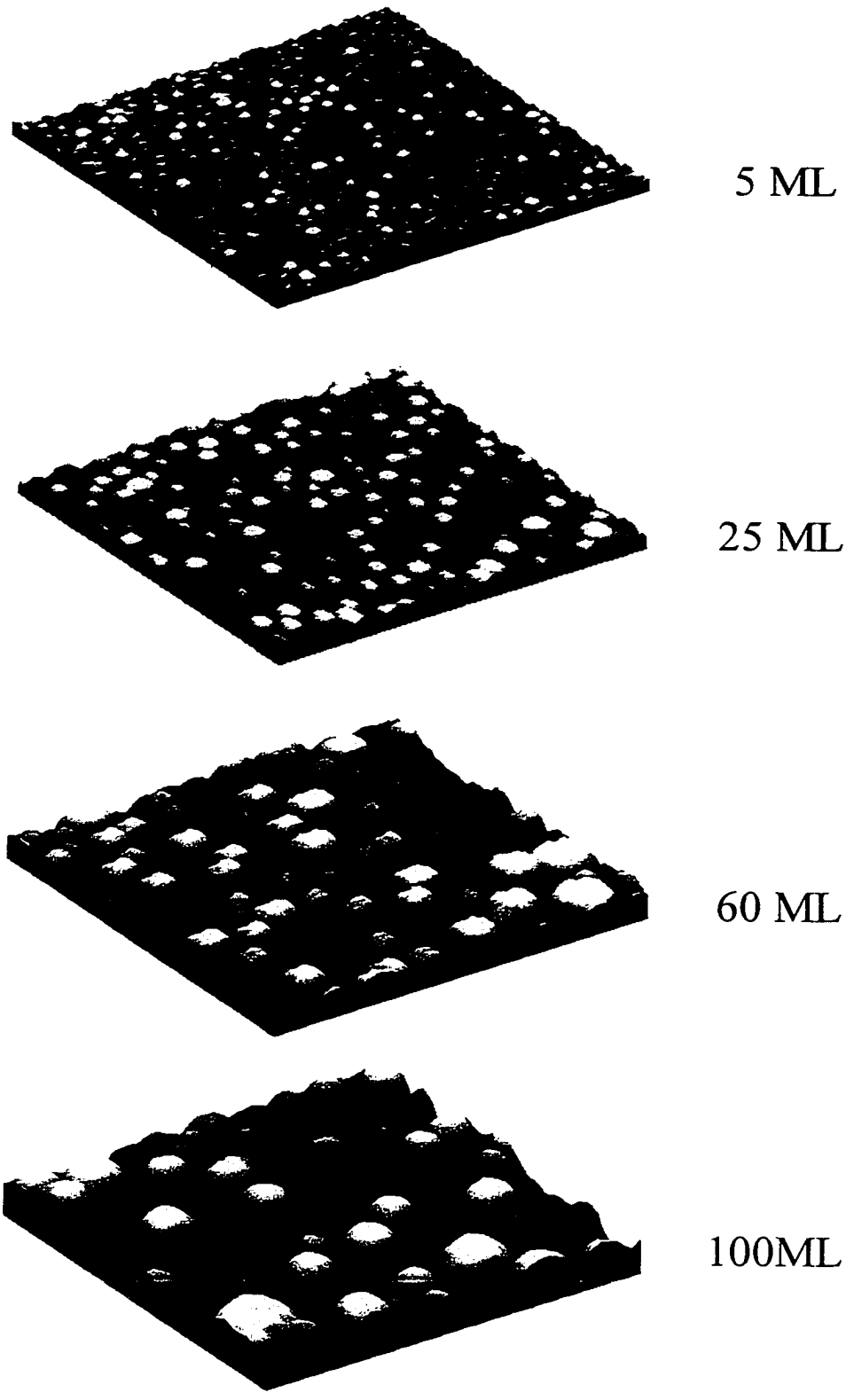

Figure 3

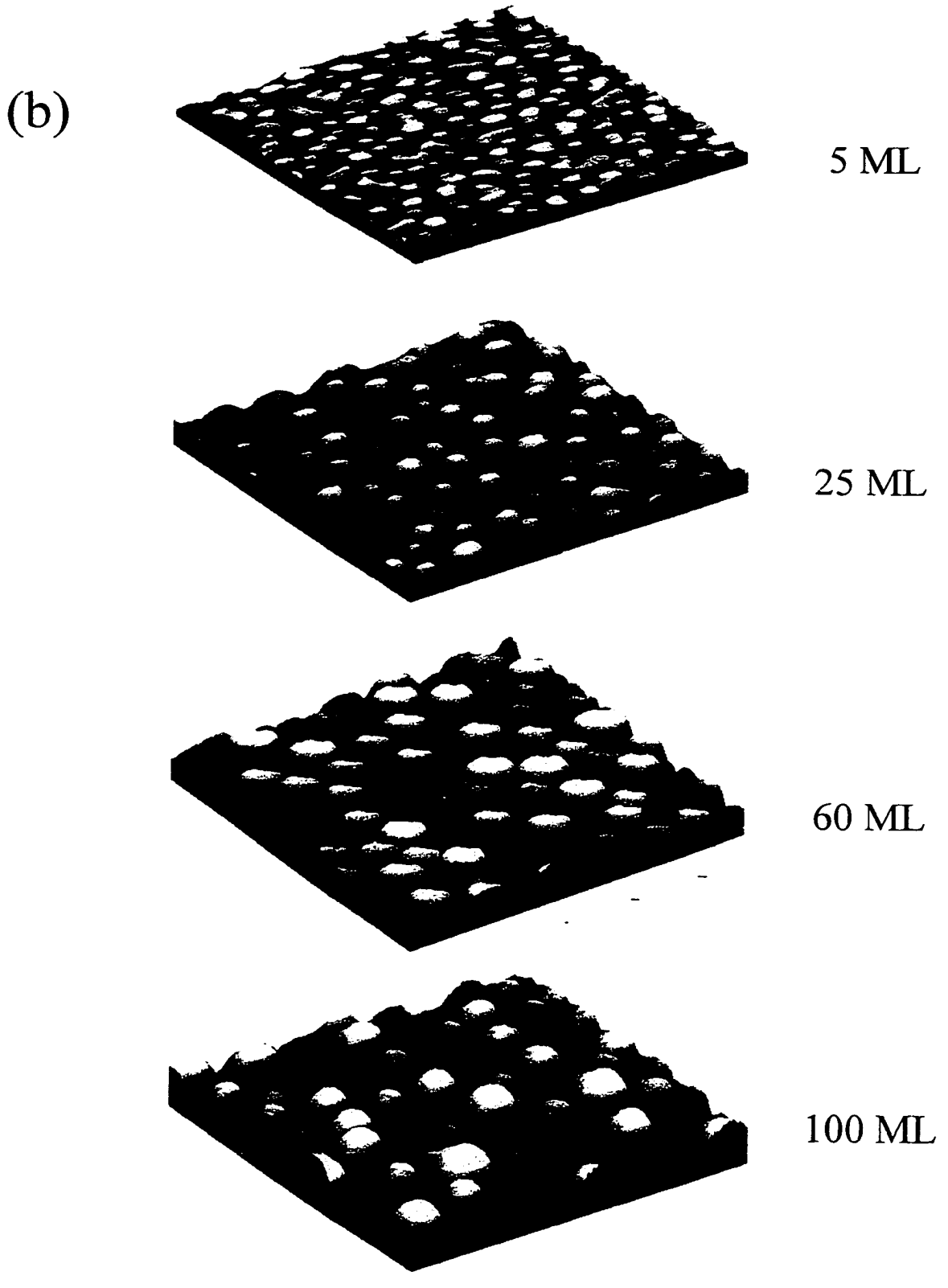

Figure 3

(c)

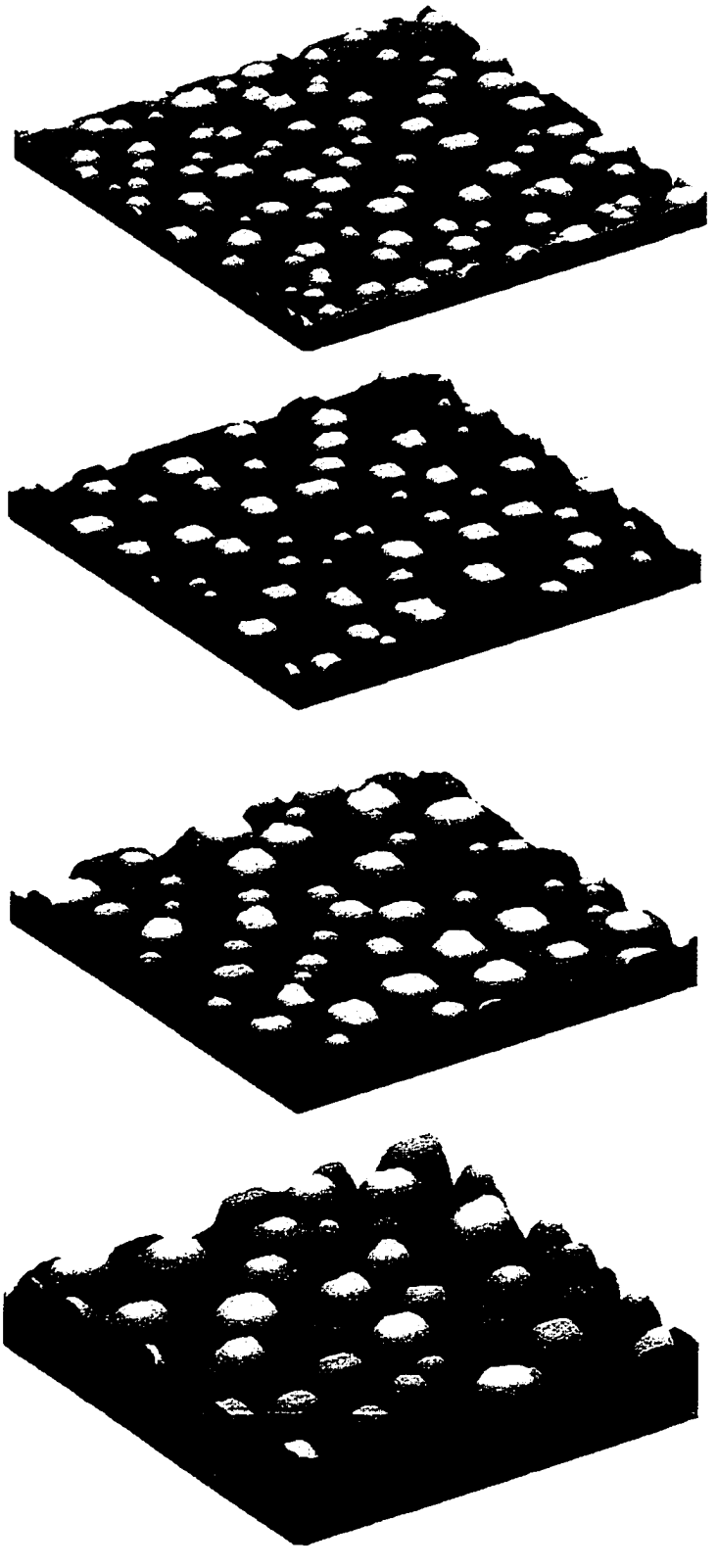

Figure 3

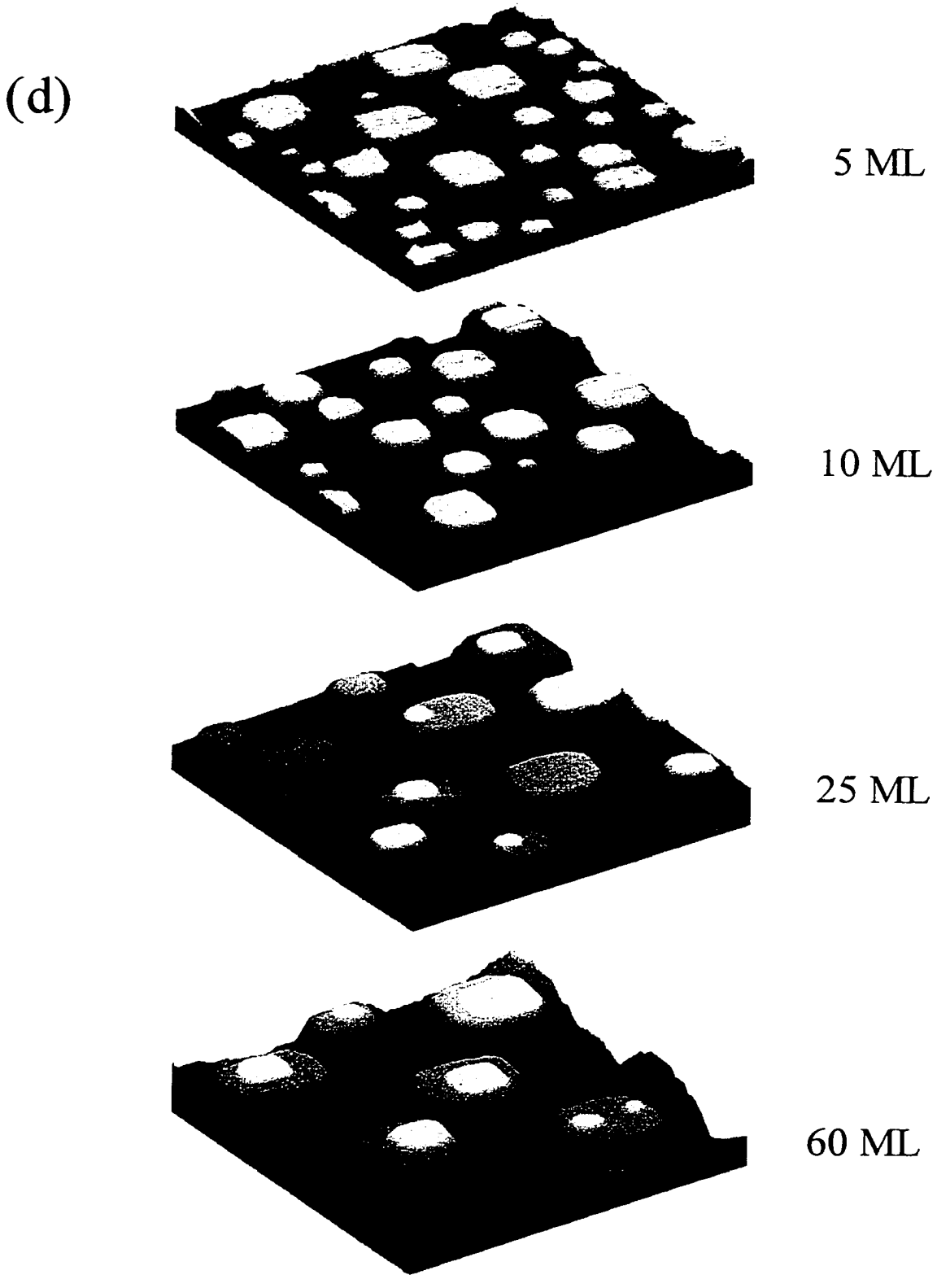

Figure 3

(a)

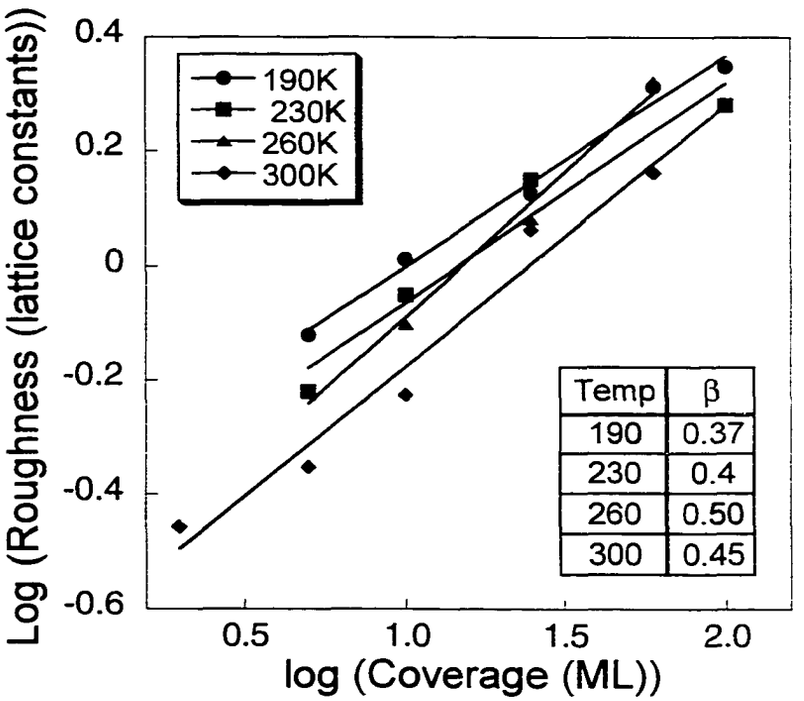
Log (Roughness (lattice constants))
log (Coverage (ML))
190K
230K
260K
300K
Temp | β
190 | 0.37
230 | 0.4
260 | 0.50
300 | 0.45

(b)

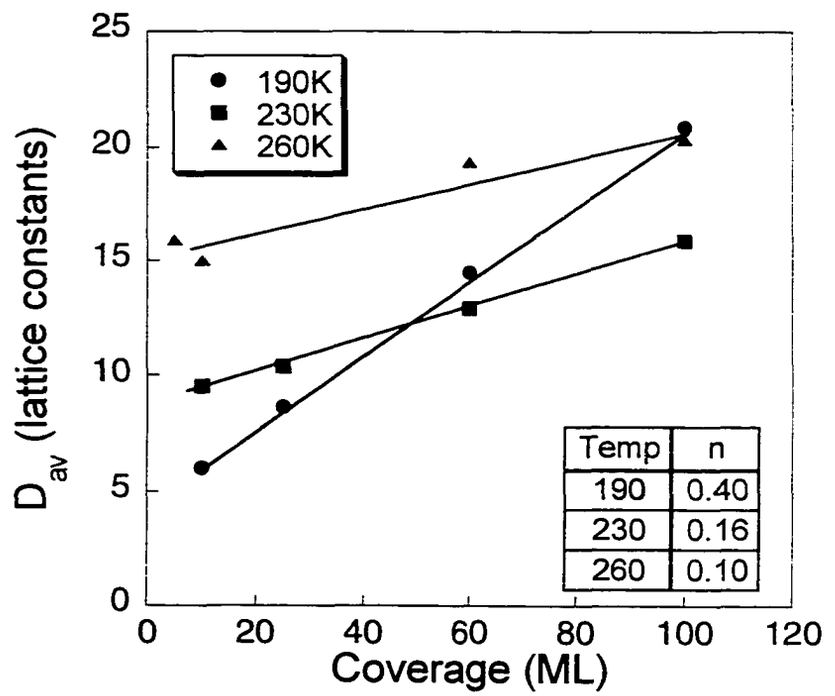
D_av (lattice constants)
Coverage (ML)
190K
230K
260K
Temp | n
190 | 0.40
230 | 0.16
260 | 0.10

Figure 4

APPENDIX D. THE STUDY OF MULTILAYER Ag FILMS ON Ag(100) USING HIGH RESOLUTION LOW ENERGY ELECTRON DIFFRACTION

In contrast to X-ray diffraction techniques, which provides information on the bulk positions of atoms in a crystal, low energy electrons probe only those atoms at or near the crystal surface. By examining the array of low energy electron diffraction spots, information on the relative positions of the surface atoms can be discerned.

Because diffraction is a reciprocal space technique, analyzing the pattern of many spots (ie. observation of large areas in reciprocal space) provides information over very small areas in real space (ie. atomic positions). Conversely, by focusing on a small area in reciprocal space, for instance a single spot in the diffraction pattern, information can be gathered for very large areas in real space. High Resolution Low Energy Electron Diffraction (HRLEED) is a technique in which data from a single diffraction spot can be used to elucidate information on surface structure. Fig. 1(a) diagrams a typical HRLEED instrument. Electrons scattered from the crystal surface are scanned over the detector by a set of deflection plates. Fig 1(b) shows a typical LEED pattern for Ag(100). The high resolution capabilities of the instrument allows for closer examination of an individual diffraction spot, which is observed in Fig. 1(c). By observing changes in spot shape and intensity, information on large-scale structures, such as islands and mounds, can be gathered. HRLEED, therefore, proves to be a very useful technique in the studying the growth and evolution of surface structures.

In chapter one, we showed that HRLEED could be used to monitor the growth and evolution of submonolayer Ag islands on Ag(100). The exact same techniques can be used

to monitor mulitlayer mound structures as well. Fig. 2 demonstrates how HRLEED is used to gather such information. Fig. 2(a) shows a clean Ag(100) surface, with several monatomic terrace steps. The resultant 2-D spot profile (Fig. 2b) shows the symmetrical round spot typical of a clean surface. A 1-D cross section of this spot (fig.1c) reveals a sharp gaussian shaped peak profile. Fig. 2(d) shows a Ag(100) surface after deposition of 0.3 ML of Ag. Small 2-D square islands now decorate the terraces observed in Fig. 2(a). The 2-D spot profile of this surface shows the central spot surrounded by a diffuse ring (Fig. 2e). The 1-D cross section (Fig. 2f) clearly shows the central peak, flanked on either side by satellite peaks that represent the ring in the 2-D plot. The diameter of the ring (d*) is inversely proportional to the 'average' distance between islands on the surface in real space. This distance is termed the correlation length. This correlated distance is not relegated to measurements of submonolayer islands only. Monitoring the 1-D ring structure also provides information on the average lengths between larger structures, such as multilayer mounds.

For the submonolayer islands, after exposure to oxygen, coarsening was monitored by observing the change in the ring diameter (d*) with time. Multilayer mound coarsening can also be monitored a similar way. By measuring d* as a function of Ag coverage, the average mound separation can be determined. Mulitlayer coarsening scales by the simple relation:

$$D_{av} \sim \theta^{n} \qquad (1)$$

Where D_{av} is the average mound separation and n is the coarsening exponent. By plotting mound separation versus Ag coverage, the coarsening exponent can be determined. Figs. 3 and 4 show coarsening data for mulitlayer films at 190 and 220 K.

Fig. 5 shows a plot for 25 ML Ag films on Ag(100) at various temperatures, as the energy of the incident electrons is changed from the in-phase to the out-of-phase conditions. At the in-phase condition, all electrons scattered from the surface interfere constructively. However, the information gained here is limited because in-phase condition is insensitive to surface structure. At the out-of-phase condition, upon diffraction, electrons from adjacent layers on the surface interfere destructively. Therefore, the out-of-phase condition is sensitive to surface structure, this being observed in the resulting ring in the spot profiles. Fig. 5 shows how the known changes in surface structure (roughness), after Ag deposition at different temperatures, affects the spot profiles. At temperatures below 240 K, the out-of-phase energy condition is not reached before the intensity of the spot becomes zero, and the spot is no longer observed.

Figure Captions:

1. (a) Diagram of a typical HRLEED instrument. (b) LEED pattern for Ag(100). (c) 2-D spot profile of the specular (0,0) reflection. The transfer width of this instrument is ≈ 1000 Å.
2. Demonstration of how HRLEED is used to monitor surface structures on Ag(100). (a) Clean Ag(100) surface. (b) and (c) Respective 2-D and 1-D profiles for the surface shown in (a). (d) Ag(100) after deposition of 0.3 ML Ag. (e) and (f) Respective 2-D and 1-D profiles for the surface shown in (e). The ring diameter (d*) is inversely proportional to average distance, between surface structures, indicated by the solid line in (d).
3. Family of 1-D spot profiles for various Ag coverages at 220 K. The intensity for all profiles is normalized for comparison. The calculated island and mound separation lengths (correlation length, L_c) are shown to the right of each profile. The deposition flux = 0.006 ML/sec. The beam energy = 110.4 eV.
4. Correlation length (Lc) versus coverage at (a) 220 K and (b) 190 K. The resultant slope gives values for the coarsening exponent (n). The exponent in (a) 0.19 and (b) 0.23. Data points in (a) were collected in a single experiment after sequential deposition of Ag from 0 – 13.5 ML. Data points in (b) were collected in separate experiments. The deposition flux = 0.006 ML/sec. The beam energy = 110.4 eV.
5. Spot profile Intensity of the (0,0) reflection as the beam energy is changed from the in-phase to the out-of-phase condition for 25 ML Ag films deposited at various temperatures. In-phase energy ~ 140.0 eV, out-of-phase energy ~ 110.4 eV.

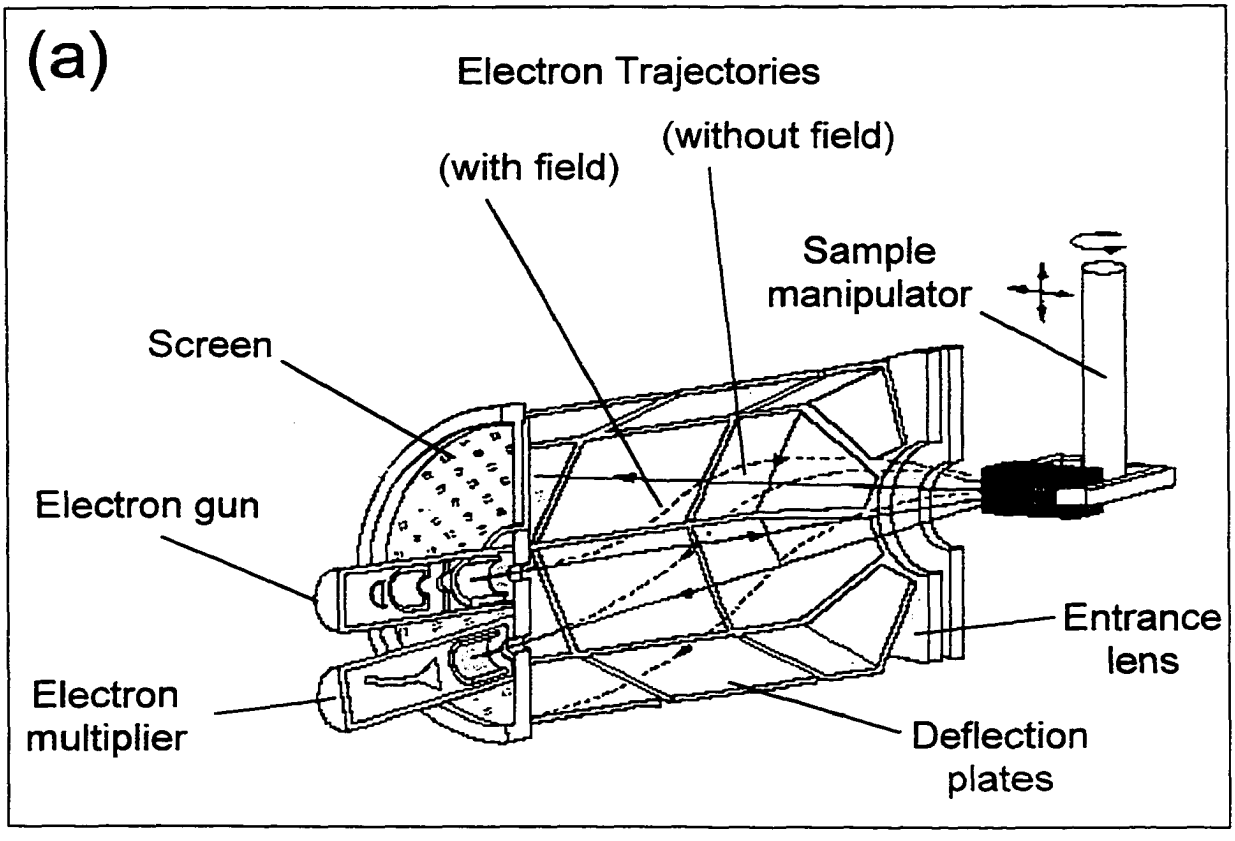
(a)
Electron Trajectories
(without field)
(with field)
Sample
manipulator
Screen
Electron gun
Entrance
lens
Electron
multiplier
Deflection
plates

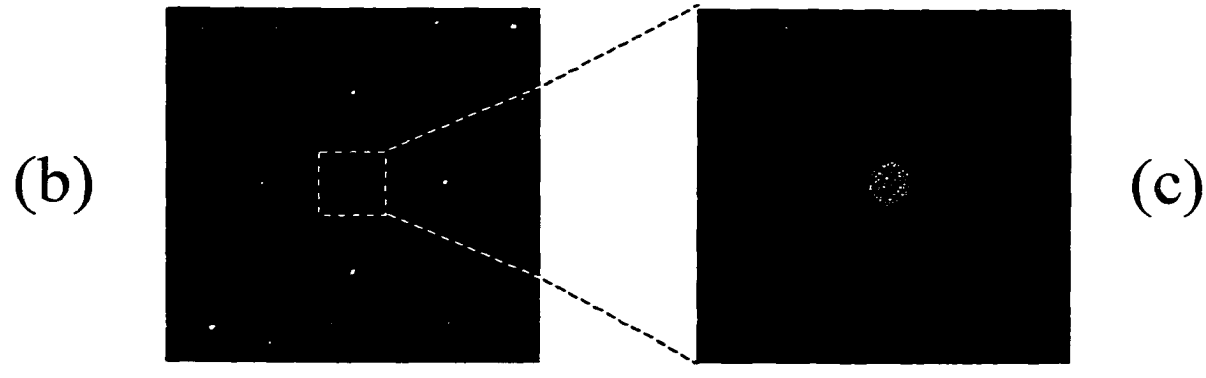
(b)
(c)

Figure 1

(a)

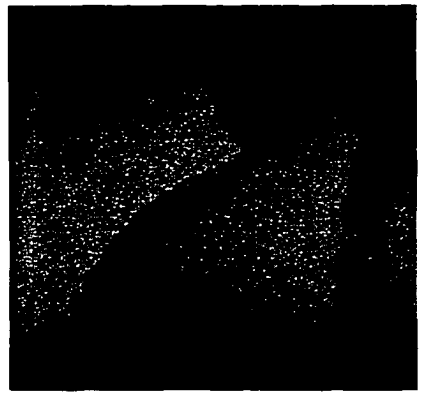

(b)

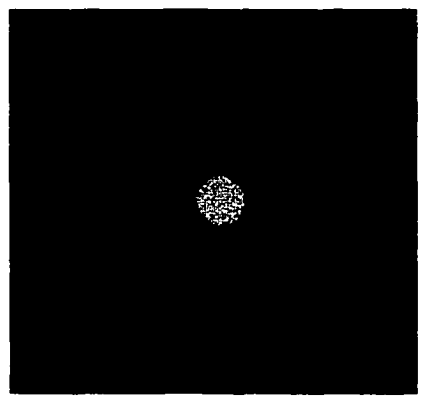

(c)

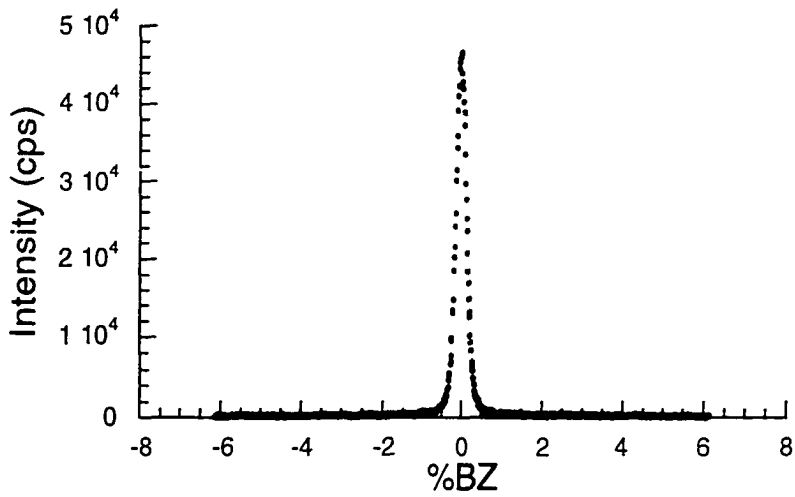

Figure 2

(d)

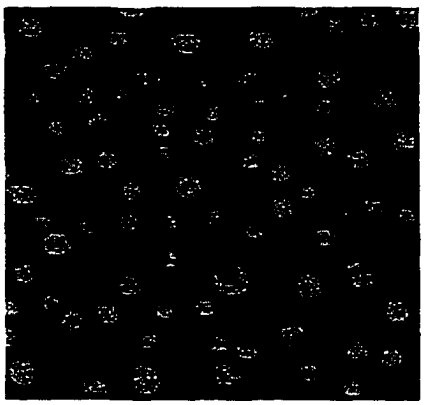

(e)

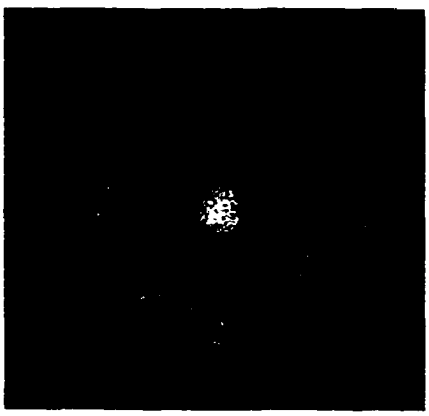

(f)

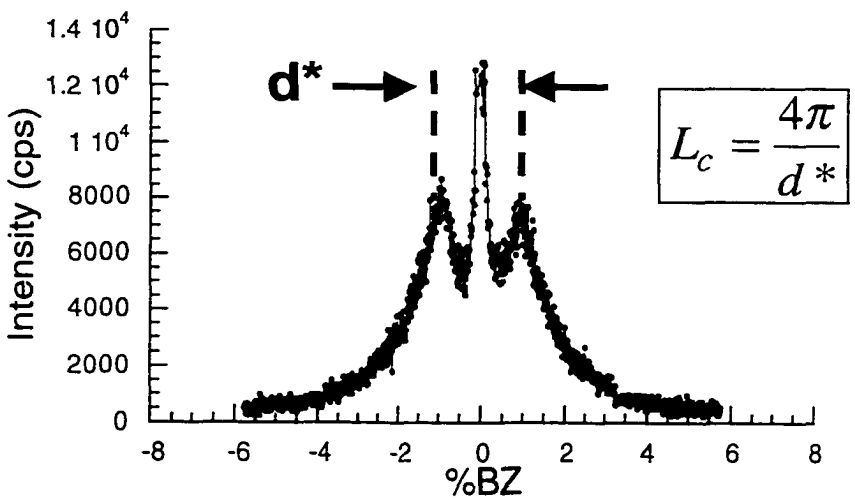
1.4 10^4
1.2 10^4
1 10^4
8000
6000
4000
2000
0
Intensity (cps)
d*
-8
-6
-4
-2
0
2
4
6
8
%BZ
$L_c = \frac{4\pi}{d*}$

Figure 2

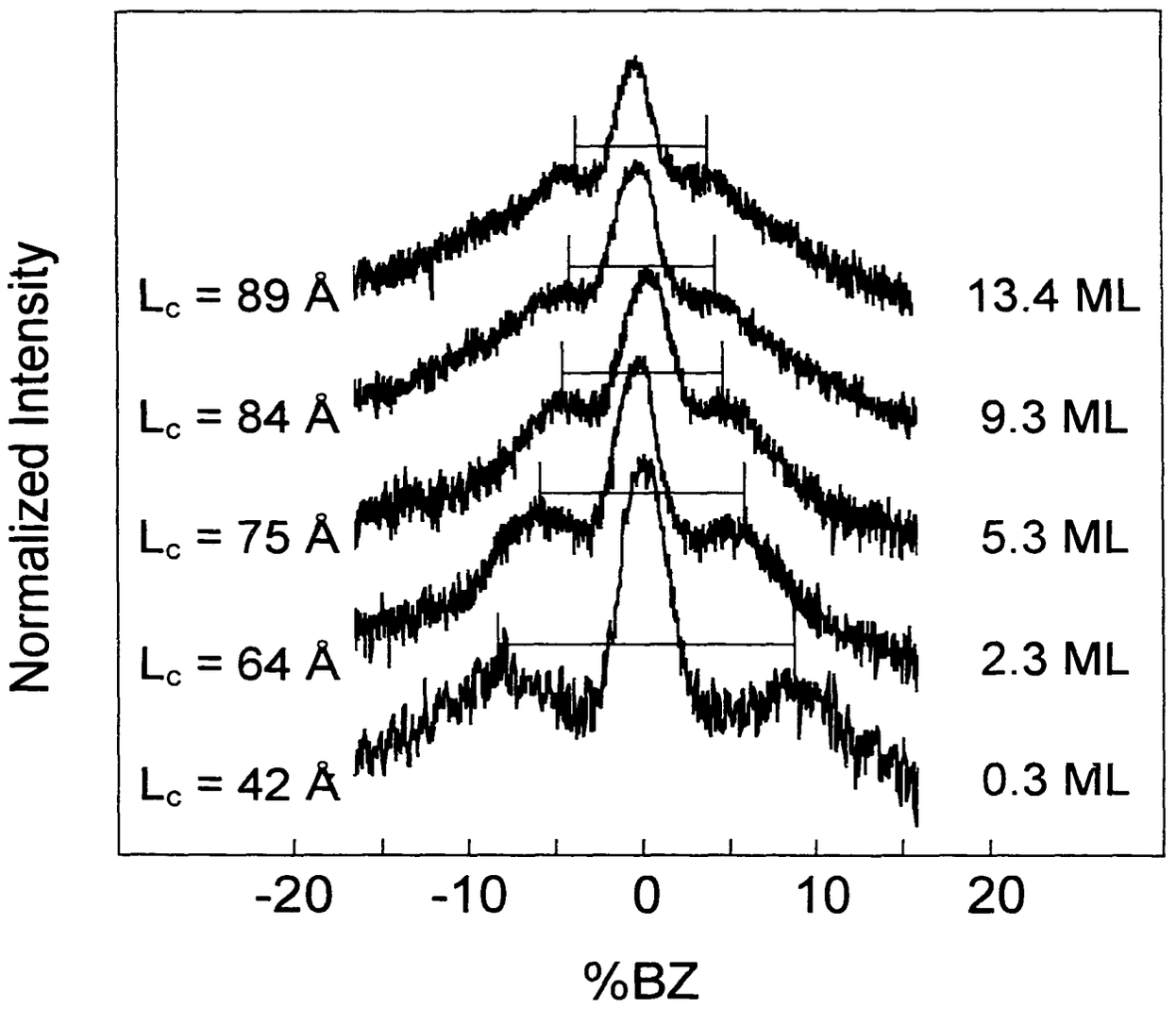
Normalized Intensity
L_c = 89 Å
13.4 ML
L_c = 84 Å
9.3 ML
L_c = 75 Å
5.3 ML
L_c = 64 Å
2.3 ML
L_c = 42 Å
0.3 ML
-20
-10
0
10
20
%BZ

Figure 3

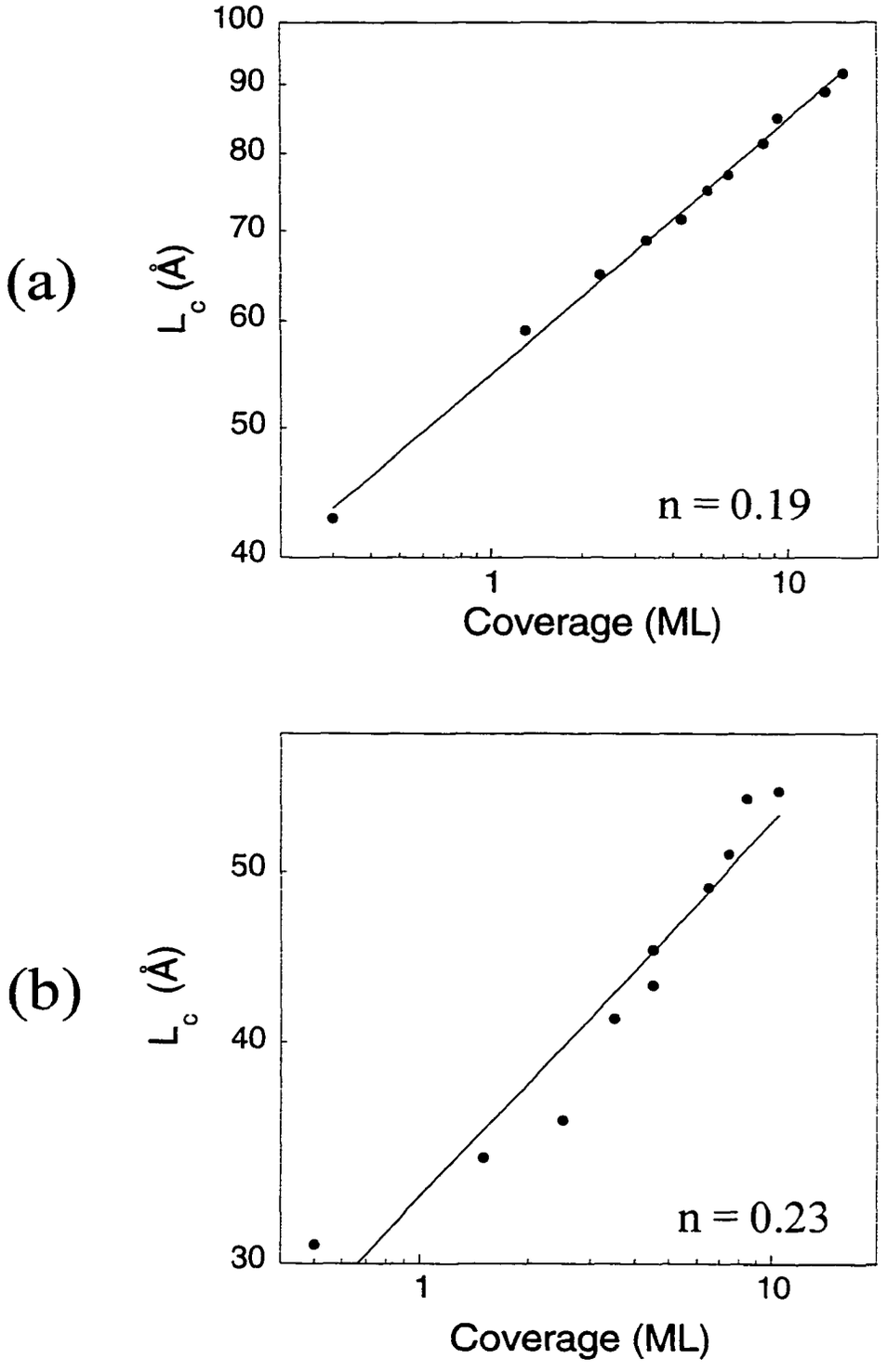
(a)
100
90
80
70
60
50
40
L_c (Å)
n = 0.19
1
10
Coverage (ML)
(b)
50
40
30
L_c (Å)
n = 0.23
1
10
Coverage (ML)

Figure 4

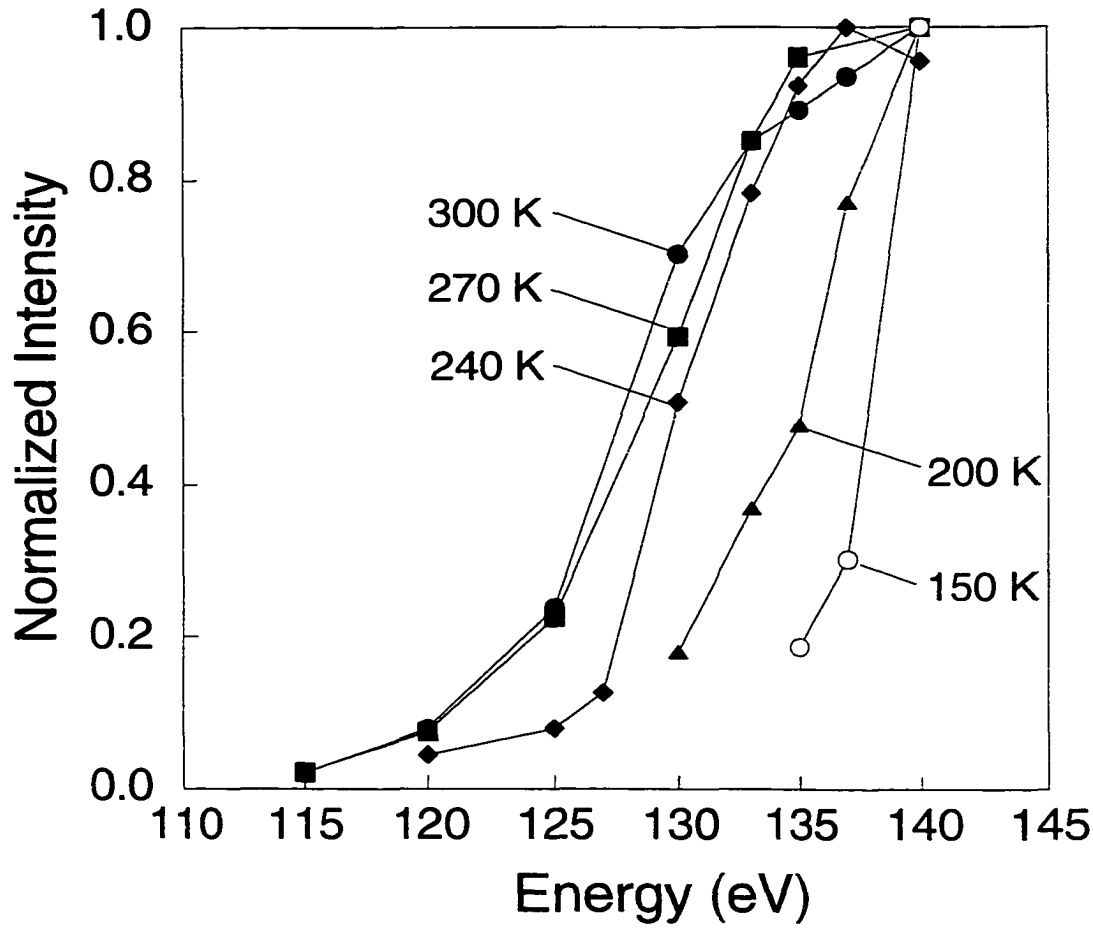
1.0
0.8
0.6
0.4
0.2
0.0
Normalized Intensity
300 K
270 K
240 K
200 K
150 K
110
115
120
125
130
135
140
145
Energy (eV)

Figure 5

APPENDIX E. FILM GROWTH ON AN ANISOTROPIC SURFACE: SUBMONOLAYER AND MULTILAYER Ag FILMS DEPOSITED ON Ag(110)

The vast majority of studies dealing with homoepitaxial nucleation, growth, and evolution of metallic thin films have focused on isotropic surfaces. Studies of such surfaces were a logical starting point due to the atomic arrangement and relative interaction energies being equal in all directions in the surface plane. Much less studied are anisotropic surfaces where the arrangement of surface atoms, and the relative energies, is not the same in all directions. Here we present preliminary results for homoepitaxial growth on an anisotropic Ag(110) surface.

The Ag(110) surface has long history and has been well documented in its use as a catalyst in epoxidation reactions [1-3]. Until recently, however, studies into growth and evolution of Ag nanostructures on this surface have not enjoyed the same level of attention. Several recent experimental studies have focused on the evolution and manipulation of surface step structure with time [4-6]. The use of STM in the decay analysis of submonolayer Ag(110) islands, has resulted in a better understanding of the atomic diffusion processes on this surface [7,8]. Multilayer studies on Ag(110) revealed a 'mound rotation' effect with deposition at very cold temperatures [9]. Finally, Monte Carlo simulations have been performed to examine the nucleation and growth characteristics of submonolayer islands [10,11]. To date, however, *experimental* studies into nucleation and growth of Ag(110) submonolayer islands have yet to be thoroughly examined.

The Ag(110) surface offers several advantages in the study of anisotropic materials. Unlike the (110) surfaces of Au [12] and Pt [13], Ag(110) does not undergo a surface

reconstruction. It is therefore possible to examine true (110) atomic interactions. Second is the relative ease for Ag film deposition. Where evaporation of refractory materials such as Ir, Pd or Pt, is very difficult due to high melting points and low vapor pressures, Ag evaporation is relatively simple.

One notable disadvantage, however, exists when studying surface structures on Ag(110). Due to the atomic arrangement of the (110) surface, atomic diffusion events are very fast. As a result, island coarsening on this surface is extremely rapid. At room temperature, islands can decay and disappear in a matter of minutes. This makes analysis, such as island density studies or island evolution studies with time, very difficult to follow at temperatures above ~ 220 K. Even at temperatures around 175 K, decay is noticeable on a time scale of minutes. Careful preparation and efficient experimental procedures are a must when working with this surface.

Fig. 1 shows a representation of a (110) surface. The atomic arrangement is such that a 'row and trough' structure is observed with rows oriented in the [110] direction. Surface islands, such as in Fig 1(a) are rectangular in shape, with the major axis oriented in [110] direction. Fig. 2 shows several high resolution STM images where the row and trough structure can be observed in the island and terrace step structure on Ag(110).

Two distinct submonolayer island nucleation experiments are shown. The first (shown in Fig. 3) monitors the initial island density as a function of temperature, with a constant deposition flux. The corresponding Arrhenius plot is shown in Fig. 3(b). The second (shown in Fig. 4 for two different temperatures) monitors the initial island density as a function of deposition flux, at constant temperature. Plots of island density versus deposition flux, for the two experiments, are shown in Figs. 4(b) and (d) respectively.

Fig. 5 shows 25 ML films deposited at different temperatures ranging from 175 – 260K. As expected, the mound structure differs greatly with temperature. At 260 K, mounds exhibit long, flat and broad terrace structure, where at colder temperatures mound are smaller and more compact. At all temperatures, the anisotropy in the mound structure is clearly evident. Comparison of the mound structure with temperature is more easily seen in Fig. 6.

References:

1. C. Backx, C.P.M. de Groot, P. Biloen, Surf. Sci. 104 (1981) 300
2. R.A. Vansanten, C.P.M. de Groot, Journal of Catal. 98 (1986) 530
3. R.A. van Santen, H.P.C.E. Kuipers, Adv. Catal. 35 (1987) 265
4. J. Li, R. Berndt, W-D. Schneider, Phys. Rev. Lett. 76 (1996) 1888
5. R. Kock, J.J. Schulz, K.F. Rieder, Europhys. Lett. 48 (1999) 554
6. J.S. Oscomert, W.W. Pai, N.C. Bartelt, J.E. Reutt-Robey, Surf. Sci. 293 (1993) 183
7. K. Morgenstern, E. Lægsgaard, I.Stensgaard, F. Besenbacher, Phys. Rev. Lett. 83 (1999) 1613
8. K. Morgenstern, E. Lægsgaard, I.Stensgaard, F. Besenbacher, M. Böhringer, W.-D. Schneider, R. Berndt, F. Mauri, A. De Vita, R. Car. Appl. Phys. 69 (1999) 559
9. F. Buatier de Mongeot, G. Constantini, C. Boragno, U. Valbusa, Phys. Rev. Lett. 84 (2000) 2445
10. C. Mottet, R. Ferrando, F. Hontinfinde, A.C. Levi, Surf. Sci. (1998) 220
11. R. Ferrando, F. Hontinfinde, A.C. Levi, Phys. Rev. B 56 (1997) R4406
12. E. Carlon, H. van Beijeren, Phys. Rev. Lett. 76 (1996) 4191
13. H.T. Lorensen, J.K. Nørskov, K.W. Jacobsen, Phys. Rev. B 60 (1999) R5149

Figure Captions:

1. The Ag(110) surface. (a) '3-D' view (b) Side view (c) Top view (d) Atomic resolution STM (28 x 39 nm^2). Inter-atomic distances for the [110] and [100] directions are labeled in (b).
2. High resolution STM images on Ag(110) at 160 K. (a) Submonolayer islands on (110) terrace (50 x 50 nm^2). (b) Submonolayer islands and [100] terrace step (65 x 65 nm^2).
3. Island density as a function of temperature. (a) STM images showing Ag islands at various temperatures. (b) Arrhenius plot for the Island density. The flux for all images was 0.045 ML/sec. All images are 100 x 100 nm^2.
4. Island density as a function of deposition flux. STM images of Ag islands for various flux values at (a) 175 K and (c) 205 K. Plots for island density versus deposition flux at (b) 175 K and (d) 205 K. All images are 100 x 100 nm^2.
5. Time evolution for 25 ML Ag films on Ag(110) at: (a) 175 K (b) 205 K (c) 260 K. Deposition flux is 0.045 ML/sec. for all temperatures. All images are 100 x 100 nm^2.
6. STM images illustrating mound size and structure for 25 ML Ag/Ag(110) just after deposition at various temperatures. All images are 100 x 100 nm^2.

(a)

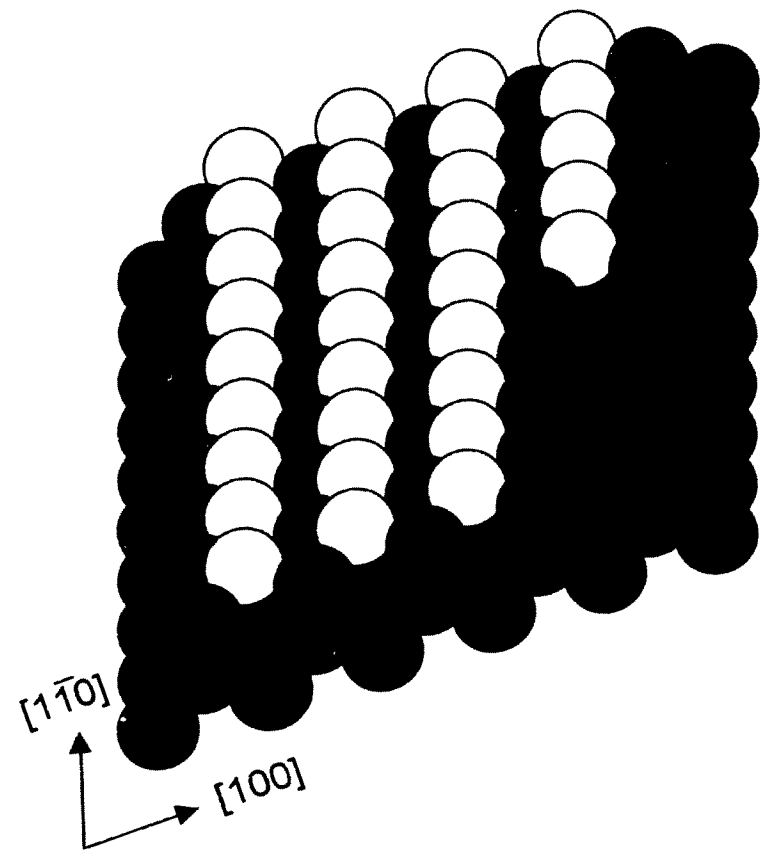

(b)

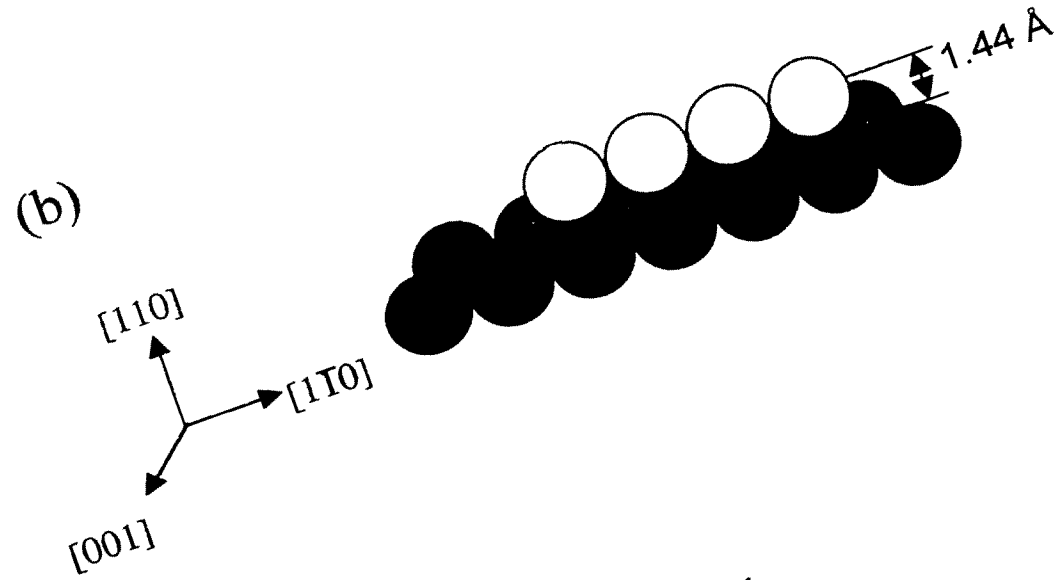

Figure 1

(c)

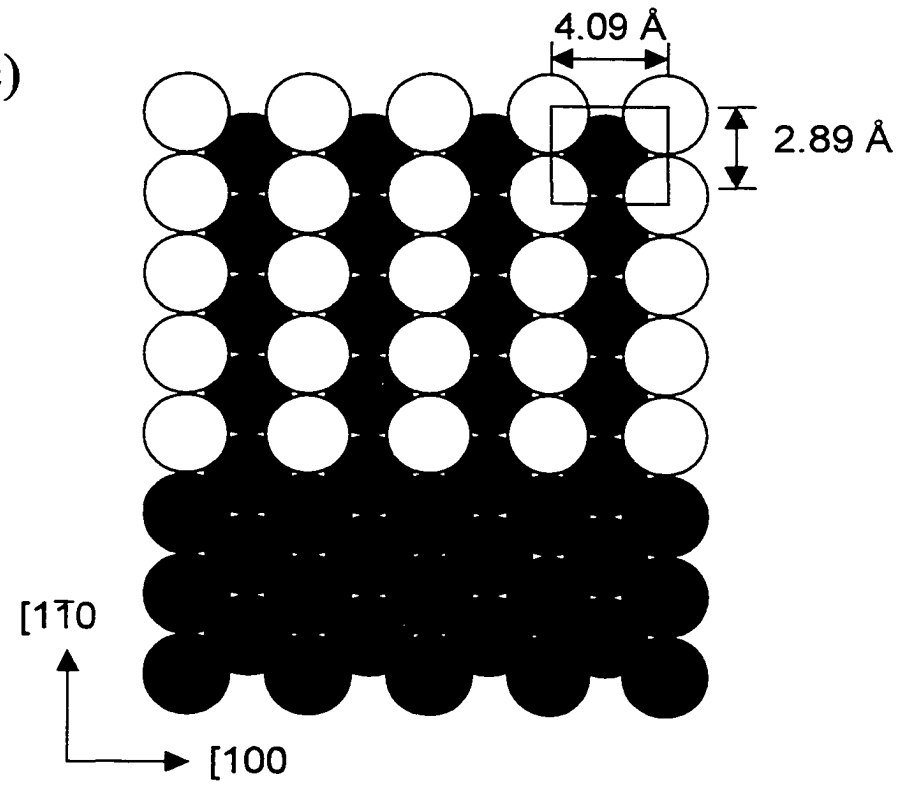

(d)

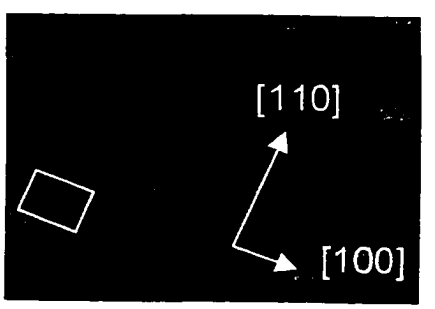

Figure 1

(a)

(b)

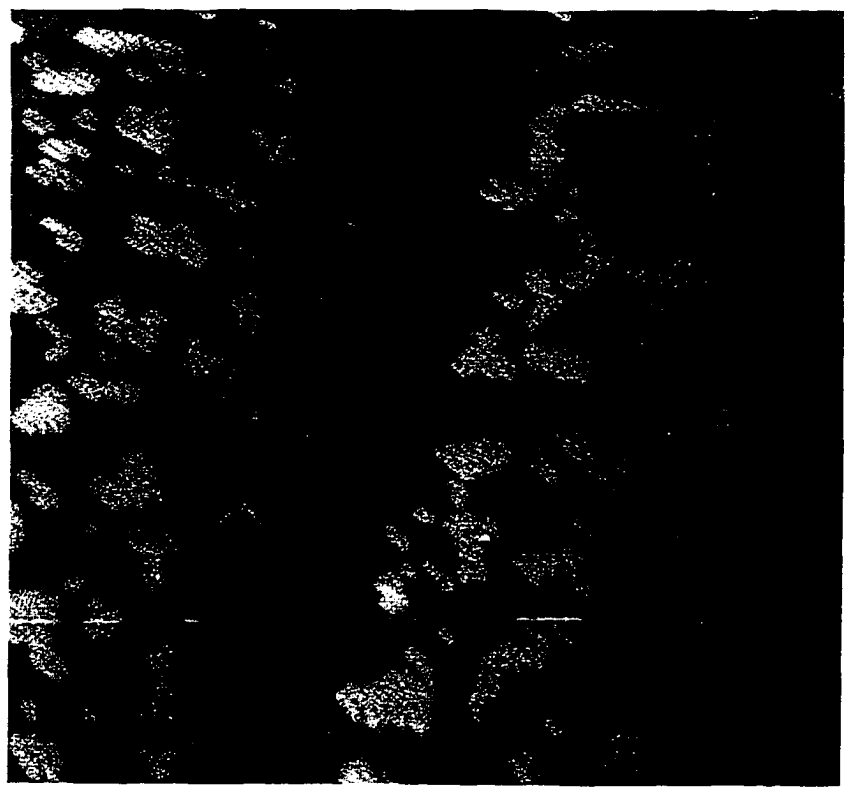

Figure 2

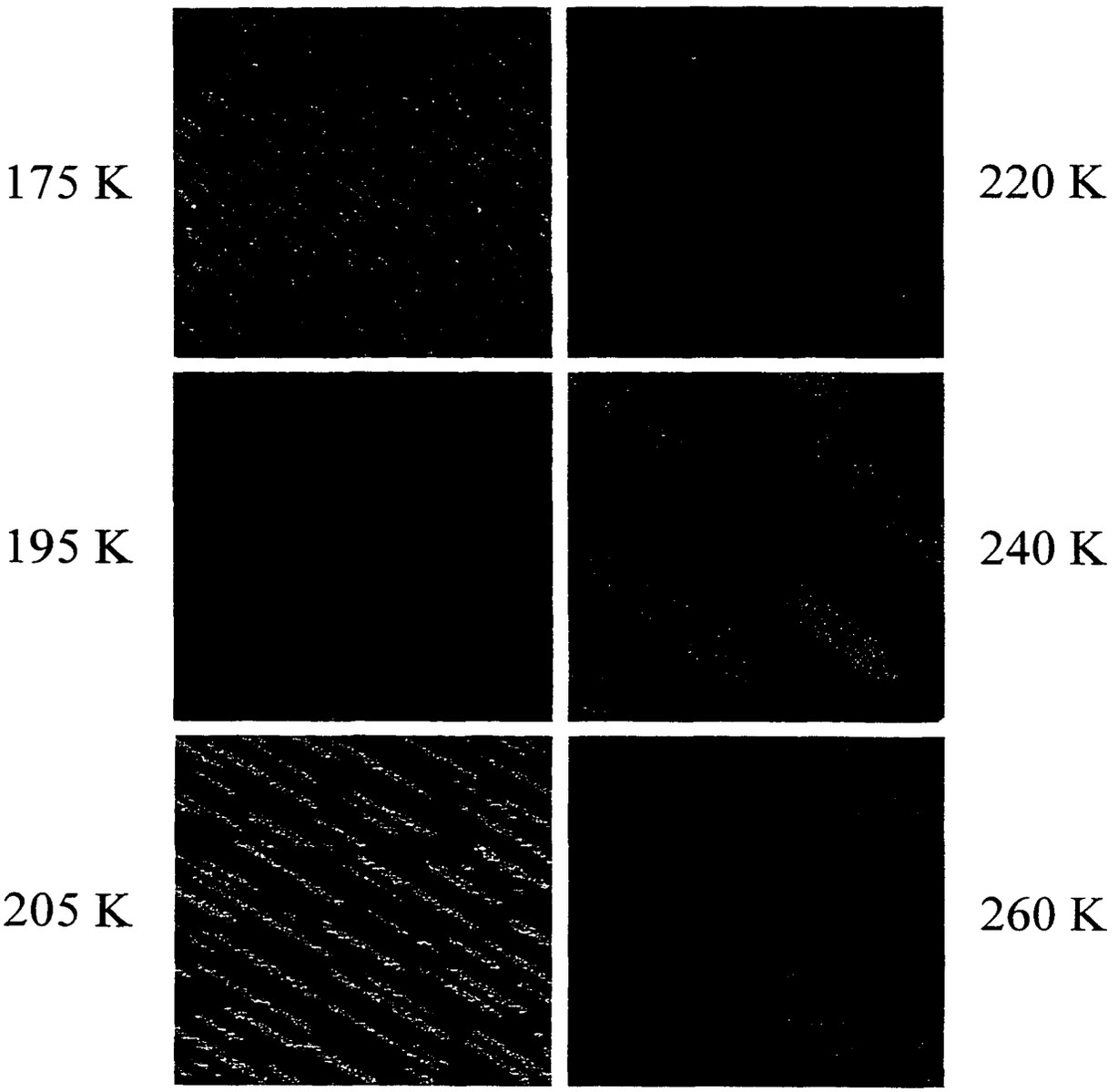

(a)

Figure 3

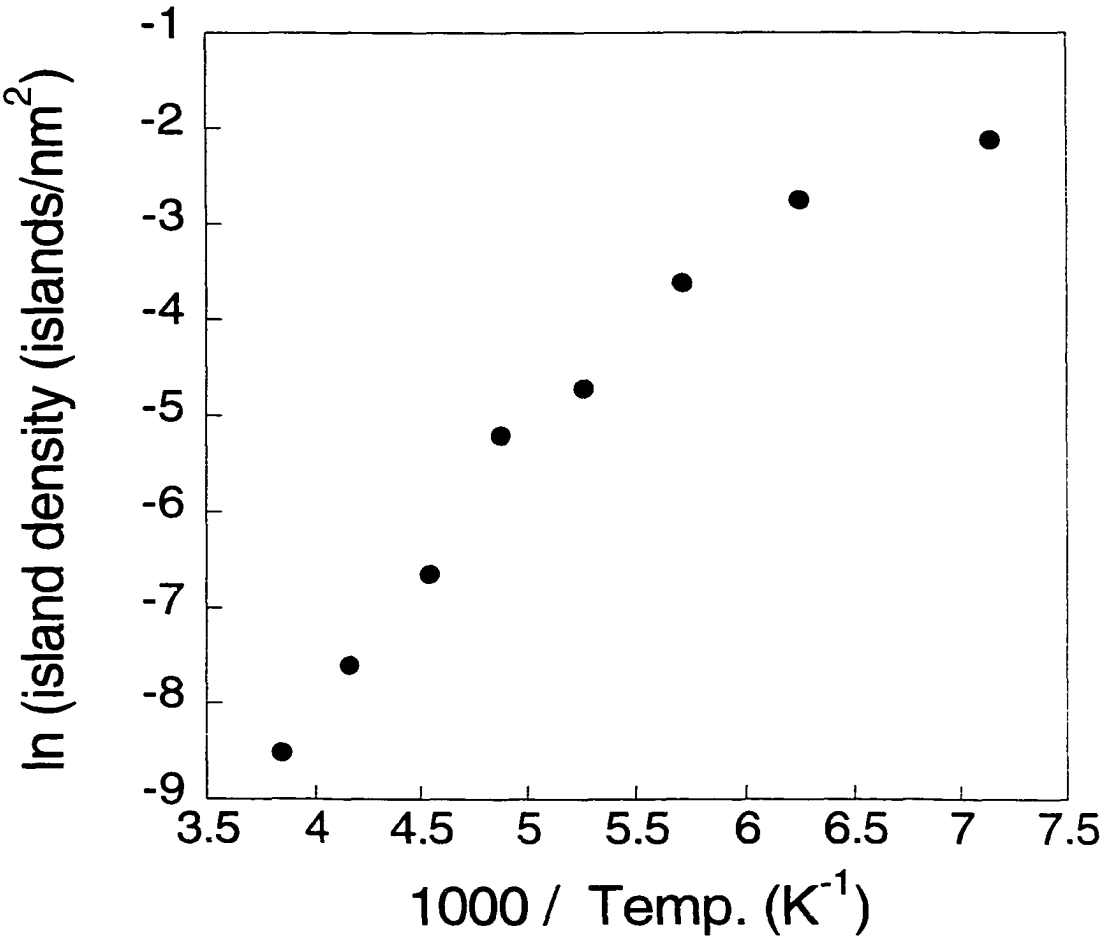
ln (island density (islands/nm^2))
-1
-2
-3
-4
-5
-6
-7
-8
-9
3.5
4
4.5
5
5.5
6
6.5
7
7.5
1000 / Temp. (K^{-1})

(b)

Figure 3

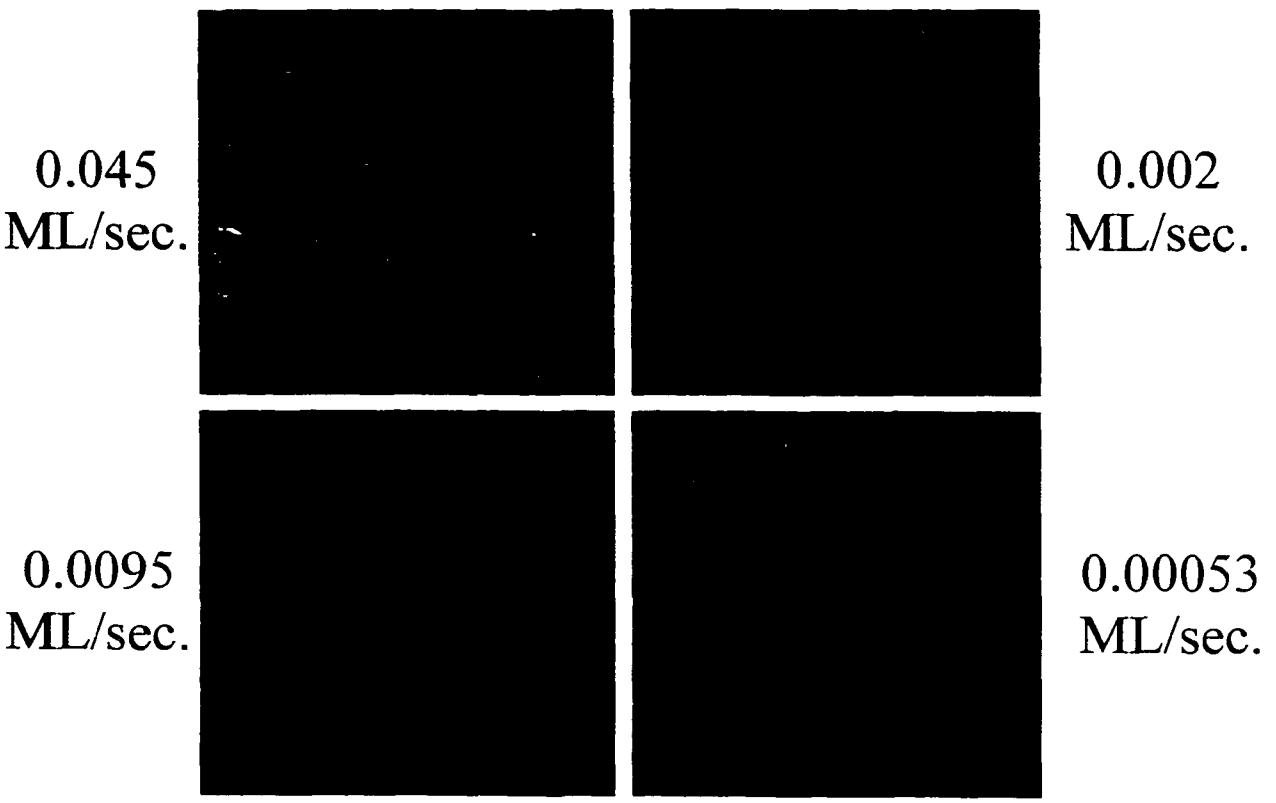

(a)

Figure 4

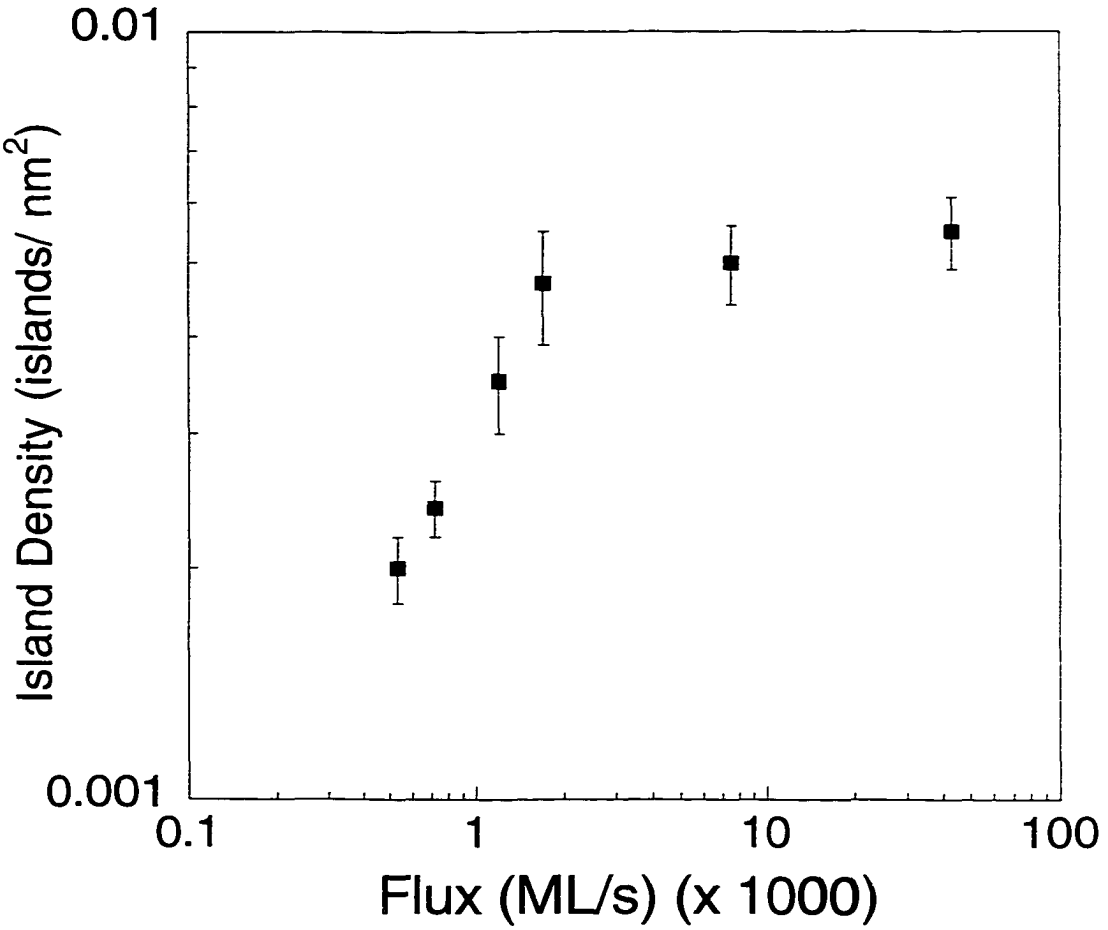
0.01
0.001
Island Density (islands/ nm^2)
0.1
1
10
100
Flux (ML/s) (x 1000)

(b)

Figure 4

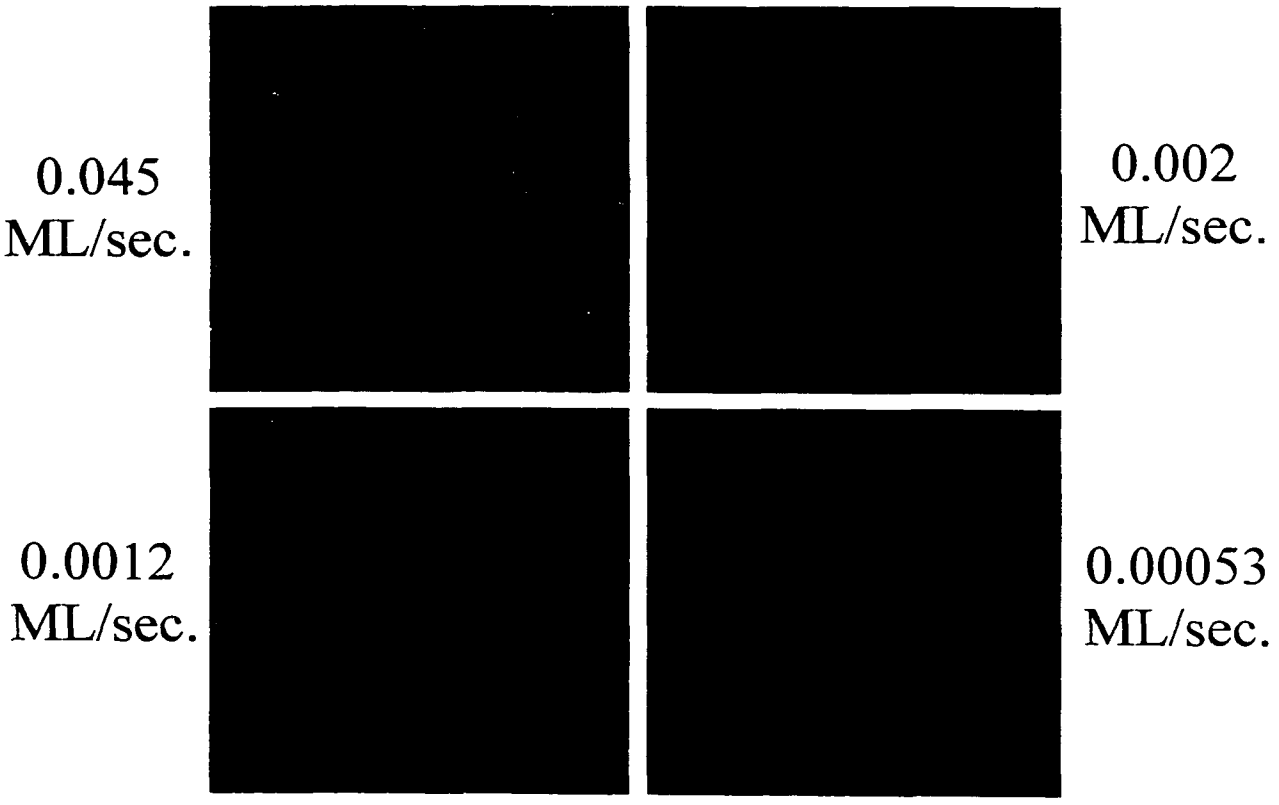

(c)

Figure 4

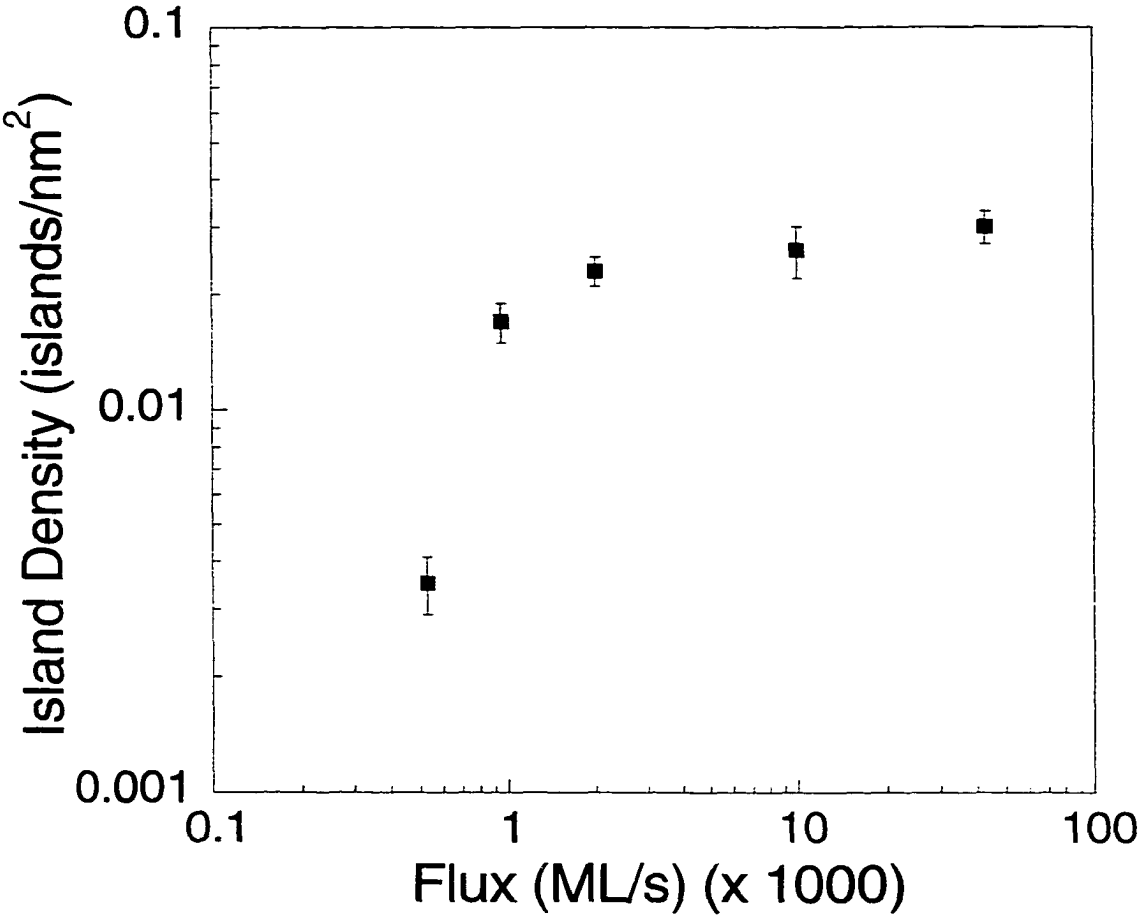
0.1
0.01
0.001
Island Density (islands/nm^2)
0.1
1
10
100
Flux (ML/s) (x 1000)

(d)

Figure 4

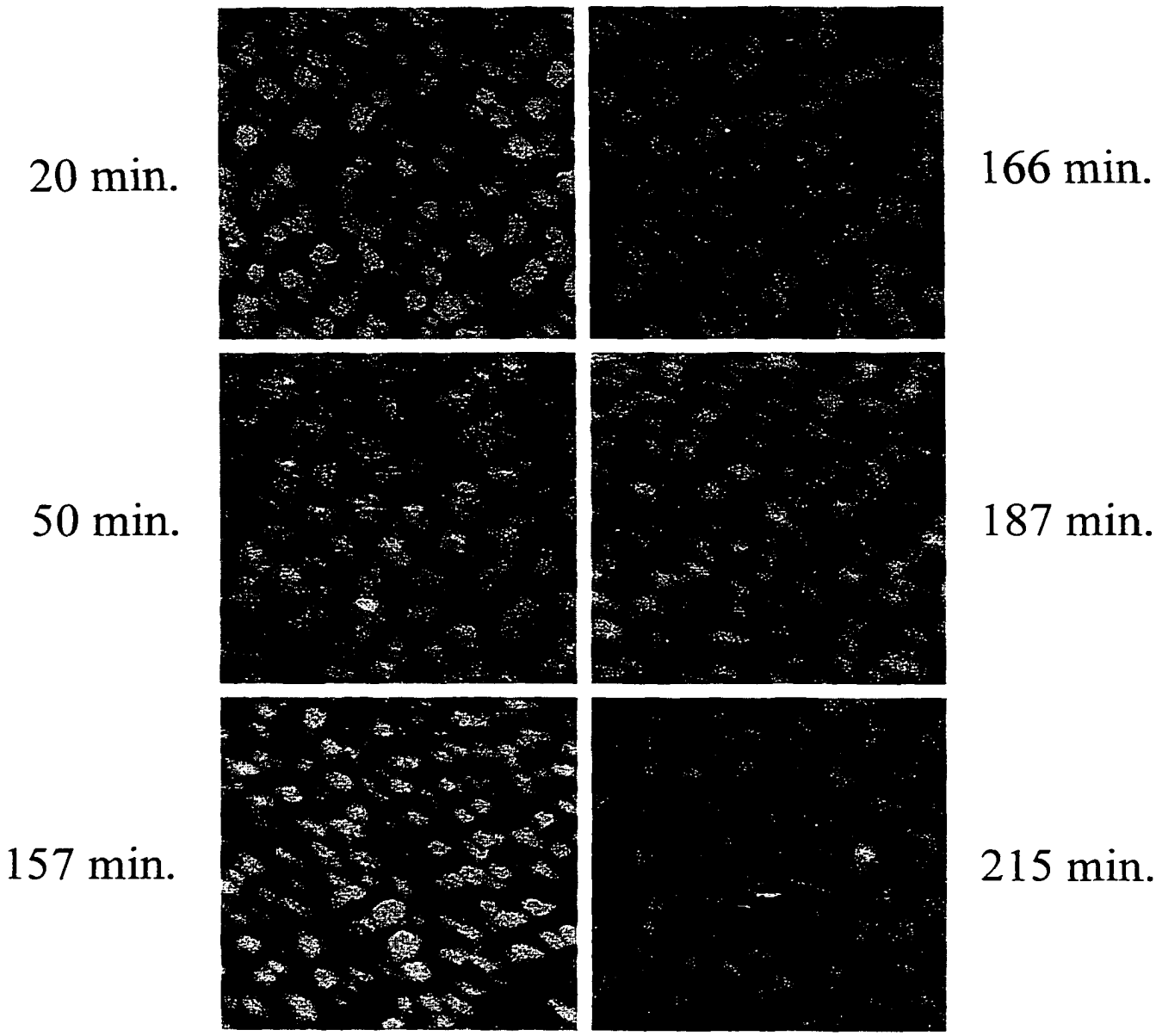

(a)

Figure 5

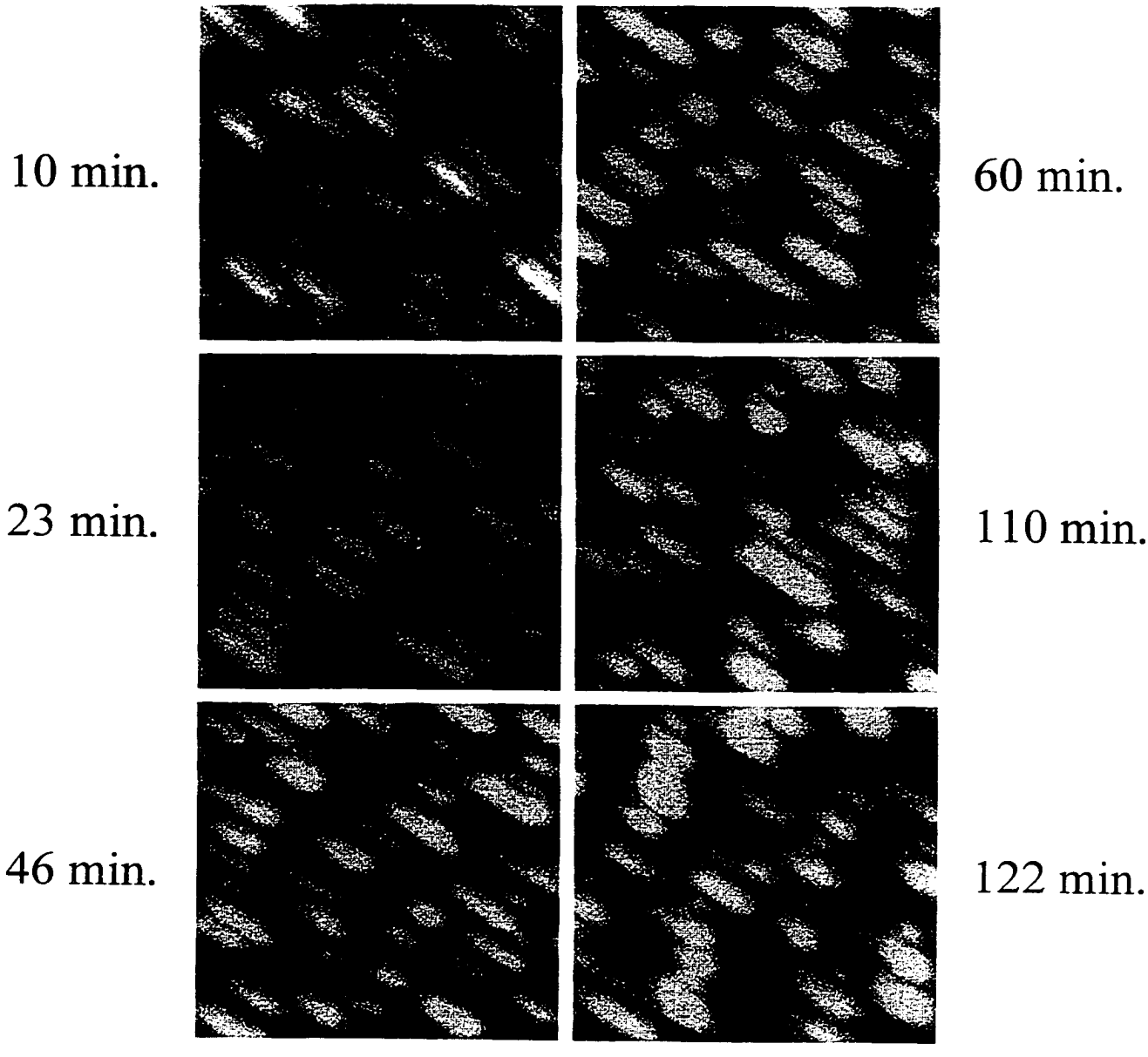

(b)

Figure 5

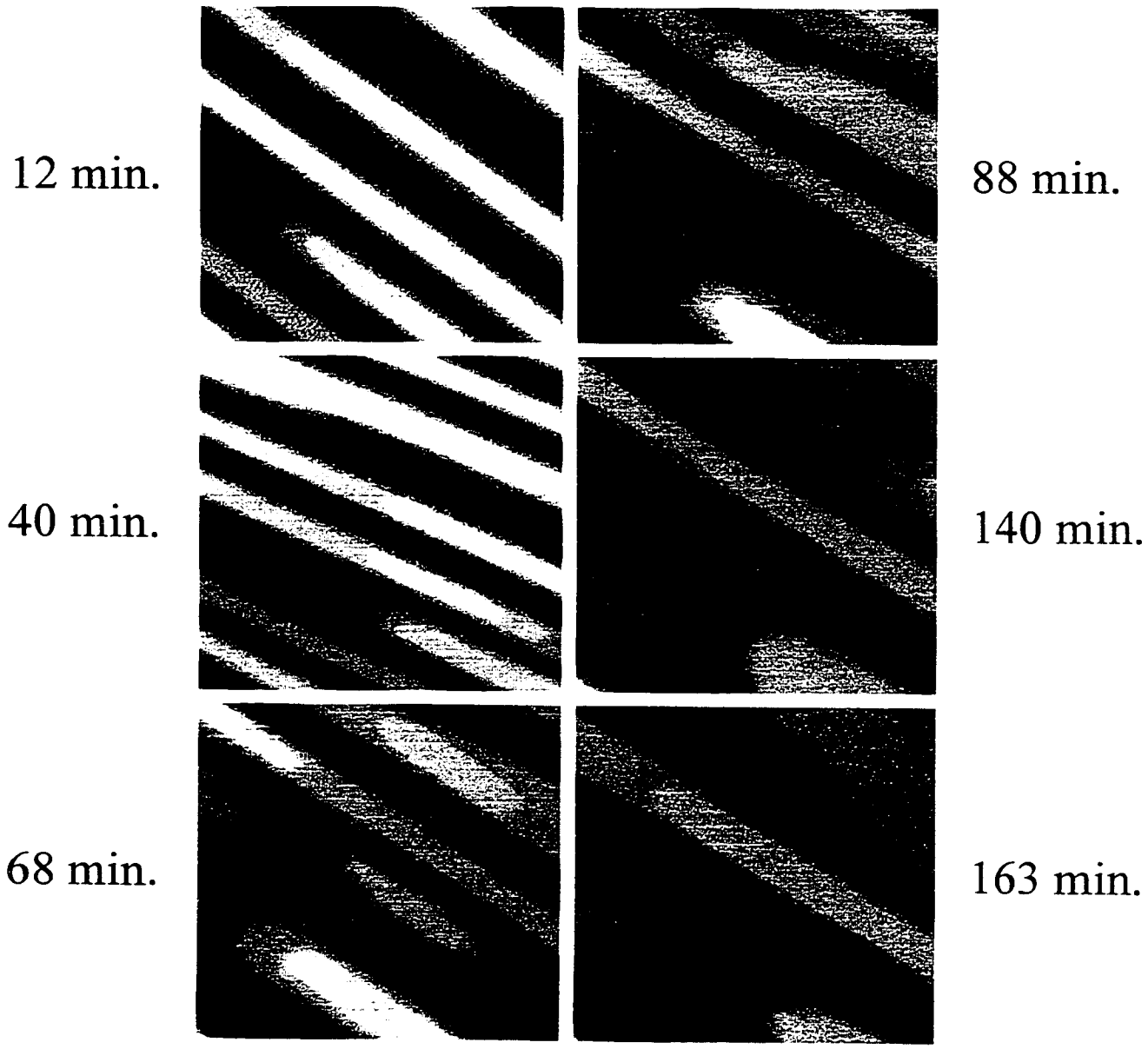

(c)

Figure 5

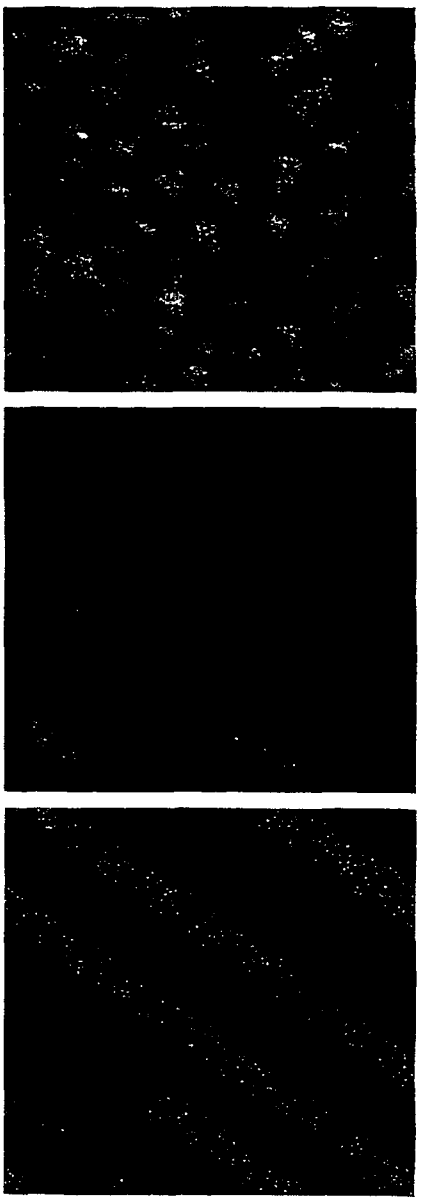

Figure 6

Appendix F. Experiment Database

Table Captions:

I. HRLEED Experiments

II. Oxygen + Ag/Ag(100) Scanning Tunneling Microscopy Experiments

III. Multilayer - Ag/Ag(100) Scanning Tunneling Microscopy Experiments

IV. Ag/Ag(110) Scanning Tunneling Microscopy Experiments

Date	Temp. (K)	Gas	Exposure Post/during dep	Pressure (Torr)	Exposure time(sec.)	Exposure (L)	Experimental Notes and comments
1/25/00	220	dry air	post	5x10-8	30		
1/25/00	220	dry air	post	5x10-6	30		
1/25/00	220	dry air	post	5x10-5	30		
1/31/00	220	N2	post	5x10-6	30		put immediately in LEED
1/31/00	220						0.2ML Ag no gas
2/1/00	220	N2	post	5x10-7	30	4	put immediately in LEED
2/2/00	220	O2	post	1x10-7	40	4	put immediately in LEED
2/2/00	220	O2	post	1x10-7	40	4	put immediately in LEED
2/3/00	220	O2	post	5x10-8	80	4	put immediately in LEED
2/3/00	220	O2	post	5x10-8	80	4	wait 20 min before placing in LEED
2/3/00	220	O2	post	5x10-8	80	4	wait 32 min before placing in LEED
2/6/00	220	O2	post	5x10-8	40	2	put immediately in LEED
2/6/00	220	O2	post	5x10-8	40	2	wait 15 min before placing in LEED
2/6/00	220	O2	post	5x10-8	20	1	wait 30 min before placing in LEED
2/8/00	220	O2	during	5x10-8	35	1.75	put immediately in LEED
2/8/00	220	O2	during	5x10-8	35	1.75	put immediately in LEED. New O2 cylinder
2/9/00	220	O2	during	1x10-7	35	3.75	wait 30 min before placing in LEED
2/9/00	220	O2	during	5x10-8	35	1.75	wait 30 min before placing in LEED
2/9/00	220	O2	during	1x10-8	35	0.35	wait 30 min before placing in LEED
2/9/00	220	O2	during	3x10-8	35	1.05	wait 30 min before placing in LEED
2/10/00	220		during	1x10-7	35	3.75	wait 30 min before placing in LEED. Flux is low
2/10/00	220		during	1x10-7	35	3.75	wait 30 min before placing in LEED. Flux is low
2/11/00	220	O2	during	1x10-7	35	3.75	put immediately in LEED. O.2 ML
2/11/00	220	O2	during	1x10-7	35	3.75	put immediately in LEED. Fixed flux
2/13/00	220	O2	during	5x10-8	35	1.75	wait 20 min before placing in LEED
2/13/00	220	O2	post	1x10-8	35	0.35	put immediately in LEED

Table I

Date	Temp. (K)	Gas	Exposure Post/during dep	Pressure (Torr)	Exposure time(sec.)	Exposure (L)	Experimental Notes and comments
2/14/00	220	O2	post	3x10-8	35	1.05	put immediately in LEED
2/14/00	250						0.3ML on Ag. NO gas
2/15/00	220	O2	during	2x10-8	36	0.7	wait 30 min before placing in LEED
2/15/00	250	O2	post	3x10-8	35	1.05	put immediately in LEED
2/15/00	250	O2	post	3x10-8	35	1.05	wait 30 min before placing in LEED
2/16/00	250	O2	post	5x10-8	35	1.75	put immediately in LEED
2/16/00	220	O2	during	3x10-8	35	1.05	put immediately in LEED
2/17/00	220	O2	post	5x10-8	35	1.75	wait 30 min before placing in LEED
2/18/00	250	O2	post	1x10-7	35	3.75	put immediately in LEED
2/18/00	250	O2	post	1x10-7	35	3.75	wait 10 min before placing in LEED
2/18/00	250	O2	post	1x10-7	35	3.75	wait 10 min before placing in LEED
2/20/00	220	O2	during	1x10-8	36	0.35	put immediately in LEED
2/20/00	220	O2	during	2x10-8	36	0.7	put immediately in LEED
2/21/00	250	O2	post	1x10-7	36	3.75	wait 10 min before placing in LEED
2/21/00	250	O2	during	5x10-8	35	1.75	put immediately in LEED
2/21/00	250	O2	during	3x10-8	35	1.05	put immediately in LEED
2/22/00	250	O2	during	1x10-7	37	3.8	put immediately in LEED
2/22/00	250	O2	during	3x10-7	37	11	put immediately in LEED
2/22/00	250	O2	during	1x10-8	37	0.38	put immediately in LEED. Didn't work
2/22/00	250	O2	during	1.5x10-8	37	0.5	put immediately in LEED.
2/22/00	250	O2	post	1.5x10-8	37	0.5	put immediately in LEED.
All data for the HRLEED experiments are on the labeled Zip Disk.							

Table I (continued)

Experiments Performed	Date	Page in Notebook	Flux ML/sec.	Oxygen Exposure (L)	Backup file name Jazz disk #3	Notes:
0.3ML Ag O2-post 250K	2/20/00	84	0.0085	2	2.20.00	
0.3ML Ag 250K No oxygen	2/21/00	85	0.0085	0	2.21.00	Didn't work. Screwed up gate valve problem
0.3ML Ag 250K No oxygen	2/23/00	87	0.008	0	2.23.00	
0.3ML Ag 250K O2-post	2/27/00	88	0.008	6	2.27.00	
0.3ML Ag 250K O2-Post	2/28/00	89	0.008	36	2.28.00	
0.3ML Ag 250K O2-Post	2/29/00	91	0.008	12	2.29.00	good data set. Small terrace data first noticed OR here
0.3ML Ag 250K O2-Post	3/2/00	93	0.008	12	3.2.00	Reproduced 2.29.00 not as good
0.1ML Ag 250K O2-Post	5/2/00	109		12	5.2.00	Did not work bad drift
0.1ML Ag 250K O2-Post	5/3/00	110		12	5.3.00	Did not work screwed up. Massive amounts of O2
0.1ML Ag 250K O2-Post	5/7/00	111	0.0025	12	5.7.00	Tried to focus on island edge for O2 some atomic images. Not good data
0.1ML Ag 250K O2-Post	5/9/00	113	0.0025	12	5.9.00	Followed island evolutin w/time was able to follow for extended time
0.1ML Ag 300K O2-Post	5/16/00	114	0.0025	12	5.16.00	Tried to focus on island edge for O2 not good
10ML Ag 260K O2-dur	5/23/00	117	0.0032	28	5.23.00	Multilayer exp watched roughness decay with time
0.05ML Ag 250K O2-post	6/5/00	120	0.0025	12	6.5.00	
25ML Ag 260K O2-dur	6/20/00	121	0.045	17	6.20.00	
25ML Ag 260K No oxygen	6/22/00	123	0.045	0	6.22.00	Did not work
25ML Ag 260K No oxygen	6/26/00	125	0.045	0	6.26.00	Roughness decreases w/No O2 at this temp

Table II

Experiments Performed	Date	Page in Notebook	Flux ML/sec.	Oxygen Exposure (L)	Backup file name Jazz disk #3	Notes:
25ML Ag 260K O2-dur	6/27/00	127	0.045	24	6.27.00	
25ML Ag 260K O2-dur	6/28/00	128	0.045	8	6.28.00	
25ML Ag 260K O2-post	7/2/00	131	0.045	17	7.2.00	
25ML Ag 250K No oxygen	7/4/00	132	0.045	0	7.4.00	Little if any decrease in Roughness at this temp w/no O2
25ML Ag 250K O2-post	74/00	134	0.045	17	7.4.00b	W decreased nicely w/time
25ML Ag 250K O2-during	7/5/00	137	0.045	17	7.5.00	Roughness decreased slower???
25ML Ag 250K O2-post	8/11/00	140	0.045	5	8.11.00	
25ML Ag 250K O2-post	8/14/00	142	0.045	0.75	8.14.00	
25ML Ag 230K O2-post	8/15/00	144	0.045	17	8.15.00	Looking at change in roughness as function of temp
25ML Ag 190K O2-post	8/16/00	148	0.045	17	8.16.00	
25ML Ag 210K O2-post	8/21/00	150	0.045	17	8.21.00	"
25ML Ag 220K O2-post	8/24/00	152	0.045	17	8.24.00	
25ML Ag 240K O2-post	8/28/00	154	0.045	17	8.28.00	"
0.3ML Ag 250K O2-post	9/19/00	156	0.002		9.19.00	island shape after long elapsed time Did not work
0.3ML Ag 250K O2-post	10/2/00	159	0.002	17	10.2.00	island shape after long elapsed time corner cropped after 24 hrs
0.3ML Ag 300K O2-post(during entire time)	10/8/00	162	0.002	17L-initial 36L/hr after	10.8.00	islands very round
0.2-0.3ML Ag @300K cool to 240K O2-post	10/15/00	167	0.002	30-initial 30 (60min) 30(120 min) 17(500 min)	10.15.00	try to stabalize [100] step edges flowery steps some islands rotated

Table II (continued)

Experiments Performed	Date	Page in Notebook	Flux ML/sec.	Oxygen Exposure (L)	Backup file name Jazz disk #3	Notes:
0.05ML Ag 250K O2-post	10/22/00	171	0.002	17	10.22.00	island width distribution expmts (also 2.28.00 5.9.00)
0.2-0.3ML Ag @300K cool to 250K O2-post redeposit @ 24hrs	10/30/00	173		30	10.30.00	did not work
0.2-0.3ML Ag @300K O2 @ 300K/evolve 24hrs cool to 250K redeposit 0.1ML	11/9/00	175	0.002	30	11.9.00	first part went OK second deposition failed
0.3 ML Ag @ 250K No oxygen	11/15/00	179	0.008	0	11.15.00	did not work STM failed IDL license problem
0.3 ML Ag @ 250K No oxygen	11/27/00	181	0.008	0	11.27.00	looking for corner/corner coalescence for comparison w/ oxygen (data OK, not great)
0.3 ML Ag @ 250K No oxygen	11/29/00	183	0.008	0	11.29.00	looking for corner/corner coalescence for comparison w/ oxygen (good examples here)
0.2-0.3ML @ 300K O2 @ 300K/evolve 24hrs cool 250K redeposit 0.1 - 0.2 ML	12/7/00	185	0.002 0.002	30	12.7.00	very weird results
0.2-0.3ML @ 320K O2 @ 300K/evolve 24hrs cool 250K redeposit 0.2 ML	12/7/00	188	1st=0.002 2nd=0.02	30	12.7.00	initial islands big 2nd layer no nucleation on top islands grew bigger
Clean sample expose to O2 @ 250 deposit 0.1 - 0.2 ML Ag	12/12/00	193	0.002	30	12.12.00	seems to affect initial island nucleation island density is lower
0.2 ML @ 320K cool to 250K No oxygen redeposit 0.2 ML Ag	12/13/00	196	1st=0.002 2nd=0.02	0	12.13.00	initial islands big was able to nucleate second layer islands

Table II (continued)

Experiments Performed	Date	Page in Notebook	Flux ML/sec.	Oxygen Exposure (L)	Backup file name Jazz disk #3	Notes:
clean sample expose to O2 @ 250K deposit 0.2ML Ag	12/15/00	199	0.02	30	12.15.00	how does initial island density change with flux
clean sample expose to O2 @ 250K deposit 0.2ML Ag	12/17/00	201	0.045	30	12.17.00	how does initial island density change with flux
clean sample expose to O2 @ 250K deposit 0.2ML Ag	12/18/00	202	0.007	30	12.18.00	how does initial island density change with flux
clean sample expose to O2 @ 250K deposit 0.2ML Ag	12/19/00	203	0.0008	30	12.19.00	how does initial island density change with flux
clean sample expose to O2 @ 250K deposit 0.2ML Ag	12/20/00	205	0.12	30	12.20.00	how does initial island density change with flux
clean sample expose to O2 @ 250K deposit 0.2ML Ag	12/21/00	206	0.01	30	" 12.21.00	how does initial island density change with flux
Clean sample expose to O2 @ 250K deposit 0.1 - 0.2 ML Ag	12/31/00	210	0.002	1	12.31.00	monitor island density with change in initial oxygen exposure (see also 12.12.00)
Clean sample expose to O2 @ 250K deposit 0.1 - 0.2 ML Ag	1/2/01	212	0.002	5	1.2.01	monitor island density with change in initial oxygen exposure
Clean sample no oxygen @ 250K deposit 0.1 - 0.2 ML Ag	1/2/01	212	0.002	0	1.2.01b	monitor island density with change in initial oxygen exposure

Table II (continued)

Experiments Performed	Date	Page in Notebook	Flux ML/sec.	Oxygen Exposure (L)	Backup file name Jazz disk #3	Notes:
Clean sample expose to O2 @ 250K deposit 0.1 - 0.2 ML Ag	1/3/01	212	0.002	15	1.3.01	monitor island density with change in initial oxygen exposure
Clean sample no oxygen @ 250K deposit 0.1 - 0.2 ML Ag	1/8/01	217	0.1	0	1.8.01	monitor island density for a clean system at 250K
Clean sample no oxygen @ 250K deposit 0.1 - 0.2 ML Ag	1/9/01	218	0.0008	0	1.9.01	monitor island density for a clean system at 250K
Clean sample no oxygen @ 250K deposit 0.1 - 0.2 ML Ag	1/9/01	218	0.0008	0	1.9.01b	monitor island density for a clean system at 250K
Clean sample expose to O2 @200K deposit 0.1 - 0.2 ML Ag	2/23/01	243	0.002	30	2.23.01	monitor island density for clean system (change temp. To get Energy (Ea)
Clean sample no oxygen @ 220K deposit 0.1 - 0.2 ML Ag	2/24/01	245	0.002	30	2.24.01	monitor island density for clean system (change temp. To get Energy (Ea)
Clean sample *no oxygen @ 270K* deposit 0.1 - 0.2 ML Ag	*2/25/01*	*246*	*0.002*	30	2.25.01	monitor island density for clean system (change temp. To get Energy (Ea)
Clean sample no oxygen @ 295K deposit 0.1 - 0.2 ML Ag	2/26/01	247	0.002	30	2.26.01	monitor island density for clean system (change temp. To get Energy (Ea)
Clean sample no oxygen @ 170K deposit 0.1 - 0.2 ML Ag	2/27/01	248	0.002	30	2.27.01	monitor island density for clean system (change temp. To get Energy (Ea)

Table II (continued)

Experiments Performed	Date	Page in Notebook	Flux ML/s	Backup file name Jazz disk #1	Notes
5 ML @ 300K	9/8/99	5	0.032	9.8.99	
100ML @ 300K	9/10/99	6	0.032	9.10.99	
100ML @ 300K	9/12/99	7	0.032	9.12.99	
25 ML @ 300K	9/13/99	8	0.032	9.13.99	W (rms) = 0.230
10 ML @ 300K	9/14/99	9	0.032	9.14.99	did not work
10 ML @ 300K	9/20/99	10	0.032	9.20.99	lot of dirt on surface
2 ML @ 300K	9/22/99	11	0.032	9.22.99	
25 ML @ 300K	9/23/99	13	0.032	9.23.99	results same as 9.13.99
100 ML @ 300K	9/27/99	16	0.032	9.27.99	
60 ML @ 300K	9/30/99	19	0.032	9.30.99	
5 ML @ 190K	10/5/99	22	0.032	10.5.99	W(RMS) 0.75X
100 ML @ 190K	10/7/99	24	0.032	10.7.99	
25 ML @ 190K	10/11/99	25	0.032	10.11.99	W(RMS) 0.26X
60 ML @ 190K	10/13/99	27	0.032	10.13.99	
100 ML @ 190K	10/15/99	28	0.032	10.15.99	res incr, W decreases
5 ML @ 260K	10/18/99	29	0.032	10.18.99	

Table III

Experiments Performed	Date	Page in Notebook	Flux ML/s	Backup file name Jazz disk #1	Notes
10 ML @ 260K	10/19/99	30	0.032	10.19.99	
25 ML @ 260K	10/21/99	32	0.032	10.21.99a	W = 1.208
60 ML @ 260K	10/21/99	33	0.032	10.21.99b	
100 ML @ 260K	10/25/99	34	0.032		Bad tip cannot resolve bad data
60 ML @ 260K	11/7/99	40	0.032	11.7.99	
100 ML @ 260K	11/16/99	45	0.032		silver in evaporator ran out
100 ML @ 230K	12/16/99	59	0.032	12.16.99	W(rms) 0.388 W = 1.90
60 ML @ 230K	12/29/99	66	0.037	12.29.99	
25 ML @ 300K	12/30/99	67	0.037	12.30.99	W(rms) = 0.214 W = 1.04
1.0ML	12/29/00	209	0.02	12.29.00	monitor 2nd layer coverage
100 ML @ 190K	1/4/01	216	03xx	1.4.01	
500 ML @ 190K	1/17/01	221	0.045	1.17.01	W(rms) 1.5 (very large)
120 ML @ 190K	1/18/01	223	0.032	1.18.01	W(rms) = 0.46xxx
60 ML @ 190K	1/23/01	229	0.032	1.23.01	W(rms) 0.36

Table III (continued)

Experiments Performed	Date	Page in Notebook	Flux ML/s	Backup file name Jazz disk #2	Notes:
0.2ML @ 230 K	12/5/99	53	0.045	12.5.99	had miscalculated flux for these exp.'s so coverages are high
0.2ML @ 175 K	12/12/99	56	0.045	12.12.99	Actual q = 0.26 ML
0.25ML @ 190 K	12/19/99	60	0.045	12.19.99	Actual q = 0.38 ML
0.20ML @ 205 K	12/21/99	63	0.045	12.21.99	Actual q = 0.25 ML
0.20ML @ 220 K	1/3/00	70	0.045	1.2.00	Actual q = 0.30 ML
0.20ML @ 240 K	1/4/00	72	0.045	1.4.00	Actual q = 0.23 ML
0.20ML @ 260 K	1/6/00	74	0.045	1.6.00	
0.2ML @ 140 K	1/17/00	77	0.045	1.17.00	Difficult exp. Resolution poor density probably higher than indicated
0.2ML @ 205K	1/21/00	78		1.21.00	great exp. For island coalescence Actual q = 0.23 ML
25ML @ 205 K	1/21/00	79		1.21b.00	multilayer exp
0.2 ML @ 160 K	1/23/00	80		1.23.00	Excellent data set three atomic row resolution!
0.2 ML @ 205 K	3/28/00	94	0.0075	3.28.00	
0.2ML @ 205 K	3/29/00	96	0.00053	3.29.00	
0.2 ML @ 205 K	4/2/00	97	0.0017	4.2.00	
0.2 ML @ 205 K	4/4/00	98	0.0012	4.4.00	

Table IV

Experiments Performed	Date	Page in Notebook	Flux ML/s	Backup file name Jazz disk #2	Notes:
0.2 ML @ 205 K	4/5/00	100	0.00072	4.5.00	
0.2 ML @ 175 K	4/17/00	101	0.0075	4.17.00	drift problems
0.2 ML @ 175 K	4/18/00	102	0.002	4.18.00	?????
0.2 ML @ 175 K	4/19/00	103	0.00095	4.19.00	hard to find large terraces
0.2 ML @ 175 K	4/20/00	104	0.00071	4.20.00	coverage too high to get acurate density
0.2 ML @ 175 K	4/24/00	105	0.0075	4.24.00	
0.2 ML @ 175 K	4/25/00	106	0.002	4.25.00	bad drift
0.2 ML @ 175 K	4/26/00	107	0.00095	4.26.00	no image until 30min bad drift
0.2 ML @ 175 K	1/30/01	233	0.00053	1.30.01	not many images good enough image initially
0.2 ML @ 175 K	2/4/01	235	0.01	2.4.01	did not work
0.2 ML @ 175 K	2/5/01	236	0.01		couldn't get image until 120 min can't use)
0.2 ML @ 175 K	2/6/01	238	0.01	2.6.01	good image at 30 min
25ML @ 175 K	2/8/01	239	0.045	2.8.01	multilayer exp
25ML @ 260K	2/9/01	241	0.045	2.9.01	multilayer exp

Table IV (continued)

ACKNOWLEDGEMENTS

I would like to express my deepest appreciation to Professors Pat Thiel and Jim Evans for their support and guidance throughout my graduate career. I thank them for the knowledge they passed along to me, as well as the opportunity to do some really cool research. While I was occasionally required to reproduce a 'Conrad data point' or two, I truly appreciate their allowing me a large degree of independence and the freedom to explore different avenues of my own research. I would like to thank them for their patience and their willingness to let me make mistakes. I have always believed that failure and mistakes pave the way to success, and I believe so now more than ever.

I have to thank all of the Thiel group members, past and present. I would especially like to acknowledge the people I worked closest with over my time at Iowa State including: Cynthia Jenks, Conrad Stold, and Kyle Caspersen.

I would like to send a special thanks to Jim Anderegg for all his help and advise on the many modifications and repairs to my equipment over the years. I will also miss our morning conversations, which were always more than intriguing.

To all the friends that I've met here I owe special thanks. Brett (whose love of Sheboygan brats may only be rivaled by my own), Mike (fellow coffee fiend), Kenny (my old 'Okey' roomate) and Rich and Christa (as well as Gus and Benny,) who are all, and will remain more than good friends. Of course I couldn't forget Zoey (my dog), who made the last year here a lot of fun.

Lastly I would like to thank my family. They have always been there when I needed them. Their thoughts and prayers mean more to me than they will ever know. I love you all.